plant, Algae, and Environment
Vol. 9, Issue 3, Sept. 2025
Table of Contents

Modelling of the Climate Change Impact on the Spatial Distributions of *Crocus* Species in Iran

Melika Tabasi[1]* , **Ahmadreza Mehrabian[2], Sadaf Sayadi[2], Hossein Mostafavi[3]**

Abstract

Global warming, droughts, widespread fires, and shifts in plant phenology contribute to a loss of biodiversity. Plant species are also facing a decrease in the desirability of their habitats due to climate change. These events result in significant genetic erosion within plant taxa. In the present study, to predict the current and future spatial distributions of *Crocus* species of Iran and possibility of expansion and reduction of their current habitats, the spatial distribution of this endangered genus, based on presence data of seven *Crocus* species, including *C. biflrous*, *C. cancellatus*, *C. caspius*, *C. haussknechtii*, *C. michelsonii*, *C. speciosus*, *C. sativus* was investigated under present and future climate change scenarios: RCP2.6 and RCP8.5 for the years 2050 and 2080 using a set of ecological variables (Sixteen environmental variables) and the MaxEnt model. The projected climate maps resulted in reductions and expansions, as well as positive and especially negative range change for the studied species in comparison to their current predicted distributions. Among all studied species, Saffron (*Crocus sativus*) showed the highest positive range change as well as the highest significant change under optimistic scenarios for 2050 and 2080, while *Crocus michelsonii* showed the highest range of negative changes under these scenarios. *C. biflorus*, *C. speciosus*, and *C. caspius* also revealed a negative range change, respectively. Finally, the results of this study revealed that the species whose current habitats are negatively affected by climate change (especially *C. michelsonii*) are the most endangered *Crocus* species in the face of climate change. Therefore, a conservation plan to protect these threatened species seems necessary.

Introduction

The increase in global temperature, along with drought and wildfires, significantly contributes to

1- Department of Biology, Faculty of Basic Sciences, Hakim Sabzevari University, Sabzevar, Iran
2-Department of Plant Sciences and Technology, Faculty of Life Sciences and Biotechnology, Shahid Beheshti University, Tehran, Iran
3-Department of Biodiversity and Ecosystem Management, Environmental Sciences Research Institute, Shahid Beheshti University, Tehran, Iran
* Corresponding author email address: me.tabasi@hsu.ac.ir

the decline of biodiversity (Amedie, 2013). Based on the IPCC (Intergovernmental Panel on Climate Change), approximately 58% of plant taxa are expected to face a sharp decrease in habitat desirability due to climate change by 2080 (Warren et al., 2013). The mentioned catastrophic event resulted in significant genetic erosion in plant taxa (Jarvis et al., 2008). Considering the available evidence, climate change is known to be a negative event for the majority of species. The effect of climate change on a wide range of taxa will probably be negative (Muths et al., 2017; Yousefi et al., 2020).

Crop Wild Relatives (CWRs) are major natural genetic resources that play an important role in the improvement and promotion of crops (Maxted et al., 1997). CWRs include valuable genetic material, which may be useful for enhancing crops, such as increasing production and resistance against natural stresses. Consequently, assessing the impacts of climate change is a crucial step in establishing conservation priorities and executing management strategies (Guillera-Arroita et al., 2015).

Saffron (*Crocus sativus* L.) is a perennial bulb cultivated mainly in Iran, India, and the Mediterranean countries (Bathaie et al., 2010; Christodouloua et al., 2015). Saffron is known as the most expensive spice in the world, as well as the most valuable industrial and medicinal crop, primarily used for its aroma and flavor in food, and as a medicinal herb (Koocheki, 2004). Iran produces about 93% (301 tons) of the world's saffron production (Ghorbani and Koocheki, 2017). Furthermore, Central Asia, the Middle East, and the islands of South West Greece are considered the origin centers of saffron (Vavilov, 1951; Tammaro, 1989). The wild relatives of saffron can be utilized to enhance its quality and mitigate environmental stresses (Negbi, 1999). Iranian *Crocus* species exhibit highly variable flower coloration due to intensive gene exchange between genotypes. Therefore, it is suggested that the considerable genetic resources found in different *Crocus* species could be utilized to genetically improve *C. sativus*. Among the wild Iranian *Crocus* species, *Crocus pallasii* Goldb. is closely related to *C. sativus* (Sheidai et al., 2018). Unfortunately, several threatening factors, including climate change, land use change, overharvesting, and overgrazing, severely threaten these species. Therefore, they are classified in critically endangered (CR) and endangered (En) categories according to IUCN (International Union for Conservation of Nature) threatened categories (Mehrabian et al., 2020).

Ecological niche modeling (ENM) is an effective methodology for predicting distribution patterns in conservation management (Margules and Pressey, 2000; Groves et al., 2002; Peterson and Soberón, 2012; Flores-Tolentino et al., 2019; Mathur et al., 2023; Waheed et al., 2025). Up to now, a wide range of diffrent algorithms based on presence and/or absence data have been developed to predict distribution patterns of target taxa (Soberón and Peterson, 2005; Elith and Leathwick, 2007, 2009). Maximum entropy (MaxEnt) modeling is recognized as one of the best-performing methods for modeling diverse taxa based on presence data (Elith et al., 2006). So far, many

studies have been conducted based on this methodology throughout the world (Rödder and Weinsheimer, 2009; Aragón et al., 2010; Rubidge et al., 2011; Khanum et al., 2013; Kujala et al., 2013; Legault et al., 2013; Adams-Hosking et al., 2015; Bleyhl et al., 2015; Luo et al., 2015; Sen et al., 2016; Ulrey et al., 2016).

Despite Iran's outstanding plant diversity, few modeling studies have been done in Iran. Saffron is an economically valuable species, and some of its wild Iranian relatives (as important breeding resources) are among the threatened taxa (Tabasi et al., 2021). To date, the distribution of these valuable taxa in Iran has not been modeled. Therefore, our study aims to predict the current and future spatial distributions of wild and cultivated *Crocus* species of Iran for the first time to forecast the possibility of expansion and reduction of their current habitats under scenarios projecting climate change, RCP2.6 (RCP, representative concentration pathway; optimistic scenario) and RCP8.5 (pessimistic scenario) for the years 2050 and 2080 using a set of ecological variables and the MaxEnt model. Finally, the results of this study can inform effective conservation decisions for these valuable species.

Material and methods

Study area

Iran is a segment of the Alpine-Himalayan geologic belt (Krinsley, 1970) that is considered one of the most seismically active regions in the world, with high natural uplands, as well as mountains that surround the irregular and lower interior (Fisher, 1968; Homke et al., 2004). The Zagros mountain-ous belt is a set of north-west to south-east trending parallel inhabits in the entire Western zones of Iran (Cucchi and Zini, 2003). In addition, the Alborz Mountain system is located in the Northern zone of Iran and stretches from the Southern parts of the Caspian Sea (Stöklin, 1974) from West (Azarbaijan) to East (Khorasan). This natural massif is located between the Caspian Sea and the Central plateau of Iran (Alavi, 1991). Other prominent mountainous systems, including the Kopet-Dagh, located in the Eastern margins of the Caspian Sea, extend into Northeastern Iran, Turkmenistan, and Northern Afghanistan (Afshar, 1979; Buryakovsky et al., 2001). Additionally, the Makran in the Southeast, as well as Jebal Barez in the Center, are other geomorphological formations of Iran (Fischer, 1968; McCall, 1997). Moreover, climatological units of Iran comprise of 35.5% hyper-arid, 29.2% arid, and 20.1% zone of the world. The precipitation shows an average of about 250 mm (about less than one-third of the average rainfall in the world, 860 mm) (Amiri and Eslamian 2010; Shakoor et al., 2010).

Species occurrence data collection

Distribution patterns originated from field assessments during 2017–2019 as well as some literature records available in several plant floras. Due to the lack of careful and reliable absence species distribution data, only presence data were used in this study. Distribution map including the presence of seven species (*Crocus biflorus* Mill., *Crocus cancellatus* Herb., *Crocus caspius* Ficher & Meyer., *Crocus michelsonii* B. Fedtsch., *Crocus speciosus* M. Bieb., *C. pallasii, C. sativus*) of the *Crocus* genus which enough data

were available for their modelling (Fig.1). A geographic distribution database of these species was established using records that corresponded to 336 distribution points of them. These records were provided based on the review of Flora of Iran (Assadi et al., 1999), Flora Iranica (Rechinger, 1975), the illustrated flora of Golestan National Park (Akhani, 2005), plant samples from several Herbaria: HSBU, TUH, FUMH, the personal Herbarium of Dr. Akhani, the Herbarium of Hakim Sabzevari University, the Herbarium of Payame Noor University of Sari, and Virtual Herbaria of Wien (http://herbarium. univie.ac.at/database/search.php), several scientific literatures, as well as field excursions by authors. Additionally, ecological factors (e.g., latitude, longitude, and altitude) for some plant samples without geographic coordinates were provided by Google Earth ver.5.1.

Selection of environmental variables

In this study, first, based on a compilation of valid experiences of experts about the ecology of this group of taxa, a total set of 16 ecological variables (i.e. BIO2 = Mean Diurnal Range, BIO4 = Temperature Seasonality, BIO8 = Mean Temperature of Wettest Quarter, BIO11 = Mean Temperature of Coldest Quarter, BIO13 = Precipitation of Wettest Month, BIO15 = Precipitation Seasonality, BIO16 = Precipitation of Wettest Quarter, BIO19 = Precipitation of Coldest Quarter, Slope, Solar Radiation, Elevation, Sand Content, pH Index, Bulk Density, Coarse Fragments, Soil Organic Carbon Content) connected to the distribution pattern of *Crocus* species was used. Subsequently, collinearity among ecological variables was tested by Pearson's correlation coefficient (r), so if two variables were highly correlated (r > |0.70|), one of them was excluded according
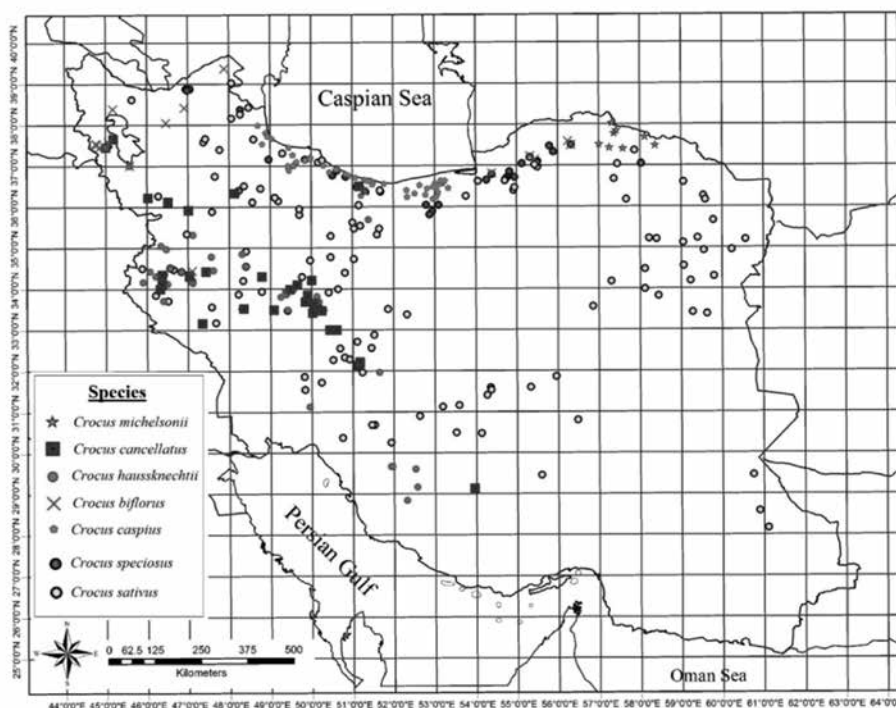

Fig. 1. Distribution map (based on presence data) of seven studied *Crocus* species: *C. biflrous, C. cancellatus, C. caspius, C. haussknechtii, C. michelsonii, C. speciosus,* and *C. sativus* in Iran

4

to our expert judgment in order to avoid collinearity (Elith et al., 2010). The source of selected variables after the correlation test is available in Table 1. To represent climate change influences, we used projected future climate variables for 2050 and 2080 (used the average of 16 General Circulation Models (GCMs) under optimistic (RCP 2.6) and pessimistic (RCP 8.5) with the 30 arc-second (ca. 1 × 1 km) resolution) with empirically downscaled bioclimatic data downloaded from the CCAFS website (Climate Change, Agriculture and Food Security; http://www.ccafs-climate.org).

Modelling process and evaluation

The MaxEnt model (Phillips et al., 2006) was applied for modelling species current and future habitat suitability. MaxEnt (jar file v3.4.1) was utilized through the dismo package v1.1-4 (Hijmans et al., 2017) in R v3.2.3 programming environment (R Core Team, 2018). The MaxEnt model is particularly used when the data points include presence-only with a limited number of records (e.g., Vasconcelos et al., 2012; Bosso et al., 2013; Fois et al., 2018). The models were evaluated using 10-fold cross-validation. In cross-validation, data is randomly divided

Table 1. Source of selected variables after correlation test, and estimates of their permutation importance

Source	Variable	Permutation importance (%)						
		C. biflorus	*C. cancellatus*	*C. caspius*	*C. haussknechtii*	*C. michelsonii*	*C. speciosus*	*C. sativus*
Bioclimatic variables (www.worldclim.org)	BIO2 = Mean Diurnal Range	18.7	3.6	27.3	0.9	-	1.9	2.4
	BIO4 = Temperature Seasonality	0.9	-	15.7	0.9	0.1	20.1	5.4
	BIO8 = Mean Temperature of Wettest Quarter	-	16.1	0.1	18.3	-	5.1	0.8
	BIO11 = Mean Temperature of Coldest Quarter	2.1	-	-	-	2.3	-	-
	BIO13 = Precipitation of Wettest Month	-	-	11.6	-	-	2.9	-
	BIO15 = Precipitation Seasonality	4.3	1	9.9	9	86.4	1	6.5
	BIO16 = Precipitation of Wettest Quarter	-	10.1	-	2	-	-	4.4
	BIO19 = Precipitation of Coldest Quarter	11.2	-	-	-	3.9	-	-
Topographic variables (www.worldgrids.org) (www.isric.org)	Slope	0.7	1.3	2	3.9	0.3	9.1	10.2
	Solar Radiation	43.4	7.1	5.3	2.6	-	29.7	19.8
	Elevation	5.9	3.5	9.8	3.2	-	8	8.1
Edaphic predictor (www.soilgrid.org) (www.isric.org)	Sand Content	0.3	45.4	8.7	34.2	0.3	0.6	30.3
	PH Index	-	-	3.1	-	-	-	-
	Bulk Density	-	-	6.7	-	-	-	-
	Coarse Fragments	-	4.9	-	0.6	0.1	4.9	9.1
	Soil Organic Carbon Content	12.6	7	-	24.5	6.7	16.8	3

into 10 parts, nine parts are used for model fitting, and the fitted model is evaluated on the holdout part (Valavi et al., 2018). We also considered permutation importance to define the main environmental variables that have influenced the potential distribution of the studied species (Abdelaal et al., 2019). To assess the accuracy of the modelling results, the Area Under the Curve (AUC) (Yi et al., 2016; Fois et al., 2018) of the Receiver Operating Characteristic Curve (ROC) was computed (Lobo et al., 2008). AUC shows the power of the model to discriminate the presence of a random background (Phillips et al., 2009).

Results

Modelling outputs for the potential habitat suitability of *C. biflorus*, *C. cancellatus*, *C. caspius*, *C. haussknechtii*, *C. michelsonii*, *C. speciosus*, and *C. sativus* with 16 environmental variables (correlation test) showed perfect predictive performance with AUC values (i.e., 0.944, 0.945, 0.990, 0.946, 0.980, and 0.898, respectively). Considering permutation importance, Precipitation Seasonality (BIO15), Sand Content, Solar Radiation, and Mean Diurnal Range (BIO2) were respectively the main environmental variables that have influenced the potential distribution of all species. In this regard, for *C. biflorus*, Solar Radiation and Mean Diurnal Range (BIO2); for *C. cancellatus*, sand content and Mean Temperature of Wettest Quarter (BIO8); for *C. caspius*, Mean Diurnal Range (BIO2) and Temperature Seasonality (BIO4); for *C. haussknechtii*, sand content and soil organic carbon content; for *C. michelsonii*, Precipitation Seasonality

(BIO15); for *C. speciosus*, Solar Radiation and Temperature Seasonality (BIO4) and finally for *C. sativus*, sand content and Solar Radiation were respectively important (Fig. 2).

The projected climate maps under optimistic and pessimistic scenarios (RCP 2.6 and RCP8.5) of 2050 and 2080 (Fig. 3) resulted in reduction and expansion as well as positive and especially negative range change for the studied species in comparison to their current predicted distributions (Tables 2 and 3). Among the studied species, *C. michelsonii* showed the highest range of negative changes based on the loss and gain of suitable habitats under these scenarios. *C. biflorus*, *C. speciosus*, and *C. caspius* also revealed a negative range change (less than *C. michelsonii*) under the scenarios mentioned above, respectively. However, among the studied species, *C. sativus* showed the highest positive range changes as well as the highest increase (significant increase) under optimistic scenarios for 2050 and 2080. Some species, like *C. cancellatus* and *C. haussknechtii*, showed different range changes under these scenarios.

The current distribution patterns of these taxa in Iran are often concentrated in Alborz (North and North West), Kopet Dagh (North East), and Zagros (West). The main area of *Crocus* species distribution is confined to the Mediterranean phyto-chorion that extends into the Irano-Turanian region (Negbi, 1999).

Discussion and Conclusion

The present study demonstrated the potential geographical distributions of seven

Crocus species in Iran under both current and future climate scenarios. The results obtained in the present study showed that BIO2 (Mean Diurnal Range), BIO15 (Precipitation Seasonality), edaphic factors (Sand Content), and topographic variables (Solar Radiation) are generally key to the geographic distributions of the studied species.

Based on Benschop (1993), temperature is the most important environmental factor controlling the growth and flowering of *crocus* species by affecting enzyme activity in plant metabolism. It is determined that bulb and corm size is a major factor in determining the capacity of bulbous plants to flower as well as efficient reproduction (Le Nard and De Hertog, 1993). In *Crocus*, flower
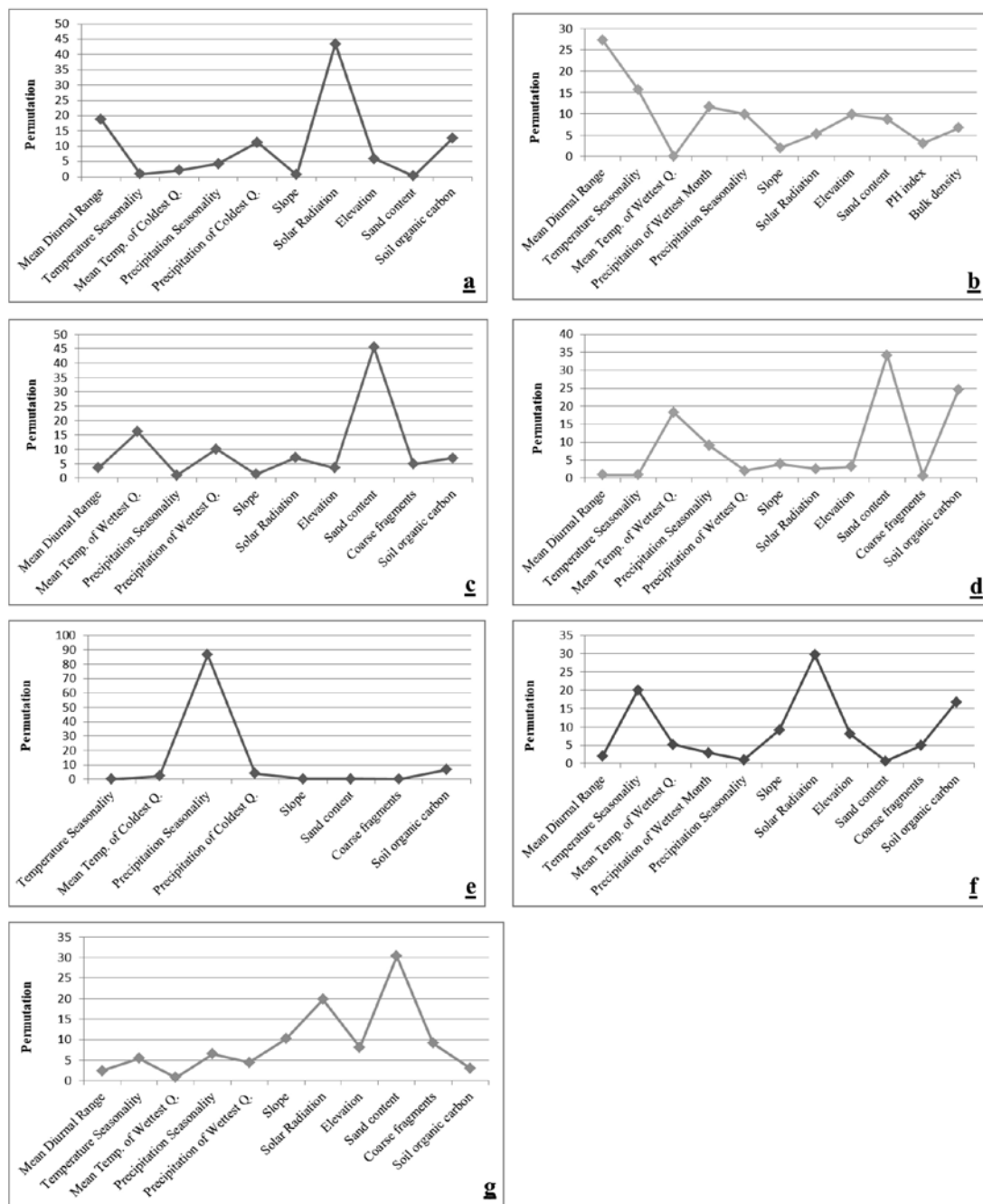

Fig. 2. permutation importance of *C. biflorus* (a), *C. caspius* (b), *C. cancellatus* (c), *C. haussknechtii* (d), *C. michelsonii* (e), *C. speciosus* (f), *C. sativus* (g)
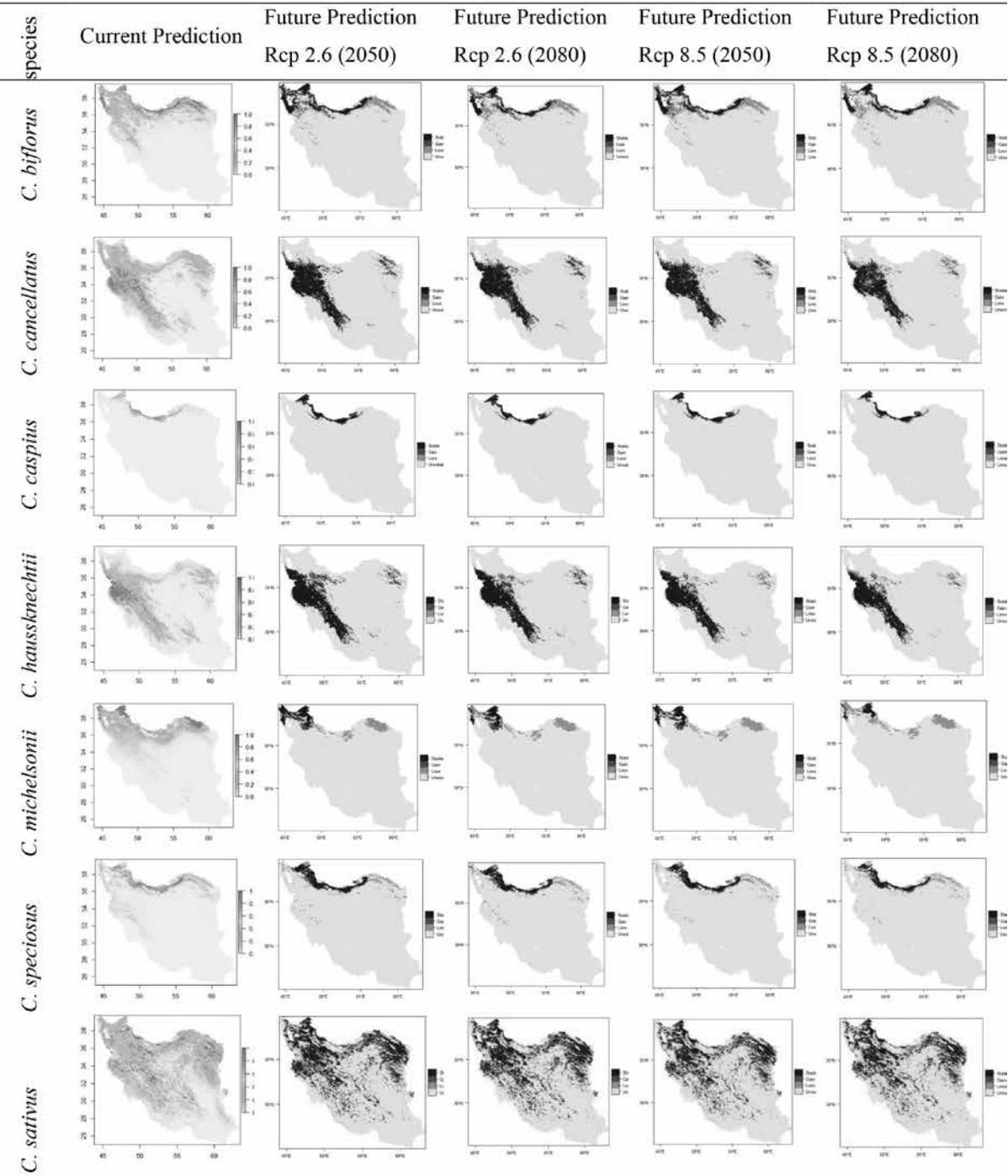
Fig. 3. Prediction of species distribution potential under climate change scenarios RCP2.6 and RCP8.5 2050 and 2080

formation is directly related to corm size (Negbi et al., 1989; De Mastro and Ruta, 1993). The previous studies showed that low growth temperatures have a positive effect on the final biomass of the corms (Badri et al., 2007; Lundmark et al., 2009) and seed germination rate (Bernareggi et al., 2016) in this genus. Therefore, an increase in temperature will damage the reproductive cycle of this taxon. Based on species distribution modeling conducted in Cyprus, *Crocus cyprius* is experiencing a significant decline in its populations as the temperature rises,

particularly evident in the warmest month (Louca et al., 2015). Moreover, the results of Baikov and Doronkin's (2020) study showed that climatic variables that influence the amount of heat in the warmest period of a year (for example, maximum average diurnal temperature of surface air in the warmest period of a year) may be taken into account as factors, limiting the population size of rare species in Iridaceae.

Furthermore, precipitation plays an important role in species richness, distribution patterns, and the diversification of plant spe-

Table 2. Percentage of gain, loss, and range change of studied species (RCP2.6 of 2050 and 2080)

Species	Time – Scenarios (2050 – RCP2.6)			Time – Scenarios (2080 – RCP2.6)		
	Gain	Loss	Range change	Gain	Loss	Range change
C. biflous	15.40	50.68	-35.29	9.45	57.17	-47.72
C. caspius	23.06	28.41	-5.35	26.21	26.98	-0.78
C. canellatus	24.45	8.88	15.57	22.54	9.33	13.20
C. haussknechtii	18.22	5.68	12.53	13.13	6.52	6.61
C. michelsonii	17.13	53.74	-36.61	16.19	66.49	-50.29
C. speciosus	17.85	39.81	-21.96	20.27	39.35	-19.09
C. sativus	41.49	9.43	32.05	47.30	8.77	38.53

Table 3. Percentage of gain, loss, and range change of studied species (RCP8.5 of 2050 and 2080)

Species	Time – Scenario (2050 – RCP8.5)			Time – Scenario (2080 – RCP8.5)		
	Gain	Loss	Range change	Gain	Loss	Range change
C. biflous	13.63	51.38	-37.76	6.32	64.80	-58.48
C. caspius	17.32	32.11	-14.78	13.74	34.85	-21.11
C. canellatus	16.38	14.97	1.41	11.95	29.65	-17.69
C. haussknechtii	6.85	15.26	-8.41	3.79	22.28	-18.49
C. michelsonii	14.20	61.89	-47.68	0.42	82.93	-82.50
C. speciosus	10.91	47.41	-36.50	4.42	59.21	-54.79
C. sativus	30.64	14.57	16.08	28.64	16.80	11.84

cies (Pausas and Austin, 2001; Yan et al., 2015). The potential distribution models of certain plant taxa in Iran, including *Astragalus caragana* Fischer & C. A. Meyer (Ardestani et al., 2015), *Daphne mucronata* Royle (Abolmaali et al., 2018), and *Onosma* L. (Khajoei Nasab et al., 2020), confirmed the importance of this environmental factor. Distribution patterns of studied taxa showing a wide range of average annual rainfall of between 300 mm (Zagros, Kopet Dagh, Central mountains as well as Southern Slopes of Alborz) to 1200 mm (Northern Slopes of Alborz), so precipitation has a great impact on the growth of these taxa in vegetative state (Jafarbeyglou and Mobaraki, 2009).

The results of the present study about the key effects of precipitation and temperature in geographic distributions of the studied species agree with the conclusions of previous studies on the effects of these factors on growth and distribution patterns of *Crocus* species (Benschop, 1993; Jafarbeyglu and Mobaraky, 2008; Louca et al., 2015; Tabasi et al., 2015).

Moreover, the distributions of plant taxa also depend on edaphic factors such as sand content as well as variables derived from topography (e.g., elevation, slope, solar radiation) (Hanson and Churchill, 1962; Guisan and Thuiller, 2005). The results of our study show that sand content plays a crucial role in the geographic distributions of the studied *crocus* species especially concerning the two closely related species, *C. sativus* and *C. haussknchtii* (Sheidai et al., 2018) as well as, *C. cancellatus*. In addition, *Crocus* species grow in a wide spectrum of soil types,

but thrive best in deep soils. Accordingly, shallow soils and rocky texture (e.g., high elevations) are unsuitable for *Crocus* (Negbi, 1999). However, as temperature rises, *Crocus* populations are likely to need to migrate to higher elevations; they will not be able to establish themselves due to the unfavorable soils (e.g., shallow soils and rocky texture) of these areas for their growth. Several studies have emphasized the role of edaphic factors in shaping the spatial patterns of plant taxa in Iran (Mehrabian, 2015; Sayadi and Mehrabian, 2016; Sayadi et al., 2017; Moradi et al., 2019; Khajoei Nasab et al., 2020). The physical and chemical properties of soils (soil pH, calcium carbonate, soil texture, nitrogen, phosphorus, potassium, and organic matter contents of the soils) in the growth place of some *Crocus* species are determined in previous studies (Satıl and Selvi, 2007; Kandemir, 2009; Şık and Candan, 2009; Khattak and Khattak, 2011; Kandemir et al., 2012). Based on these studies, the levels of nitrogen (N), phosphorus (P), potassium (K), and organic matter are elevated in the soils that support the growth of various *Crocus* species.. The role of edaphic factors in geographic distributions of the studied *Crocus* species in the present study, especially about *C. haussknechtii*, is highly influenced by sand content and Soil Organic Carbon, supporting the suggestions of Kandemir et al. (2009, 2012) and Satıl and Selvi (2007) studies about this subject that *Crocus* species (for example, *Crocus* pallasii, synonym *C. haussknechtii*) prefer to grow in soils with rich organic matter contents.

Solar radiation is another key factor that affects the distribution of the studied *Cro-*

cus species. Solar radiation affects vegetation pattern, plant distribution, and growth by influencing near-surface air temperature, soil temperature, and soil moisture within a region (Coblentz and Riitters, 2004; Bennie et al., 2008; Yilmaz et al., 2016). The special importance of solar radiation in the crop production process is determined in several previous studies (Monteith, 1973; Penning de Vries et al., 1989). It is also considered a significant factor in the growth and distribution of *C. sativus* as noted by Kumar et al. (2009). Based on this study, saffron plants show poor growth in shaded conditions, whereas they exhibit the highest under direct sunlight.

The findings of our study revealed that the response of the studied species to environmental changes varies somewhat. Habitat loss occurs when a region that is predicted to be suitable under current climate conditions turns unsuitable as a result of climate change (Randin et al., 2009). Numerous studies have revealed the possibility of decline or loss of currently suitable habitats of certain plant taxa, such as *Thuja korainsis* Nakai. (Wang et al., 2016), *Alsophila denticulate* Baker. (Wang et al., 2016), *Bruguiera gymnorrhiza* (L.) Lam. (Cao et al., 2020) and *Pedicularis longiflora* Rudolph. (Cao et al., 2020) in light of future climate change scenarios. The findings of the present study suggest that the habitats of *C. michelsonii* are experiencing the most significant negative changes due to climate change. The distribution of *C. michelsonii* is limited to the Kopet Dagh. This area is recognized as a top conservation priority in Iran (Mehrabian et al., 2020). Furthermore, given that the

growth of this species is significantly influenced by precipitation levels (Table 1), the potential loss of the appropriate habitat of *C. michlsonii* in Iran due to decreasing rainfall is highly predictable. Other species such as *C. biflorus*, *C. speciosus*, and *C. caspius* are also experiencing negative impact on their current habitats by climate change. The distribution of *C. caspius* is limited to the Hyrcanian region of Iran (Assadi et al., 1999). The lowest belt of the Hyrcanian forests, which serves as a primary habitat for this species, is currently diminishing following an intensification of land use in the area, mainly cattle grazing and cultivation of rice, cotton, and tea (Frey and Probst, 1986). In addition to the Hyrcanian region, *C. biflorus* and *C. speciosus* are also distributed in the Irano-Turanian region (Assadi et al., 1999). Based on Tabasi et al. (2021), the threatened *Crocus* species in Iran are mainly distributed in the Irano-Turanian region. The mountainous ecosystems of Almeh and Western Alborz, which are among the distribution areas for these two species, are considered significant distribution centers of the threatened *Crocus* species in this region. Furthermore, the findings of the current study (Table 1) indicated that temperature factors (Mean Diurnal Range for *C. caspius* and *C. biflorus* and Temperature Seasonality for *C. speciosus*) are critical bioclimatic variables influencing the growth of these species. Consequently, it is anticipated that a reduction in suitable habitats for these species will occur as a result of climate change and global warming, given that lower temperatures positively affect the growth of *Crocus* species (Badri et al., 2007; Lundmark et al., 2009).

On the other hand, numerous studies have revealed the possibility of habitat expansion among certain plant taxa (for example, Capparis spinosa L. (Ashraf et al., 2018), *Ambrosia artemisiifolia* L. (Adhikari et al., 2019), *Ambrosia trifida* L. (Adhikari et al., 2019), *Solanum carolinense* L. (Adhikari et al., 2019), and *Onosma* L. (Khajoei Nasab et al., 2020)) in light of future climate change scenarios. The anticipated expansions of the distribution range of various taxonomic plant groups in Iran are projected under these scenarios (Kafash et al., 2016; Farashi and Erfani, 2018; Kafash et al., 2018; Khajoei Nasab et al., 2020). According to the findings of the present study, the suitable habitat for *C. cancellatus*, *C. Haussknechtii*, and *C. sativus* is expected to increase under the RCP 2.6 scenario. These three species, especially *C. sativus*, benefit from a change in climate under this scenario. However, *C. sativus* is the sole species that benefits from climate changes associated with the RCP 8.5 scenario. Two other mentioned species showed stability or even a slight decrease in distribution under this scenario. Therefore, among the species examined, *C. sativus* is the only species that exhibited a positive range change in both scenarios. *C. sativus* (saffron) is a plant that requires a minimum level of water and nutritional treatment. This species thrives in temperate and dry climates. Consequently, it appears that various areas in Iran, particularly in the North East of Iran, are well-suited for saffron cultivation, as it requires a minimum level of water, resistance to dryness, and at the same time can be of economic significance to the country (Monazzam EsmaeilPour and Kar-

davani, 2011). Due to this subject, the increase in cultivation points of this species in Iran is predictable.

Among the studied species, *C. michelsonii*, whose current habitat in Kopet Dagh is significantly affected by climate change, is the most endangered species in the face of these changes. Consequently, this study prioritizes the conservation of *C. michelsonii*. Additionally, *C. biflorus*, *C. speciosus*, and *C. caspius* which have also revealed a negative shift in their range, are identified as other conservation priorities, respectively. Moreover, *C. michelsonii* and *C. caspius*, both exhibiting a Species Specialization Index (SSI) of less than 0.5, were considered as species of high conservation value in our previous study (Tabasi et al., 2021).

In this study, we employed MaxEnt as a tool to identify conservation priorities for seven *Crocus* species in Iran. The application of this tool appears to predict the potential habitats of these taxa effectively. Based on the findings, *C. michelsonii*, *C. biflorus*, *C. speciosus*, and *C. caspius* are the most threatened species among those studied, as they face a loss or reduction of their currently suitable habitats in the future. Conservation planning to protect these species, especially *C. michelsonii*, which has the possibility of losing its entire habitat in the Northeastern area of Iran (Kopet Dagh) and, as a result, facing extinction in the future, is necessary.

To ensure the effective conservation of plants amidst climate change, it is recommended to regularly monitor them as indicators at various levels: environmental, community, population, and individual. This monitoring aims to detect how ecosystems

are responding to change. Observation can be conducted by investigating the presence, absence, richness, and composition of plants at designed monitoring stations. Moreover, tracking these variations in species over time is crucial. Our previous study established the current distribution pattern of *Crocus* species and determined the primary distribution centers of these taxa in Iran. Additionally, this study predicts the future distribution status of *Crocus* species. This data can assist in planning in situ conservation and guide ex situ conservation methods such as gene banks, field gene banks, and in vitro conservation for protecting this valuable genus and addressing climate change in Iran.

Acknowledgments

References

Abdelaal, T., Michielsen, L., Cats, D., Hoogduin, D., Mei, H., Reinders, M.J.T., and Mahfouz, A., 2019. A comparison of automatic cell identification methods for single-cell RNA sequencing data. *Genome Biology*, 20(1), p.194. DOI: 10.1186/s13059-019-1795-z.

Abolmaali, S.M.R., Tarkesh, M., and Bashari, H., 2018. MaxEnt modeling for predicting suitable habitats and identifying the effects of climate change on a threatened species, Daphne mucronata, in central Iran. *Ecological Informatics*, 43, 16-123. DOI: 10.1016/j. ecoinf.2017.10.002.

Adams, J., 2007. *Vegetation–Climate Interaction*: *How Vegetation Makes the Global Environment*. Springer Berlin Heidelberg, Heidelberg, Berlin.

Adams-Hosking, C., McAlpine, C.A., Rhodes, J.R., Moss, P.T., and Grantham, H.S., 2015. Prioritizing regions to conserve a specialist folivore: considering probability of occurrence, food resources, and climate change. *Conservation Letters*, 8(3), 162-170. DOI: https: 10.1111/conl.12125

Adhikari, P., Jeon, J., Kim, H.W., Shin, M.S., Adhikari, P., and Seo, C., 2019. Potential impact of climate change on plant invasion in the Republic of Korea. *Journal of Ecology and Environment*, 43(4), 352-363. DOI: 10.1186/s41610-019-0134-3

Afshar-Harb, A., 1979. The stratigraphy, tectonics, and petroleum geology of the Kopet-Dagh region, northern Iran. PhD dissertation, 316 p. Imperial College London, London, England.

Akhani, H., 2005. *The Illustrated Flora of Golestan National Park, Iran*, Vol. 1. University of Tehran Press, Tehran.

Alavi, M., 1991. Tectonic map of the Middle East. Geological Survey of Iran, Tehran.

Amedie, F.A., 2013. Impacts of Climate Change on Plant Growth, Ecosystem Services, Biodiversity, and Potential Adaptation Measures. Master's dissertation, University of Gothenburg, Sweden.

Amiri, M.J., and Eslamian, S.S. 2010. Investigation of climate change in Iran. *Journal of Environmental Science and Technology*, 3(4), 208-216. DOI: 10.3923/jest.2010.208.216.

Aragón, P., Rodríguez, M.A., Olalla-

Tárraga, M.A., and Lobo, J.M., 2010. Predicted impact of climate change on threatened terrestrial vertebrates in central Spain highlights differences between endotherms and ectotherms. Animal Conservation, 13(4), 363-373. DOI: 10.1111/j.1469-1795.2009.00343.x.

Ardestani, G.E., Tarkesh, M., Bassiri, M., and Vahabi, M.R. 2015. Potential habitat modeling for reintroduction of three native plant species in central Iran. *Journal of Arid Land*, 7, 381-390. DOI: 10.1007/s40333-014-0050-4.

Ashraf, U., Chaudhry, M.N., Ahmad, S.R., Ashraf, I., Arslan, M., Noor, H., and Jabbar, M., 2018. Impacts of climate change on *Capparis spinosa* L. based on ecological niche modeling. *PeerJ*, 6, e5792. DOI: 10.7717/peerj.5792.

Assadi, M., Khatamsaz, M., Masoumi, A., Mozafarian, V., Babakhanlu, P., and Zehzad, B., 1999. *Flora of Iran (Iridaceae)*, Vol 31. Research Institute of Forests and Rangelands Publication, Tehran (in persian).

Badri, M.A., Minchin, P.E.H., and Lapointe, L., 2007. Effects of temperature on the growth of spring ephemerals: *Crocus vernus* (L.) Hill. *Physiologia Plantarum*, 130, 67-76. DOI: 10.1111/j.1399-3054.2007.00882.x.

Baikov, K., and Doronkin, V., 2020. Towards the conservation of rare species *Iris glaucescens* (Iridaceae) in Novosibirsk oblast: ecoinformative multimodal analysis of the area. International Conferences "Plant Diversity: Status, Trends, Conservation Concept". BIO Web of Conferences, Vol 24. DOI:

10.1051/bioconf/20202400007.

Bellard, C., Bertelsmeier, C., Leadley, P., Thuiller, W., and Courchamp, F., 2012. Impacts of climate change on the future of biodiversity. *Ecology Letters*, 15(4), 365-377. DOI: 10.1111/j.1461-0248.2011.01736.x.

Bennie, J., Huntleya, B., Wiltshirea, A., Hill, M.O., and Baxtera, R., 2008. Slope, aspect, and climate: Spatially explicit and implicit models of topographic microclimate in chalk grassland. *Ecological Modelling*, 216, 47-59. DOI: 10.1016/j.ecolmodel.2008.04.010.

Benschop, M., 1993. *Crocus*, In: De Hertog, A., and Le Nard, M. eds. The *Physiology* of Flower *Bulbs*, Chap 19. Elsevier, Amsterdam, Netherlands.

Bernareggi, G., Carbognani, M., Mondoni, A., and Petraglia, A., 2016. Seed dormancy and germination changes of snowbed species under climate warming: the role of pre- and post-dispersal temperatures, *Annals of Botany*, 118(3), 529-539. DOI: 10.1093/aob/mcw125.

Bleyhl, B., Sipko, T., Trepet, S., Bragina, E., Leitão, P.J., Radeloff, V.C., and Kuemmerle, T., 2015. Mapping seasonal European bison habitat in the Caucasus Mountains to identify potential reintroduction sites. *Biological Conservation*, 191, 83-92. DOI: 10.1016/j.biocon.2015.06.011.

Bosso, L., Rebelo, H., Garonna, A.P., and Russo, D., 2013. Modelling geographic distribution and detecting conservation gaps in Italy for the threatened beetle Rosalia alpina. *Journal of Nature Conservation*, 21(2), 72-80. DOI:

10.1016/j.jnc.2012.10.003.

Buryakovsky, L.A., Chilinger, G.V., and Aminzadeh, F., 2001. *Petroleum geology of the South Caspian Basin*. Gulf Professional Publishing, USA, 442 pp.

Cao, B., Bai, C., Xue, Y., Yang, J., Gao, P., Liang, H., Zhang, L., Che, L., Wang, J., Xu, J., and Duan, C., 2020. Wetlands rise and fall: six endangered wetland species showed different patterns of habitat shift under future climate change. *Science of the Total Environment*, 731, 138518. DOI: 10.1016/j.scitotenv.2020.138518.

Coblentz, D., and Riitters, K.H., 2004. Topographic controls on the regional-scale biodiversity of the south-western USA. *Journal of Biogeography*, 31, 1125-1138. DOI: 10.1111/j.1365-2699.2004.00981.x.

Cucchi, F., and Zini, L., 2003. Gypsum karst of Zagros mountains (I.R. Iran). *Acta carsologica*, 32(1), 69-82. DOI: 10.3986/ac.v32i1.365.

De Mastro, G., and Ruta, C., 1993. Relation between corm size and saffron (*Crocus sativus* L.) flowering. *Acta Horticulturae*, 344, 512-517. DOI: 10.17660/ActaHortic.1993.344.58

Elith, J., Graham, C., Anderson, R., Dudík, M., Ferrier, S., Guisan, A., J. Hijmans, R., Huettmann, F., R. Leathwick, J., Lehmann, A., and Li, J., 2006. Novel methods improve prediction of species' distributions from occurrence data. *Ecography*, 29(2), 129-151. DOI: 10.1111/j.2006.0906-7590.04596.x.

Elith, J., and Leathwick, J.R., 2007. Predicting species distributions from museum and herbarium records using multiresponse models fitted with multivariate adaptive regression splines. Diversity and Distributions, 13(3), 165-175. DOI: 10.1111/j.1472-4642.2007.00340.x.

Elith, J., and Leathwick, J.R., 2009. Species distribution models: ecological explanation and prediction across space and time. *Annual Review of Ecology, Evolution, and Systematics*, 40, 677-697. DOI: 10.1146/annurev.ecolsys.110308.120159.

Elith, J., Kearney, M., and Phillips, S., 2010. The art of modelling range-shifting species. *Methods in Ecology and Evolution*, 1(4), 330-342. DOI: 10.1111/j.2041-210X.2010.00036.x.

Farashi, A., and Erfani, M., 2018. Modeling of habitat suitability of Asiatic black bear (Ursus thibetanus gedrosianus) in Iran in future. *Acta Ecologica Sinica*, 38(1), 9-14. DOI: 10.1016/j.chnaes.2017.07.003.

Fischer, R.A., 1968. Stomatal opening: role of potassium uptake by guard cells. *Science* 160(3829): 784-785. DOI: 10.1126/science.160.3829.784.

Fisher, W.B., 1968. The land of Iran. In: Fisher, W.B., eds. *Cambridge history of Iran*. Cambridge University Press, Cambridge, U. K.

Flores-Tolentino, M., Ortiz, E., and Villaseñor, J. L., 2019. Ecological niche models as a tool for estimating the distribution of plant communities. *Revista mexicana de biodiversidad,* 90. DOI: 10.22201/ib.20078706e.2019.90.2829.

Fois, M., Cuena-Lombraña, A., Fenu, G., and Bacchetta, G., 2018. Using species distribution models at local scale to guide

the search of poorly known species: Review, methodological issues and future directions. *Ecological Modelling*, 385, 124-132. DOI: 10.1016/j. ecolmodel.2018.07.018.

Frey, W., and Probst, W., 1986. A synopsis of the vegetation in Iran. Contributions to the vegetation of southwest Asia. In: Kürschner, H. eds. *Contributions to the Vegetation of Southwest Asia*. Ludwig Riechert, Wiesbaden, Germany.

Ghorbani, R., and Koocheki, A.R., 2017. Sustainable Cultivation of Saffron in Iran. In: Litchfouse, E. eds. *Sustainable agriculture reviews*. Springer, Cham, Germany.

Graham, C.H., Ferrier, S., Huettman, F., Moritz, C., and Peterson, A.T., 2004. New developments in museum-based informatics and applications in biodiversity analysis. *Trends in Ecology & Evolution*, 19(9), 497-503. DOI: 10.1016/j.tree.2004.07.006.

Groves, C.R., Jensen, D.B., Valutis, L.L., Redford, K.H., Shaffer, M.L., Scott, J.M., Baumgartner, J.V., Higgins, J.V., Beck, M.W., and Anderson, M.G., 2002. Planning for biodiversity conservation: Putting conservation science into Practice. *Bioscience*, 52(6), 499-512. DOI: 10.1641/0006-3568(2002)052[0499:PF-BCPC]2.0.CO;2.

Guillera-Arroita, G., Lahoz-Monfort, J.J., Elith, J., Gordon, A., Kujala, H., Lentini, P.E., McCarthy, M.A., Tingley, R., and Wintle, B.A., 2015. Is my species distribution model fit for purpose? Matching data and models to applications. *Global Ecology and Biogeography*, 24(3), 276-292. DOI: 10.1111/ geb, 12268.

Guisan, A., and Thuiller, W., 2005. Predicting species distribution: Offering more than simple habitat models. *Ecology Letters*, 8(9), 993-1009. DOI: 10.1111/j.1461-0248.2005.00792.x.

Guisan, A., Tingley, R., Baumgartner, J.B., Naujokaitis-Lewis, I., Sutcliffe, P.R., Tulloch, A.I., Regan, T.J., Brotons, L., McDonald-Madde, E., Mantyka-Pringle, C., and Martin, T.G., 2013. Predicting species distributions for conservation decisions. *Ecology Letters*, 16(12), 1424-1435. DOI:10.1111/ele.12189.

Hanson, H.C., and Churchill, E.D., 1962. *The Plant Community*. Reinhold Publishing Corp, New York, pp 1-218.

Hijmans, R.J., Phillips, S., Leathwick, J., Elith, J., and Hijmans, M.R.J., 2017. Package 'dismo'. *Circles*, 9(1), 1-68.

Homke, S., Verges, J., Emami, H., and Karpuz, R., 2004. Magnetostratigraphy of Miocene–Pliocene Zagros foreland deposits in the front of the Push–e Kush Arc (Lurestan Province, Iran). *Earth and Planetary Science Letters*, 225(3-4), 397-410. DOI: 10.1016/j.epsl.2004.07.002.

Hopkins, J., and Maxtend, N., 2011. *Crop Wild Relatives: Plant conservation for food security*. Natural England Publications, U.K, 58pp.

Jafarbeyglou, M., and Mobaraki, Z. 2009. land suitability evaluation of Qazvin province for saffron cultivation based on Multi-Criteria decision making approach. *Physical Geography Research*, 66, 101-119. (In Persian with English Summary).

Jarvis, A., Lane, A., and Hijmans, R., 2008.

The effect of climate change on crop wild relatives. *Agriculture, Ecosystems and Environment,* 126, 13-23. DOI: 10.1016/j.agee.2008.01.013.

Jarvis, A., Upadhyaya, H., Gowda, C., Agrawal, P., Fujisaka, S., and Anderson, B., 2008. Climate change and its effect on conservation and use of plant genetic resources for food and agriculture and associated biodiversity for food security. Monograph, Food and Agriculture Organization of the United Nations, UK.

Kafash, A., Kaboli, M, Köhler., Yousefi, M., and Asadi, A., 2016. Ensemble distribution modeling of the Mesopotamian spiny-tailed lizard (Saara loricata) in Iran: an insight into the impact of climate change. *Turkish of Journal Zoology*, 40(2), 262-271. DOI: 10.3906/zoo-1504-10.

Kafash, A., Ashrafi, S., Ohler, A., Yousefi, M., Malakoutikhah, S., Koehler, G., and Schmidt, B.R., 2018. Climate change produces winners and losers: differential responses of amphibians in mountain forests of the Near East. *Global Ecology and Conservation*, 16, e00471. DOI: 10.1016/j.gecco.2018.e00471.

Kandemir, N., 2009. morphology, anatomy and ecology of critically endangered endemic *Crocus pestalozzae* Boiss. (Iridaceae) in North-West Turkey. *Bangladesh Journal of Botany*, 38(2), 127-132. DOI: 10.3329/bjb.v38i2.5136.

Kandemir, N., Çelik, A., and Yayla, F., 2012. Comparative anatomic and ecologic investigations on some endemic *Crocus* taxa (Iridaceae) in Turkey. *Pakistan Journal of Botany,* 44(3), 1065-1074.

Khajoei Nasab, F., Mehrabian, A., and Mostafavi, H., 2020. Mapping the current and future distributions of *Onosma species* endemic to Iran. *Journal of Arid Land*, 12, 1031-1045. DOI: 10.1007/s40333-020-0080-z.

Khanum, R., Mumtaz, A.S., and Kumar, S., 2013. Predicting impacts of climate change on medicinal asclepiads of Pakistan using MaxEnt modeling. A*cta Oecologica*, 49, 23-31. DOI: 10.1016/j.actao.2013.02.007.

Khattak, I.M., and Khattak, M.I., 2011. Study of heavy trace metals in some medicinal-herbal plants of *Pakistan. Pakistan Journal of Botany*, 43, 2003-2009.

Koocheki, A., 2004. Indigenous knowledge in agriculture with particular reference to saffron production in Iran. *Acta Horticulturae*, 650, 175-182. DOI: 10.17660/ActaHortic.2004.650.17

Krinsley, D.B., 1970. A *geomorphological and paleoclimatological study of the playas of Iran*. U.S. Geological Survey. U.S. Government Printing Office, contract. PROCP 700–800. Air Force Cambridge Research, U.S, 329 pp.

Kujala, H., Moilanen, A., Araujo, M.B., and Cabeza, M., 2013. Conservation planning with uncertain climate change projections. *PLoS One* 8(2), e5331. DOI: 10.1371/journal.pone.0053315

Kumar, R., Singh, V., Devi, K., Sharma, M., Singh, M.K., and Ahuja, P.S., 2009. State of art of saffron (*Crocus sativus* L.). Agronomy: a comprehensive review. *Food Reviews International*, 25, 44-85. DOI: 10.1080/87559120802458503

Legault, A., Theuerkauf, J., Chartendrault,

V., Rouys, S., Saoumoé, M., Verfaille, L., Desmoulins, F., Barré, N., and Gula, R., 2013. Using ecological niche models to infer the distribution and population size of parakeets in New Caledonia. *Biological Conservation*, 167, 149-160. DOI: 10.1016/j.biocon.2013.07.041.

Le Nard, M., and De Hertog, A., 1993. Bulb growth and development and flowering. In: De Hertog, A., and Le Nard, M. eds. *The Physiology of Flower Bulbs*, Chapt 4. Elsevier, Amsterdam, pp. 29-43.

Lobo, J.M., Jiménez-Valverde, A., and Real, R., 2008. AUC: a misleading measure of the performance of predictive distribution models. *Global Ecology and Biogeography*, 17(2), 145-151. DOI: 10.1111/j.1466-8238.2007.00358.x.

Louca, M., Vojiatakis, I.N., and Moustakas, A., 2015. Modelling the combined effects of land use and climatic changes: coupling bioclimatic modelling with Markov-chain cellular automata in a case study in Cyprus. *Ecological Informatics*, 30, 241-249. DOI: 10.1016/j.ecoinf.2015.05.008

Lundmark, M., Hurry, V., and Lapointe, L., 2009. Low temperature maximizes the growth of *Crocus vernus* (L.) Hill via changes in carbon partitioning and corm development. *Journal of Experimental Botany*, 60(7), 2203-2213. DOI: 10.1093/jxb/erp103.

Luo, Z., Jiang, Z., and Tang, S., 2015. Impacts of climate change on distributions and diversity of ungulates on the Tibetan Plateau. *Ecological Applications,* 25(1), 24-38. DOI: 10.1890/13-1499.1

Margules, C.R., and Pressey, R.L., 2000. Systematic conservation planning. Nature, 405, 243-253.

Mathur, M., Mathur, P., and Purohit, H., 2023. Ecological niche modelling of a critically endangered species, *Commiphora wightii* (Arn.) Bhandari uses bioclimatic and non-bioclimatic *variables. Ecological Processes*, 12(1), 8. DOI: 10.1186/s13717-023-00423-2.

Maxtend, N., Ford-Lloydm, B.V., and Hawkes, J.G., 1997. *Plant genetic conservation: the in situ approach*. Chapman & Hall, London.

McCall, G.J.H., 1997. The geotectonic history of the Makran and adjacent areas of southern Iran. *Journal of Asian Earth Sciences*,15(6), 517-531. DOI: 10.1016/S0743-9547(97)00032-9

Mehrabian, A.R., 2015. Distribution patterns and diversity of *Onosma* in Iran: with emphasis on endemism conservation and distribution pattern in SW Asia. *Rostaniha*, 16(1), 36-60. (in Persian). DOI: 10.22092/botany.2015.101996.

Mehrabian, A.R., Amini Rad, M., and Pahlevani, A.H., 2015. The map of distribution patterns of Iranian endemic monocotyledons. Shahid Beheshti University, Tehran.

Mehrabian, A.R., Khajoei Nasab, F., and Amini Rad, M., 2020. Distribution patterns and priorities for conservation of Iranian Endemic Monocots: determining the Areas of Endemism(AOEs). *Journal of Wildlife and Biodiversity*, 5(2), 69-87. DOI: 10.22120/jwb.2020.136616.1188.

Memmott, J., Craze, P.G., Waser, N.M., and Price, M.V., 2007. Global warming and the disruption of plant–pollinator interactions. *Ecology Letters*, 10,

710-717. DOI: 10.1111/j.1461-0248.2007.01061.x.

Monazzam EsmaeilPour, A., and Kardavani, P., 2011. Saffron (*Crocus sativus*) potentials for sustainable rural development: A case study of Balavelayat village in Kashmar, North Eastern Iran. *African Journal of Agricultural Research*, 6(13), 3149-3160. DOI: 10.5897/AJAR11.212.

Monteith, J.L., 1973. *Principles of Environmental Physics*. Edward Arnold, London, UK, 281 pp.

Moradi, Z.H., Mehrabian, A.R., Naghizadeh, S., Mostafavi, H., and Khajoi Nasab, F., 2019. Distribution patterns, diversity, and conservation priorities of *Onosma* L. (Boraginaceae Juss.) in some sections of the northwestern geomorphologic unit of Iran. *Environmental Sciences*,17(1),73-94. (In Persian). DOI: 10.29252/ENVS.17.1.73.

Moustakas, A., and Evans, M.R., 2013. Integrating Evolution into Ecological Modelling: Accommodating Phenotypic Changes in Agent Based Models. *PloS ONE*, 8, e71125. DOI: 10.1371/journal.pone.0071125.

Muths, E., Chambert, T., Schmidt, B.R., Miller, D.A.W., Hossack, B.R., Joly, P., Grolet, O., Green, D.M., Pilliod, D.S., Cheylan, M., and Fisher, R.N., 2017. Heterogeneous responses of temperate-zone amphibian populations to climate change complicate conservation planning. *Scientific Reports*, 7(1), 17102. DOI: 10.1038/s41598-017-17105-7.

Negbi, M., Dagan, B., Dror, A., and Basker, D., 1989. Growth, flowering, vegetative reproduction, and dormancy in the saffron crocus (*Crocus sativus* L.). Journal of Botany, 38, 95-113.

Negbi, M., 1999. *Saffron: Crocus sativus* L. Harwood Academic, Amsterdam, 154 pp.

Pausas, J.G., and Austin, M.P., 2001. Patterns of plant species richness in relation to different environments: An appraisal. J*ournal of Vegetation Science*, 12(2), 153-166. DOI: 10.2307/3236601

Penning de Vries, F.W.T., Jansen, D.M., ten Berge, H.F.M., and Bakema, A., 1989. *Simulation of ecophysiological processes of growth in several annual crops*. IRRI, Los Baños, and Pudoc, Wageningen.

Peterson, A.T., and Soberón, J., 2012. Species distribution modeling and ecological niche modeling: Getting the concepts right. *Nature Conservation*, 10(2), 102-107. DOI: 10.4322/natcon.2012.019.

Phillips, K.W., Northcraft, G.B., and Neale, M.A., 2006. Surface-level diversity and decision-making in groups: When does deep-level similarity help?. *Group Processes & Intergroup Relations*, 9(4), 467-482. DOI: 10.1177/1368430206067557.

Phillips, S.J., Dudík, M., Elith, J., Graham, C.H., Lehmann, A., Leathwick, J., and Ferrier, S., 2009. Sample selection bias and presence-only distribution models: implications for background and pseudo-absence data. *Ecological Applications*, 19(1), 181-197. DOI: 10.1890/07-2153.1.

Randin, C.F., Engler, R., Normand, S., Zappa, M., Zimmermann, N.E., Pearman, P.B., Vittoz, P., Thuiller, W., and Guisan, A., 2009. Climate change and plant distribution: local models predict

high-elevation persistence. *Global Change Biology*, 15, 1557-1569. DOI: 10.1111/j.1365-2486.2008.01766.x.

R Core Team., 2018. R: A Language and Environment for Statistical Computing. R Foundation for Statistical Computing, Vienna, Austria. [2019-05-21]. http://www.R-project.org/.

Reshinger, K.H., 1975. *Flora Iranica*. Vol. 112. Academische Drucku, Verlagasantalt, Graz – Austria.

Rödder, D., and Weinsheimer, F., 2009. Will future anthropogenic climate change increase the potential distribution of the alien invasive Cuban treefrog (Anura: Hylidae)?. J*ournal of Natural History*, 43(19-20), 1207-1217. DOI: 10.1080/00222930902783752.

Rosenzweig, C., Casassa, G., Karoly, D.J., Imeson, A., Liu, C., Menzel, A., Rawlins, S., Root, T.L., Seguin, B., and Tryjanowski, P., 2007. Assessment of observed changes and responses in natural and managed systems. In: Parry, M.L., Canziani, O.F., Palutikof, J.P., et al. eds. *Climate Change 2007: Impacts, Adaptation and Vulnerability Contribution of Working Group II to the Fourth Assessment Report of the Intergovernmental Panel on Climate Change*. Cambridge University Press, Cambridge, UK, pp. 79-131.

Rubidge, E.M., Monahan, W.B., Parra, J.L., Cameron, S.E., and Brashares, J.S., 2011. The role of climate, habitat, and species co-occurrence as drivers of change in small mammal distributions over the past century. *Global Change Biology*, 17(2), 696-708. DOI: 10.1111/j.1365-2486.2010.02297.x

Satıl, F., and Selvi, S., 2007. An anatomical and ecological study of some Crocus L. taxa (Iridaceae) from the western part of Turkey. *Acta Botanica Croatica*, 66, 25-33.

Sayadi, S., and Mehrabian, A., 2016. Diversity and distribution patterns of Solanaceae in Iran: Implications for conservation and habitat management with emphasis on endemism and diversity in SW Asia. *Rostaniha* 17(2), 136-160. DOI: 10.22092/botany.2017.109408.

Sayadi, S., Mehrabian, A.R., and Nikjoyan, M.J., 2017. Some notes on taxonomy and diversity of *Onosma* with emphasis on important evidence and complex groups in Flora Iranica. *Rostaniha* 18(1), 50-58. DOI: 10.22092/botany.2017.113233.

Sen, S., Gode, A., Ramanujam, S., Ravikanth, G., and Aravind, N.A., 2016. Modeling the impact of climate change on wild *Piper nigrum* (Black Pepper) in Western Ghats, India using ecological niche models. *Journal of Plant Research*, 129(6), 1033-1040. DOI: 10.1007/s10265-016-0859-3.

Shakoor, A., Roshan, G.R, and Najafi Kani, A.A., 2010. Evaluating climatic potential for palm cultivation in Iran with emphasis on degree–day index. *African Journal of Agricultural Research*, 5, 1616-1626. DOI: 10.5897/AJAR09.081.

Sheidai, M., Tabasi, M., Mehabian, A.R., Koohdar, F., Ghasemzadeh-Baraki, S., and Noormohammadi, Z., 2018. Species delimitation and relationship in *Crocus* L. (Iridaceae). Acta *Botanica Croatica*, 77(1), 10-17. DOI: 10.1515/

botcro-2017-0015.

Şık, L., and Candan, F., 2009. Ecological properties of some *Crocus* taxa in Turkey. *African Journal of Biotechnology*, 8, 1895-1899.

Soberón, J., and Peterson, A.T., 2005. Interpretation of models of fundamental ecological niches and species' distributional areas. *Biodiversity Information*, 2, 1-10. DOI: 10.17161/bi.v2i0.4

Stöcklin, J., 1974. *Northern Iran: Alborz Mountains*. Geological Society, London, Special Publications, 4(1), 213-234.

Tabasi, M., Sheidai, M., Mehrabiam, A.R., and Noormohammadi, Z., 2015. population assessment of some *Crocus* species in Iran based on morphological and habitat characteristics. 2nd National confrance on climate change and engineering sustainable agriculture and natural resourses, Shahid Beheshti university, Tehran.

Tabasi, M., Mehrabian, A., and Sayadi, S., 2021. Distribution patterns and conservation status of *Crocus species* in Iran, one of the diversity centers of *Crocus* in the Middle East. *Folia Oecologica*, 48(2), 156–168. DOI: 10.2478/foecol-2021-0016.

Tammaro, F., 1987. Notiziestorico-colturalisullo zafferano (*Crocus* sativus L., Iridaceae) nell'area mediterranea. *Micol Veget Medit*, 2, 44-59.

Ulrey, C., Quintana-Ascencio, P.F., Kauffman, G., Smith, A.B., and Menges, E.S., 2016. Life at the top: Long-term demography, microclimatic refugia, and responses to climate change for a high-elevation southern Appalachian endemic plant. *Biological Conservation*, 200, 80-92. DOI: 10.1016/j.biocon.2016.05.028.

Valavi, R., Shafizadeh-Moghadam, H., Matkan, A.A., Mirbagheri, B., and Kia, H., 2018. Modelling climate change effects on Zagros forests in Iran using individual and ensemble forecasting approaches. *Theoretical and Applied Climatology*, 137, 1015-1025. DOI:10.1007/s00704-018-2625-z.

Valavi, R., Elith, J., Lahoz-Monfort, J.J., and Guillera-Arroita, G., 2019. block CV: An r package for generating spatially or environmentally separated folds for k-fold cross-validation of species distribution models. *Methods in Ecology and Evolution*, 10(2), 225-232. DOI: 10.1101/357798.

Vasconcelos, R., Santos, X., and Carretero, M.A., 2012. High temperatures constrain microhabitat selection and activity patterns of the insular Cape Verde wall gecko. *Journal of Arid Environments*, 81, 18-25. DOI: 10.1016/j.jaridenv.2012.01.013.

Vavilov, N.I., 1951. The origin, variation, immunity and breeding of cultivated plants. *Chester Chron Botany*, 13, 1-366.

Waheed, M., Arshad, F., Sadia, S., Fonge, B. A., Al-Andal, A., Jabeen, A., and Dilshad, S., 2025. From Ecological Niche to Conservation Planning: Climate-Driven Range Dynamics of Ephedra intermedia in Central Asia. *Ecology and Evolution*, 15(3), e71127. DOI: 10.1002/ece3.71127.

Wang, C., Liu, C., Wan, J., and Zhang, Z., 2016. Climate change may threaten

habitat suitability of threatened plant species within Chinese nature reserves. *PeerJ*, 2091, 1-20. DOI: 10.7717/peerj.2091.

Warren, R., VanDerWal, J., Price, J., Welbergen, J.A., Atkinson, I., Ramirez-Villegas, J., Osborn, T.J., Jarvis, A., Shoo, L.P., Williams, S.E., and Lowe, J., 2013. Quantifying the benefit of early climate change mitigation in avoiding biodiversity loss. *Nature Climate Change*, 3(7), 678-682. DOI: 10.1038/NCLIMATE1887.

Yan, H., Liang, C., Li, Z., Liu, Z., Miao, B., He, C., and Sheng, L., 2015. Impact of precipitation patterns on biomass and species richness of annuals in a dry steppe. *PLoS ONE*, 10(4), e0125300. DOI: 10.1371/ journal.pone.0125300.

Yi, C., An, S.M., Kim, K., Kwon, H.G., and Min, J.S., 2016. Surface micro-climate analysis based on urban morphological characteristics: Temperature deviation estimation and evaluation. *Atmosphere*, 26(3), 445-459. DOI:10.14191/Atmos.2016.26.3.445.

Yilmaz, H., Yilmaz, O.Y., Akyüz., and Y.F., 2017. Determining the factors affecting the distribution of Muscari latifolium, an endemic plant of Turkey, and a mapping species distribution model. *Ecology and Evolution*, 7, 1112-1124. DOI: 10.1002/ece3.2766.

Yousefi, M., Jouladeh-Rodbar, A., and Kafash, A., 2020. Using endemic freshwater fishes as proxies of their ecosystems to identify high priority rivers for conservation under climate change. *Ecological Indicators*, 112, 106137. DOI: 10.1016/j.ecolind.2020.106137.

Synergistic Effects of Thyme Essential Oil and Thyme Honey on Biofilm Formation by *Candida albicans*

Running title: Synergistic Effects of Thyme Oil and Honey on Candida Biofilms

Ahmad Abdullah Ismail [1], Shahrzad Asgari [1], Parastoo Saniee [1*] , Ahmadreza Mehrabian [2]

Abstract

Candida albicans is a major pathogenic yeast responsible for numerous systemic infections. Its ability to form biofilms significantly complicates treatment, leading to high rates of treatment failure and mortality. This study investigates the synergistic effects of thyme essential oil and thyme monofloral honey on *Candida albicans* biofilm formation, exploring them as a potential natural therapeutic strategy. The inhibition of biofilm formation was assessed using a crystal violet microtiter plate assay. Various concentrations of thyme monofloral honey (100%, 75%, 50%, and 25% v/v) and thyme essential oil were tested both individually and in combination. A clinical isolate of *Candida albicans* served as the target organism for the study. The effectiveness of the treatments in inhibiting biofilm formation was measured, and fluorescent microscopy was employed to visualize the effects on yeast cell density and morphology. The results indicated a significant synergistic effect of combining thyme essential oil and honey, achieving the highest inhibition rate of 59% at the 75% concentration of honey and thyme essential oil, compared to individual treatment rates of 28% for thyme essential oil and 31% for honey alone. Microscopy imaging revealed a marked reduction in the density of *Candida albicans* cells and changes in cell morphology in treated samples, highlighting the effectiveness of the combined treatment in inhibiting biofilm formation.

The combined action of thyme essential oil's antimicrobial properties and the bioactive compounds found in thyme honey suggests a promising strategy for overcoming *Candida albicans* biofilm-associated infections. These findings support the exploration of natural antimicrobials as alternatives to synthetic antifungal agents, particularly in an era of rising antifungal resistance. Further research, including *in vivo* studies, is necessary to validate the clinical efficacy of these natural products against multidrug-resistant pathogens.

Keywords: *Candida albicans*, Honey, Thyme Essential Oil, Anti-biofilm, Synergistic Effect

1-Department of Microbiology and Microbial Biotechnology, Faculty of Life Sciences and Biotechnology, Shahid Beheshti University, Tehran, Iran
2-Department of Plant Sciences and Biotechnology, Faculty of Life Sciences and Biotechnology, Shahid Beheshti University, Tehran, Iran
*Corresponding author email address: p_saniee@sbu.ac.ir

Introduction

Recent estimates indicate that Earth is home to approximately 8.7 million eukaryotic species, with fungi comprising about 7% of this total, which translates to around 611,000 species (Mora et al., 2011). Among these fungi, approximately 600 species are recognized as human pathogens (Brown et al., 2012). This relatively small group includes fungi responsible for mild skin infections, such as Dermatophytes and *Malassezia* species, as well as certain fungi that pose significant risks of life-threatening systemic infections, including notable pathogens like *Aspergillus fumigatus*, *Cryptococcus neoformans*, *Histoplasma capsulatum*, and *Candida albicans* (Köhler et al., 2017).

Candida species are particularly concerning, ranking as the fourth most common cause of hospital-acquired systemic infections in the United States, with an alarming mortality rate that can reach up to 50% (Pfaller and Diekema, 2007). These pathogens are prevalent and can affect skin and mucosal surfaces, and even progress to systemic infections. They are implicated in around 400,000 cases of systemic fungal diseases (Mukaremera et al., 2017). Among the various species, *Candida albicans* is the most common cause of mucosal and systemic infections, accounting for approximately 70% of fungal infections worldwide (Morad et al., 2018). This fungus has been a major contributor to life-threatening invasive infections over the past several decades, and despite available treatments, the mortality rate remains close to 40%, particularly in hospital settings (Enoch et al., 2017).

C. albicans commonly inhabit the human body, especially in the gastrointestinal tract, typically without causing any harm. However, under certain conditions, it can shift to a pathogenic form and lead to infections (Köhler et al., 2017). One of the most significant challenges in treating *C. albicans* infections is its ability to form biofilms (Tsui et al., 2016). Biofilms are complex communities of microorganisms that adhere to surfaces such as medical devices, tissues, or mucosal membranes and are enveloped by a protective matrix of extracellular substances (Blankenship and Mitchell, 2006). This biofilm formation makes *C. albicans* particularly resistant to conventional antifungal treatments, complicating efforts to fully eradicate the infection. Consequently, the presence of *C. albicans* biofilms is often associated with persistent and recurring infections, further complicating treatment strategies (Nobile and Johnson, 2015).

Traditional antifungal therapies frequently struggle to completely eradicate *C. albicans* infections due to the protective characteristics of *Candida* biofilms. The biofilm matrix serves as a barrier, hindering antifungal agents from effectively reaching the underlying fungal cells (Mathé and Van Dijck, 2013). This resistance often results in recurrent infections, necessitating prolonged treatment (Atriwal et al., 2021). Moreover, extended use of antifungal medications can lead to adverse side effects and the emergence of drug-resistant strains of *C. albicans*. It exhibits significant antifungal resistance, particularly to azoles, through mechanisms such as overexpression of membrane transporters. Resistance to other

antifungal classes, including polyenes and echinocandins, has also been observed due to genomic changes and enzyme inactivation, complicating treatment strategies for infections. (Bhattacharya et al., 2020). As a result, there is an urgent need for alternative approaches that can disrupt biofilms and improve the efficacy of antifungal treatments. Recent studies have emphasized a growing interest in natural substances with antifungal properties. More than 300 herbal species are recognized for their pesticidal properties, with numerous specifically demonstrating antifungal efficacies. These natural products have been utilized in clinical practice for centuries, often providing an alternative or complementary approach to conventional antifungal treatments (Liu et al., 2011). The historical use of these herbs, combined with emerging scientific evidence supporting their effectiveness, underscores their potential to enhance treatment strategies against infections caused by *C. albicans* and other fungi (Tseung and Zhao, 2016).

Essential oils (EOs) are secondary metabolites produced by plants, existing in the aromatic and volatile liquids found in various plant parts. Many EOs exhibit antimicrobial properties which are believed to be associated with their phenolic compounds (Nazzaro et al., 2013). Thyme (*Thymus vulgaris*) EO is celebrated for its antimicrobial, antioxidant, and anti-inflammatory properties (Kowalczyk et al., 2020). It contains several bioactive compounds, particularly thymol and carvacrol, which are types of monoterpene phenols. These compounds have demonstrated potential antifungal properties against *C. albicans*.

(Alshaikh and Perveen, 2021). Not only do these compounds inhibit the growth of *C. albicans*, but research showed that they also disrupt its biofilm matrix, making thyme effective against biofilm-related infections (Alves et al., 2019). By targeting the fungal cell wall, thymol and carvacrol induce membrane damage, ultimately leading to cell death, which addresses the persistent challenges posed by biofilms in clinical settings (Shariati et al., 2022).

Honey, a natural product produced by *Apis mellifera* bees from the nectar of flowers or from the secretions of plant-sucking insects, is another significant source of bioactive compounds originating from plants (Pattamayutanon et al., 2015). This sweet substance is not only valued for its flavor but also for its rich nutritional profile, comprising numerous vitamins and bioactive compounds. Throughout history, honey has been utilized as a medicinal remedy, prescribed by physicians for a wide array of human health issues (Boukraâ, 2023). One type of honey, known as monofloral honey, is derived when bees predominantly gather nectar from a single type of flower. Certain monofloral honeys have gained recognition as medical-grade honey (MGH). MGH is characterized by its high sugar content, low water activity, acidic pH, and significant bioactive compounds such as hydrogen peroxide, methylglyoxal, and bee-derived peptides (Holubová et al., 2023). These qualities create an unfavorable environment for the growth and survival of various microorganisms, including pathogenic fungi (Mandal and Mandal, 2011). Honey exhibits diverse antimicrobial

properties that can effectively kill or inhibit the growth of a range of microorganisms, including multidrug-resistant pathogens (Mandal and Mandal, 2011). Since the foundational study by Molan in 1992, which highlighted honey's antimicrobial activity (Molan, 1992), extensive research has been conducted to explore the efficacy of honey from differing geographical and botanical origins, its chemical composition, and its therapeutic potential.

Research has indicated that darker honeys, such as thyme honey, are particularly rich in antioxidant compounds, including phenolic compounds and flavonoids, which underpin their powerful antioxidant and antibacterial properties (Alissandrakis et al., 2007, Karabagias et al., 2016). Thyme honey is not only nutritious but also beneficial for various health issues. It contains vitamins B, A, and E, which contribute to the health of the brain and nervous system, alleviate intestinal discomfort, relieve coughs and sore throats, combat joint pain, and reduce menstrual pain. Additionally, thyme honey has been noted for its positive effects on conditions such as epilepsy, convulsions, headaches, and migraines (Alissandrakis et al., 2007). It is also one of the few honey types used in managing diabetes (Lafraxo et al., 2021).

Considering the individual health benefits and bioactive properties of EOs and honey, there has been considerable interest in studying extracts from various plants that are high in phenolic compounds when used alongside honey (Nagy-Radványi et al., 2024). Studies suggest that these two substances may work together synergistically. Additionally,

combining EOs, which are typically made up of inedible and poorly soluble components, with honey may enhance the solubility of the EOs and improve their absorption in the digestive system (Assaggaf et al., 2022).

In this context, examining the interactions between thyme EO and thyme monofloral honey could yield important insights for innovative uses in natural medicine and functional foods. This investigation is part of a larger research project focusedon understanding MGHs and their interactions with herbal EOs. The specific objective of this study is to assess the potential synergistic effects of thyme EO and thyme monofloral honey when used together, particularly by analyzing their antibiofilm activity against clinical strains of *C. albicans*.

Material and methods

Thyme Essential Oil (EO) Preparation

EO from thyme was extracted using steam distillation. Fresh or dried thyme leaves were washed to remove contaminants and placed in a round-bottom flask, which was filled halfway with distilled water. The flask was equipped with a condenser and a receiving flask, and heated to a boiling point of approximately 100 °C to produce steam that passed through the plant material, facilitating the extraction of the essential oil. After 2-4 hours of distillation, the mixture was allowed to cool, and the distillate was collected. The aqueous layer was carefully removed to separate the EO, which was then stored in dark glass bottles, labeled with the extraction date for future use.

Honey Selection

Monofloral honey samples were collected

from 2023 to 2024 directly from beekeepers across various ecological regions of Iran. Each sample, weighing 250-300 g, was sourced from individual colonies and transported to the laboratory at temperatures below 20 °C. To verify authenticity, the samples were tested for physicochemical and phytochemical properties, emphasizing parameters relevant to medical use. Key physicochemical factors, including reducing sugars (before and after hydrolysis), 5-Hydroxymethylfurfural, proline, diastase activity, pH, sucrose, and the fructose/glucose ratio, were analyzed following International Honey Commission (IHC) guidelines and methodologies from Nayik et al.(Nayik and Nanda, 2016) and Oroian and Ropciuc (Oroian and Ropciuc, 2017). Additionally, melissopalynological analysis was conducted for botanical and geographical identification based on Louveaux et al.'s methods (Louveaux et al., 1978)(data not shown). After a thorough analysis, thyme honey emerged as a candidate for further analysis.

Yeast Cultivation

One clinical isolate of *C. albicans*, previously obtained from a gastric biopsy and stored at -80 °C, was used in this study. Previous research has demonstrated that this isolated yeast exhibits a high capacity for biofilm formation. After thawing, the recruited isolate was inoculated onto Brain Heart Infusion (BHI) agar and incubated at 37°C for 24 hours. The identity of the isolate as *C. albicans* was confirmed by the appearance of green colonies on Chromagar. To evaluate the resistance profile of this isolate, susceptibility testing was performed using the broth microdilution method according to the Clinical and Laboratory Standards Institute (CLSI) guidelines, assessing resistance to azoles (e.g., fluconazole), echinocandins (e.g., caspofungin), and polyenes (e.g., amphotericin B) (CLSI, 2020)

Determination of minimum inhibitory concentration (MIC) and minimum bactericidal concentration (MBC)

The minimum inhibitory concentration (MIC) of thyme essential oil (EO) and thyme honey against *C. albicans* was assessed using the broth microdilution method in 96-well microplates. Fresh yeast cultures were diluted to a 0.5 McFarland standard, and each well received 90 μL of brain-heart infusion (BHI) medium. A 10 μL aliquot of yeast suspension was added to each well, followed by 50 μL of honey at four concentrations (100%, 75%, 50%, and 25% v/v, corresponding to final concentrations of 25%, 18.75%, 12.5%, and 6.25% v/v) and 50 μL of thyme EO. Control wells were included for evaluating the individual effects of thyme EO and honey, as well as negative controls without any additives. Each treatment was replicated three times for statistical reliability, and the plates were incubated for 24 hours at 37 °C in a shaking incubator. The MIC was defined as the lowest concentration of honey that inhibited yeast growth. Following this, 50 μL from wells with no visible yeast growth were inoculated onto BHI agar plates and incubated for another 24 hours at 37 °C. The minimum bactericidal concentration (MBC) was determined as the lowest concentration of honey that showed no bacterial growth on

the agar plates (CLSI, 2020).

Anti-biofilm Activity Assay

The crystal violet (CV) microtiter plate assay was performed to evaluate the effect of thyme EO and thyme honey on the biofilm formation of *C. albicans*, as described by(Shukla and Rao, 2017). Initially, yeast cultures were incubated on BHI agar plates for 24 hours. Yeast suspensions were then prepared by diluting a 0.5 McFarland standard to obtain a final concentration of 1×10^3 to 3×10^3 colony-forming units per mL, which was utilized for the anti-biofilm assay. Each well of a 96-well plate received 90 μL of liquid BHI medium. Subsequently, 10 μL of the yeast suspension was added to each well, followed by the addition of 50 μL of four concentrations of honey (100%, 75%, 50% and 25% V/V final concentrations 25, 18.75, 12.5, and 6.25% V/V) and 50 μL of thyme EO. Control wells were set up to assess the individual contributions of the components: wells that lacked honey but contained EO and yeast were utilized to evaluate the impact of EO by itself, while wells that lacked EO but included honey and yeast were used to determine the effect of honey independently. Additionally, wells containing neither yeast nor honey nor EO served as negative controls. Each treatment group was replicated three times to ensure statistical validity. The plates were then incubated for 24 hours at 37 °C. After incubation, the culture medium was discarded, and the wells were rinsed with sterile phosphate-buffered saline (PBS). The microplate was inverted and allowed to air dry at room temperature for one hour. After drying, 200 μL of a 2% crystal violet solution

was added to each well, and the microplate was incubated for 15 minutes without agitation. Following this, the wells were rinsed with phosphate buffer to eliminate any residual dye. Subsequently, 200 μL of a 30% acetic acid solution was added to extract the bound dye from the wells. Finally, the optical absorbance was measured at 595 nm using a microplate reader. The inhibitory effect on biofilm formation was analyzed using the formula: Inhibitory rate $= (1 - S/C) \times 100\%$, where S represents the average absorbance of the sample group treated with thyme EO and honey, while C reflects the average absorbance of the control group.

Statistical analysis

To assess the effectiveness of each treatment in preventing biofilm formation compared to the control group, a paired samples t-test was performed using Excel version 2021. The optical absorption values obtained from the treatment groups compared with those of the control group following crystal violet staining, with a p-value of ≤ 0.05, was considered statistically significant.

Microscopy imaging

To illustrate the inhibitory effects of honey and thyme EO oil on the biofilm formation of *Candida albicans*, Evans Blue solution (0.01% in PBS) was utilized to stain the treated *Candida albicans* samples that were exposed to a combination of thyme EO and various concentrations of honey. These treated samples were then compared to a control group. Observations were conducted using immersion oil with a fluorescent microscope which was configured with a 1000X objective lens to examine biofilm formation, using a FITC filter set for

effective fluorescence detection.

Results

Resistance profile

The resistance profile of the *C. albicans* isolate was assessed using disk diffusion tests. The results revealed resistance to fluconazole, caspofungin, and amphotericin B, characterized by an average inhibition zone of less than 15 mm, confirming the isolate's multidrug-resistant phenotype.

Susceptibility assay by MIC and MBC

The MIC and MBC tests indicated that the thyme EO and honey were ineffective in inhibiting the growth of *C. albicans*. However, subsequent tests were conducted to evaluate their ability to inhibit biofilm formation.

Anti-biofilm activity assay

The light absorption for biofilm quantification was measured at a wavelength of 595 nm using a microplate reader (Table 1). All p-values obtained from the treatments were below 0.05, demonstrating statistically significant differences when compared to the negative control. Notably, the combination of thyme essential oil and honey, across all concentrations tested, exhibited the lowest p-value. This finding suggests that the synergistic effect of these two components is more effective in inhibiting the biofilm formation of *C. albicans*. Subsequently, the inhibition rate was measured using the formula (Inhibitory rate = $(1 - S/C) \times 100\%$), and the mean is presented in Table 1. Notably, the combination treatments exhibited markedly higher inhibition rates than either treatment alone at each concentration level. At the concentration of 75% (final concentration 18.75% V/V), the synergistic treatment achieved an average inhibition rate of 58.40%, while individual treatments with thyme EO and honey yielded average inhibition rates of 27.10% and 22.45%, respectively. Interestingly, the lowest concentration of 25% honey (final

Table 1. Optical Absorption Values and Inhibitory Rates (%) Obtained after Treatment of Clinical *C. albicans* Isolates

samples (Final concentration) % V/V	Optical Absorption Values				Mean of inhibition rate (%)
	Repeat 1	Repeat 2	Repeat 3	Mean	
Honey 100 (25)	0.70	0.71	0.72	0.71	26.10
Honey 75 (18.75)	0.65	0.67	0.68	0.67	30.30
Honey 50 (12.5)	0.75	0.76	0.74	0.75	21.90
Honey 25 (6.25)	0.85	0.84	0.86	0.85	11.5
Thyme EO	0.72	0.69	0.70	0.70	27.10
Honey 100 (25) + Thyme EO	0.50	0.52	0.51	0.51	46.90
Honey 75 (18.75) + Thyme EO	0.40	0.39	0.41	0.40	58.40
Honey 50 (12.5) + Thyme EO	0.55	0.56	0.54	0.55	42.80
Honey 25 (6.25) + Thyme EO	0.65	0.66	0.64	0.65	32.30
Negative Control (no treatment)	0.95	0.93	1.00	0.96	0.00

concentration 6.25% V/V) demonstrated an enhanced inhibition rate of 32.30% when combined with thyme EO, compared to an average of 12% for the honey treatment alone, further emphasizing the synergistic interaction between these treatments. The control group, which received no treatment, exhibited the highest optical absorption value of 0.96, confirming the absence of any inhibitory effect in untreated samples (Table 1, Figure 1).

Microscopy imaging

The fluorescent imaging analysis demonstrated that treatment with a combination of honey 75% V/V (final concentration 18.75% V/V) and thyme EO led to a notable decrease in the populations of *C. albicans* yeast cells. In contrast to the control group, the treated samples exhibited significantly fewer fluorescently labeled yeast cells. The cells appeared more scattered, exhibiting reduced numbers and altered cell shapes, which suggests effective inhibition of yeast biofilm formation (Figure 2).
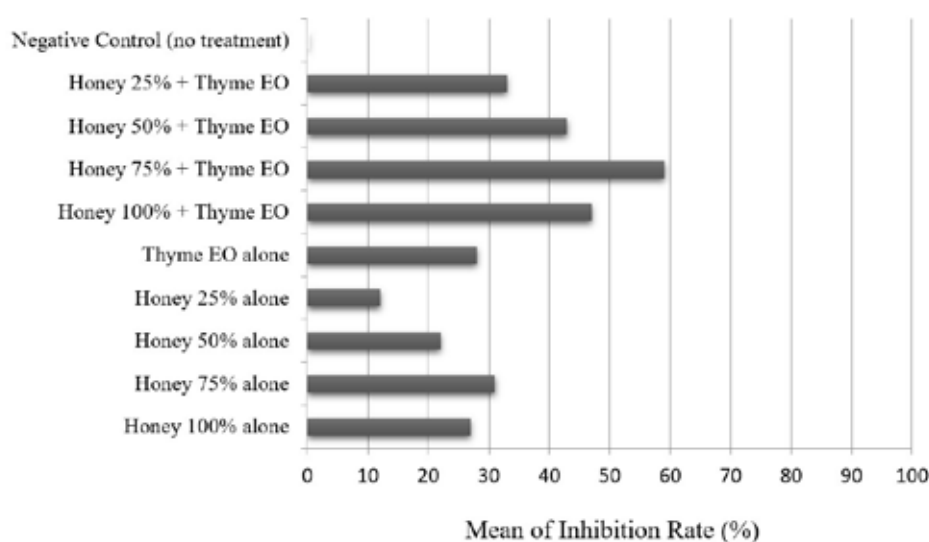

Figure 1. Comparison of inhibition rates (%) for various combinations of Thyme EO and honey against clinical isolates of *C. albicans*
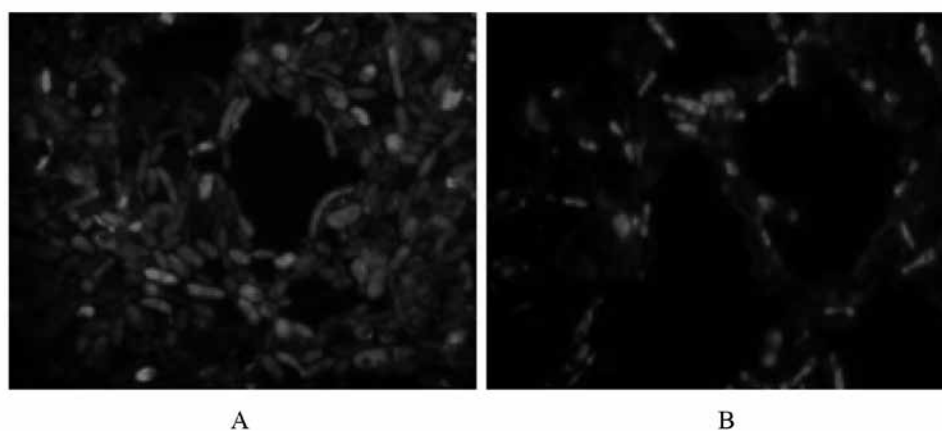

Figure 2. A: dense populations of *C. albicans* oval cells within biofilm; B: significant reduction in *C. albicans* cell density following treatment with a combination of thyme EO and honey 75% V/V, final concentration 18.75% V/V, (Magnification 1000X)

Discussion

Biofilms are critical to the pathogenesis of *Candida albicans* infections, as they significantly enhance resistance to antifungal agents, immune responses, and mechanical removal efforts (Pierce et al., 2017). The biofilm matrix offers a protective environment for *Candida* cells, complicating eradication efforts with conventional therapies. Thus, disrupting this matrix is essential for rendering *Candida* cells susceptible to antifungal treatment and ensuring successful therapeutic outcomes (Sardi et al., 2013).

Research has evaluated the antimicrobial properties of thyme EO against several bacterial strains, including *Bacillus subtilis*, *Staphylococcus aureus*, *Staphylococcus epidermidis*, *Pseudomonas aeruginosa*, *Escherichia coli*, and *Mycobacterium smegmatis*, as well as fungal species like *C. albicans* (Nazzaro et al., 2013). The results indicate that thyme EO exhibits significant bactericidal and antifungal activity against these microorganisms. Thymol, the main bioactive element found in thyme, demonstrates its antimicrobial properties by engaging with membrane proteins via hydrophobic interactions and hydrogen bonding, which subsequently modifies the permeability of cellular membranes. (Kowalczyk et al., 2020). Furthermore, thymol and carvacrol interfere with the biofilm matrix and inhibit the production of extracellular substances necessary for biofilm formation (Swetha et al., 2020). Thyme honey demonstrate bacteriostatic and microbicidal effects that are affected by its distinctive characteristics, the concentration of active compounds, and the type of bacteria present. Phenolic compounds, including flavonoids and phenolic acids, which confer antioxidant and antibacterial effects, can disrupt microbial membranes, inhibit essential enzymes, interfere with DNA, and ultimately lead to microbial death (Özkök et al., 2016).

The results of this study demonstrated a significant reduction in *C. albicans* biofilm formation when treated with a combination of honey and thyme EO. This combined treatment showed markedly higher inhibition rates compared to treatments with thyme EO or honey alone across all concentration levels tested. In this regard, Thyme honey combined with thyme EO shows promise in disrupting *C. albicans* biofilms through various mechanisms. While thyme EO is rich in potent monoterpenes, thyme honey contains a diverse array of phenolic compounds, and their interaction could yield a broader spectrum of biological activity, addressing complex health issues more efficiently than either component alone (Assaggaf et al., 2022). In this study, the combination of 75% honey and thyme EO showed a greater inhibitory effect compared to a 100% honey mixture with EO. This phenomenon may be attributed to the dilution of honey, which could activate certain bioactive compounds. When honey is diluted, the changes in osmotic pressure and the solubility of its components might enhance the availability and reactivity of specific phytochemicals and enzymes that exhibit antimicrobial and anti-biofilm properties (Mandal and Mandal, 2011).

In an era of increasing interest in natural

remedies as alternatives to synthetic pharmaceuticals, understanding the synergistic effects of thyme EO and honey may facilitate the development of novel natural therapeutics that harness their combined benefits. Additionally, the implications for functional foods are considerable, as the synergistic properties of these products could enhance their applications in promoting health and wellness through innovative nutritional strategies. Given the substantial challenges posed by biofilms in clinical settings, investigating the combined effects of thyme EO and honey could provide valuable insights into new strategies for managing infections stemming from multidrug-resistant pathogens, ultimately contributing to improved healthcare outcomes. Despite these encouraging findings, it is imperative to highlight the necessity for comprehensive studies to validate the clinical efficacy of these natural products. Future research should encompass in vivo experiments and clinical trials to fully unravel the therapeutic potential of honey and its derivatives in combination with other natural agents against *Candida* infections. This is especially important in light of the increasing antifungal resistance, necessitating the development of innovative strategies to combat multidrug-resistant pathogens effectively.

Conclusion

The study demonstrates that the combination of honey and thyme EO significantly reduces biofilm formation by *C. albicans*, highlighting the potential of these natural substances as effective antifungal agents. The synergistic effects of thyme EO and honey contribute to a promising therapeutic strategy to combat the challenges posed by biofilms in clinical settings. As the search for alternative treatments intensifies, the integration of natural antimicrobials into therapeutic protocols provides a multifaceted approach to enhance treatment efficacy against biofilm-associated infections. Increasing the number of strains examined would enhance the applicability of the results to other *Candida* strains and various clinical conditions. Continued exploration of these natural remedies is deemed essential for the development of innovative treatment options aimed at managing infections related to *C. albicans* and other multidrug-resistant pathogens, especially through studies involving a broader spectrum of clinical isolates.

References

Alissandrakis, E., Tarantilis, P.A., Harizanis, P.C. and Polissiou, M., 2007. Comparison of the volatile composition in thyme honeys from several origins in Greece. *Journal of Agricultural and Food Chemistry*, 55(20), pp.8152-8157. DOI: 10.1021/jf071442y.

Alshaikh, N.A. and Perveen, K., 2021. Susceptibility of fluconazole-resistant *Candida albicans* to thyme essential oil. *Microorganisms*, 9(12), p.2454. DOI: 10.3390/microorganisms9122454.

Alves, M., Gonçalves, M.J., Zuzarte, M., Alves-Silva, J.M., Cavaleiro, C., Cruz, M.T. and Salgueiro, L., 2019. Unveiling the antifungal potential of two Iberian thyme essential oils: effect

on *C. albicans* germ tube and preformed biofilms. *Frontiers in Pharmacology*, *10*, p.446. DOI: 10.3389/fphar.2019.00446.

Assaggaf, H.M., Naceiri Mrabti, H., Rajab, B.S., Attar, A.A., Hamed, M., Sheikh, R.A., Omari, N.E., Menyiy, N.E., Belmehdi, O., Mahmud, S., and Alshahrani, M.M., 2022. Singular and combined effects of essential oil and honey of *Eucalyptus globulus* on anti-inflammatory, antioxidant, dermatoprotective, and antimicrobial properties: in vitro and in vivo findings. *Molecules*, *27*(16), p.5121. DOI: 10.3390/molecules27165121.

Atriwal, T., Azeem, K., Husain, F.M., Hussain, A., Khan, M.N., Alajmi, M.F. and Abid, M., 2021. Mechanistic understanding of *Candida albicans* biofilm formation and approaches for its inhibition. *Frontiers in Microbiology*, 12, p.638609. DOI: 10.3389/fmicb.2021.638609.

Bhattacharya, S., Sae-Tia, S. and Fries, B.C., 2020. Candidiasis and mechanisms of antifungal resistance. *Antibiotics*, 9(6), p.312. DOI: 10.3390/antibiotics9060312.

Blankenship, J.R. and Mitchell, A.P., 2006. How to build a biofilm: a fungal perspective. *Current Opinion in Microbiology*, 9(6), pp.588-594. DOI: 10.1016/j.mib.2006.10.003.

Boukraâ, L., 2023. Honey in traditional and modern medicine. CRC Press. DOI: 10.1201/b15608.

Brown, G.D., Denning, D.W. and Levitz, S.M., 2012. Tackling human fungal infections. *Science*, 336(6082), pp.647-647. DOI: 10.1126/science.1222236.

Clinical and Laboratory Standards Institute, 2020. Performance standards for antimicrobial susceptibility testing. DOI: 10.1128/JCM.01864-19.

Enoch, D.A., Yang, H., Aliyu, S.H. and Micallef, C., 2016. The changing epidemiology of invasive fungal infections. *Human Fungal Pathogen Identification: Methods and Protocols*, pp.17-65. DOI: 10.1007/978-1-4939-6515-1_2.

Holubová, A., Chlupáčová, L., Krocová, J., Cetlová, L., Peters, L.J., Cremers, N.A. and Pokorná, A., 2023. The use of medical grade honey on infected chronic diabetic foot ulcers—a prospective case-control study. *Antibiotics*, 12(9), p.1364. DOI: 10.3390/antibiotics12091364.

Karabagias, I.K., Dimitriou, E., Kontakos, S. and Kontominas, M.G., 2016. Phenolic profile, colour intensity, and radical scavenging activity of Greek unifloral honeys. *European Food Research and Technology*, 242(8), pp.1201-1210. DOI: 10.1007/s00217-015-2624-6.

Köhler, J.R., Hube, B., Puccia, R., Casadevall, A. and Perfect, J.R., 2017. Fungi that infect humans. *Microbiology Spectrum*, 5(3), pp.10-1128. DOI: 10.1128/microbiolspec. funk-0014-2016.

Kowalczyk, A., Przychodna, M., Sopata, S., Bodalska, A. and Fecka, I., 2020. Thymol and thyme essential oil— new insights into selected therapeutic applications. *Molecules*, 25(18), p.4125. DOI: 10.3390/molecules25184125.

Lafraxo, H., Bakour, M., Laaroussi, H., El Ghouizi, A., Ousaaid, D., Aboulghazi, A. and Lyoussi, B., 2021. The synergistic beneficial effect of thyme honey and olive oil against diabetes and its complications

induced by alloxan in wistar rats. *Evidence-Based Complementary and Alternative Medicine*, 2021(1), p.9949056. DOI: 10.1155/2021/9949056.

Liu, X., Han, Y., Peng, K., Liu, Y., Li, J. and Liu, H., 2011. Effect of traditional Chinese medicinal herbs on *Candida* spp. from patients with HIV/AIDS. *Advances in Dental Research*, 23(1), pp.56-60. DOI: 10.1177/0022034511399286.

Louveaux, J., Maurizio, A. and Vorwohl, G., 1978. Methods of melissopalynology. *Bee World*, 59(4), pp.139-157. DOI: 10.1080/0005772X.1978.11097714.

Mandal, M.D. and Mandal, S., 2011. Honey: its medicinal property and antibacterial activity. *Asian Pacific Journal of Tropical Biomedicine*, 1(2), pp.154-160. DOI: 10.1016/S2221-1691(11)60016-6.

Mathé, L. and Van Dijck, P., 2013. Recent insights into *Candida albicans* biofilm resistance mechanisms. *Current Genetics*, 59(4), pp.251-264. DOI: 10.1007/s00294-013-0400-3.

Molan, P.C., 1992. The antibacterial activity of honey: 1. The nature of the antibacterial activity. *Bee World*, 73(1), pp.5-28. DOI: 10.1080/0005772X.1992.11099109.

Mora, C., Tittensor, D.P., Adl, S., Simpson, A.G. and Worm, B., 2011. How many species are there on Earth and in the ocean?. *PLoS Biology*, 9(8), p.e1001127. DOI: 10.1371/journal.pbio.1001127.

Morad, H.O., Wild, A.M., Wiehr, S., Davies, G., Maurer, A., Pichler, B.J. and Thornton, C.R., 2018. Pre-clinical imaging of invasive candidiasis using immunoPET/MR. *Frontiers in Microbiology*, 9, p.1996. DOI: 10.3389/fmicb.2018.01996.

Mukaremera, L., Lee, K.K., Mora-Montes, H.M. and Gow, N.A., 2017. *Candida albicans* yeast, pseudohyphal, and hyphal morphogenesis differentially affects immune recognition. *Frontiers in Immunology*, 8, p.629. DOI: 10.3389/fimmu.2017.00629.

Mukaremera, L., Lee, K.K., Mora-Montes, H.M. and Gow, N.A., 2017. *Candida albicans* yeast, pseudohyphal, and hyphal morphogenesis differentially affects immune recognition. *Frontiers in Immunology*, 8, p.629.DOI: 10.3390/microorganisms12112309.

Nayik, G.A. and Nanda, V., 2016. A chemometric approach to evaluate the phenolic compounds, antioxidant activity and mineral content of different unifloral honey types from Kashmir, India. *LWT*, 74, pp.504-513. DOI: 10.1016/j.lwt.2016.08.016.

Nazzaro, F., Fratianni, F., De Martino, L., Coppola, R. and De Feo, V., 2013. Effect of essential oils on pathogenic bacteria. *Pharmaceuticals*, 6(12), pp.1451-1474. DOI: 10.3390/ph6121451.

Nobile, C.J. and Johnson, A.D., 2015. *Candida albicans* biofilms and human disease. *Annual Review of Microbiology*, 69(1), pp.71-92. DOI: 10.1146/annurev-micro-091014-104330.

Oroian, M. and Ropciuc, S., 2017. Honey authentication based on physicochemical parameters and phenolic compounds. *Computers and Electronics in Agriculture*, 138, pp.148-156. DOI: 10.1016/j.compag.2017.04.020.

Özkök, A., Koru, Ö. and Sorkun, K.,

2016. Microbiological analysis and antibacterial effects of Turkish thyme honey. *Bee World*, 93(4), pp.98-101. DOI: 10.1080/0005772X.2016.1275489.

Pattamayutanon, P., Angeli, S., Thakeow, P., Abraham, J., Disayathanoowat, T. and Chantawannakul, P., 2015. Biomedical activity and related volatile compounds of Thai honeys from 3 different honeybee species. *Journal of Food Science*, 80(10), pp.M2228-M2240. DOI: 10.1111/1750-3841.12993.

PFALLER, M. A. & DIEKEMA, D. 2007. Epidemiology of invasive candidiasis: a persistent public health problem. *Clinical Microbiology Reviews,* 20**,** 133-163. DOI: 10.1128/cmr.00029-06.

Pfaller, M.A. and Diekema, D., 2007. Epidemiology of invasive candidiasis: a persistent public health problem. *Clinical Microbiology Reviews*, 20(1), pp.133-163. DOI: 10.3390/jof3010014.

Sardi, J.C.O., Scorzoni, L., Bernardi, T., Fusco-Almeida, A.M. and Mendes Giannini, M.J.S., 2013. *Candida* species: current epidemiology, pathogenicity, biofilm formation, natural antifungal products and new therapeutic options. *Journal of Medical Microbiology*, 62(1), pp.10-24. DOI: 10.1099/jmm.0.045054-0.

Shariati, A., Didehdar, M., Razavi, S., Heidary, M., Soroush, F. and Chegini, Z., 2022. Natural compounds: a hopeful promise as an antibiofilm agent against *Candida* species. *Frontiers in Pharmacology*, 13, p.917787. DOI: 10.3389/fphar.2022.917787.

Shukla, S.K. and Rao, T.S., 2017. An improved crystal violet assay for biofilm quantification in 96-well microtitre plate. *Biorxiv*, p.100214. DOI: 10.1101/100214.

Swetha, T.K., Vikraman, A., Nithya, C., Hari Prasath, N. and Pandian, S.K., 2020. Synergistic antimicrobial combination of carvacrol and thymol impairs single and mixed-species biofilms of *Candida albicans* and *Staphylococcus epidermidis*. *Biofouling*, 36(10), pp.1256-1271. DOI: 10.1080/08927014.2020.1869949.

Tseung, K. S. Y. N. H. & Zhao, J. 2016. Update on the fungal biofilm drug resistance and its alternative treatment. *Journal of Biosciences and Medicines,* 4**,** 37-47. DOI: 10.4236/jbm.2016.45004.

Tsui, C., Kong, E.F. and Jabra-Rizk, M.A., 2016. Pathogenesis of *Candida albicans* biofilm. *FEMS Pathogens and Disease*, 74(4), p.ftw018. DOI: 10.1093/femspd/ftw018.

Efficiency of Microalga *Dunaliella tertiolecta* in Cultivation and Removal of Pollutants from Dairy Industry Wastewater

Fariba Khamar[1], Javad Mirdar Harijani[2*] , Ahmad Gharaei[3], Abdolali Rahdari[4], Siroos Shojaei[5]

Abstract

Dunaliella tertiolecta is increasingly recognized as a valuable bioindustry microalga due to its ability to produce high-value pigments and biologically active compounds. However, the high cost of conventional culture media remains a major challenge for its large-scale cultivation. To address this issue, using nutrient-rich industrial wastewaters, such as dairy effluent, offers a promising, sustainable, and economical alternative. This study investigated the growth performance and pigment production of *D. tertiolecta* cultivated for 21 days in five concentrations of dairy wastewater (0%, 25%, 50%, 75%, and 100%) under controlled laboratory conditions (light intensity of 2500 lux; salinity of 1.5 M; temperature of $25 \pm 2°C$; pH of 7.5 ± 0.15). Algal cell density, chlorophyll a, chlorophyll b, and carotenoid content were measured every three days, while levels of ammonia, nitrate, and phosphate were assessed every five days. The results showed that the 25% wastewater treatment (T_2) produced the highest cell density on day 12 ($54.20 \times 10^6 \pm 1$ cells/mL). This treatment also resulted in the highest pigment concentrations, with chlorophyll a at 2.76 ± 0.04 mg/mL, chlorophyll b at 7.24 ± 0.06 mg/mL, and carotenoids at 2.24 ± 0.06 mg/mL concentrations. In terms of nutrient removal, T_2 achieved the greatest reduction in phosphate (0.052 ± 0.02 mg/mL) and nitrate (0.059 ± 0.94 mg/mL), while the highest ammonia removal (0.062 ± 2.23 mg/mL) occurred in the 50% treatment (T_3). Overall, the findings indicate that dairy wastewater, when properly diluted, can serve as an effective and low-cost culture medium for *D. tertiolecta*, supporting both biomass production and wastewater bioremediation.

Keywords: *D. tertiolecta*, Wastewater, Pigments, Biological treatment, Nutrients

Introduction

Microalgae are increasingly recognized as functional food ingredients due to their rich content of bioactive compounds,

---

1-Department of Fisheries, Faculty of Natural Resources, University of Zabol, Zabol, Iran.
2-Department of Fisheries, Faculty of Natural Resources, University of Zabol, Zabol, Iran
3-Department of Fisheries, Faculty of Natural Resources, University of Zabol, Zabol, Iran
4-Department of Aquatic Science, Hamoun International Wetland Institute, Research Institute of Zabol, Zabol, Iran
5-Faculty of Sciences, University of Sistan and Baluchestan, Zahedan, Iran.
*Corresponding author email address: Javadmirdar@uoz.ac.ir

such as carotenoids, polyunsaturated fatty acids, phycobiliproteins, and essential vitamins. These compounds contribute to antioxidant, anti-inflammatory, and immunomodulatory effects, aligning with the rising consumer demand for health-promoting and sustainable dietary sources. Among them, the *Dunaliella* genus of halophilic unicellular green microalgae has garnered attention for its ability to thrive in hypersaline environments, coastal lagoons, and rocky marine habitats, while producing high levels of β-carotene and other valuable metabolites. Martínez-Ruiz et al., 2025). Species within the genus *Dunaliella* demonstrate remarkable physiological plasticity, allowing them to thrive under extreme environmental conditions such as high salinity and variable light intensities. These adaptive traits—particularly the modulation of photosynthetic pigments and the production of osmoprotective metabolites—position *Dunaliella* as a perfect model for investigating stress tolerance mechanisms and cellular responses in plant-like systems (Barbosa et al., 2023; Mishra et al., 2008). *Dunaliella tertiolecta* has gained industrial and agricultural relevance due to its ability to synthesize valuable bioproducts, such as glycerol, β-carotene, single-cell proteins, and essential micronutrients, which are particularly beneficial in aquafeed formulations. Its biotechnological importance is further underscored by its exceptional capacity to accumulate high concentrations of β-carotene under stress conditions, making it one of the most efficient natural sources of this antioxidant pigment (Barbosa et al., 2023؛ Celente

et al., 2024). Plants are a rich source of various carotenoids beyond β-carotene, including lutein, zeaxanthin, violaxanthin, α-carotene, and neoxanthin, which contribute significantly to human health due to their antioxidant, anti-inflammatory, and photoprotective properties (Demmig-Adams et al., 2020).

The growing global population and the expansion of the food industry, especially the dairy sector, have produced large amounts of wastewater rich in organic matter and nutrients. Discharging this wastewater directly into the environment poses a serious threat to water resources and ecosystem health (Costa et al., 2021). On the other hand, microalgae are microorganisms with high potential for absorbing nutrients, producing biomass, and synthesizing bioactive compounds such as pigments. These features have attracted wide interest in biotechnology, agriculture, and environmental fields (Yang et al., 2011). Wastewater is typically defined as water that contains a mixture of organic matter, pathogens, nutrients, and chemical pollutants. When released untreated into natural ecosystems, it poses significant risks to public health and environmental integrity, including contamination of drinking water sources, eutrophication, and the spread of waterborne diseases (Lin et al., 2022؛ Babuji et al., 2023؛ Jayaswal et al., 2017). Dairy wastewater is a significant environmental concern due to its high organic load and nutrient content. With the global rise in dairy consumption, the volume of wastewater generated by dairy processing facilities has increased substantially. This

effluent typically contains elevated levels of proteins, soluble carbohydrates, nitrogenous compounds, phosphorus, and other nutrients, which can lead to eutrophication and oxygen depletion in receiving water bodies if not properly treated (Jimeto et al., 2025; Tayawi et al., 2025).

Although various chemical and physical techniques have been explored for treating dairy wastewater, many of these approaches remain economically unfeasible due to high operational and maintenance costs (Al-Tayawi et al., 2023; Radwan, 2020). Several studies have explored the cultivation of microalgae in wastewater. For example, Khalaji et al. (2019) used two concentrations of *Chlorella vulgaris* in dairy wastewater at different dilution levels. Their results showed that as the concentration of microalgae increased, nutrient uptake decreased, but nitrate absorption improved. In another study, *Chlamydomonas polypyrenoideum* was grown in diluted dairy wastewater mixed with distilled water. The findings indicated that dairy wastewater, due to its high nutrient content, can serve as a valuable medium for microalgal biomass production (Rodrigues-Sousa et al., 2021). Recent investigations have demonstrated that cultivating *Chlorella vulgaris* in dairy wastewater using a tubular photobioreactor significantly enhances nitrogen removal efficiency while simultaneously improving both the yield and biochemical composition of the algal biomass. These findings highlight the dual benefit of microalgae-based treatment systems: effective nutrient recovery and cost-efficient biomass generation for downstream applications

(Sudhanthiran et al., 2022).

Although species like *C. vulgaris* have been widely studied, *D. tertiolecta* remains underexplored in the context of dairy wastewater cultivation. Therefore, in this study, attempted to different concentrations of dairy wastewater were used as a cost-effective, nutrient-rich culture medium to grow the microalga *D. tertiolecta*. The aim was to evaluate its effects on pigment content, growth, and nutrient uptake efficiency, to identify the most suitable wastewater concentration for optimal cultivation of *D. tertiolecta*.

Material and methods

Microalgae stock preparation and cultivation conditions

A pure stock culture of *D. tertiolecta* was obtained from the Food Industry Biotechnology Research Institute in Tabriz, Iran. The strain had been taxonomically confirmed at both the genus and species levels using molecular methods and was reactivated by a specialist at the institute. Initial cultivation was carried out using Zarrouk medium (Richmond, 2003). The microalgae were grown in 500 mL (50 mL alga + 450 mL culture medium) glass flasks without shake under the following conditions: continuous gentle and continuous aeration, salinity of 1.5 M (equivalent to 87 g/L NaCl), temperature of 25 ± 1 °C, light intensity of 2500 lux with a light/dark cycle of 16:8 h, and a pH of 7.5 (Martinez et al., 2000).

Dairy wastewater collection and preparation

Dairy wastewater was collected after equipment washing at the Kerman Dairy

Factory, located in Zahak County, Sistan and Baluchestan Province, Iran. (Table 1). The wastewater was stored in polyethylene containers and transported to the laboratory at 4 °C (Hamoun International Wetland Research Institute, Zabol, Iran). Before experimentation, large particulate matter was removed using Whatman filter paper. The filtered wastewater was then sterilized in an autoclave at 120 °C and 1.6 atm pressure for 20 min, followed by a second filtration through Whatman paper to ensure clarity.

Experimental design

The experimental treatments included volumes of 5 mL culture medium and 50 mL *D. tertiolecta* inoculum, but with different concentrations of dairy wastewater: 0%, 25%, 50%, 75%, and 100%, each diluted with distilled water. The total duration of the experiment was set to 21 days. It should be noted that all sampling was performed with three replicates.

Cell counting

Cell counts were performed every three days using a light microscope and a Neubauer counting chamber at 40× magnification. Five squares of the chamber were counted, and cell density was calculated using Eq. (1) (Mokhberi et al., 2015). It should be noted that all cells were counted visually.

$$\text{Number of cells/mL= Average cell count} \times 10^4 \times \text{Dilution factor} \qquad (1)$$

Measurement of chlorophyll (a, b) and total carotenoids

The concentrations of chlorophyll a, chlorophyll b, total chlorophyll (a + b), and total carotenoids were measured every three days using a UV/Vis spectrophotometer (UV/Vis 2100, Unico). For each measurement, 5 mL of the algal culture was centrifuged at 5000 rpm for 10 min. The supernatant was carefully removed using a micropipette. Then, 5 mL of 85% acetone was added to the pellet. After vortexing, the tubes were kept in the dark for 5 minutes. The mixture was centrifuged again at 5000 rpm for another 10 minutes. The supernatant was then transferred to a cuvette, and absorbance was measured

Table 1. Physicochemical properties of dairy wastewater

Compound	Concentration (mg/L)
Sulfate (SO$_4$)	185
Magnesium carbonate (MgCO$_3$)	38
Manganese (Mn)	0.001
Calcium carbonate (CaCO$_3$)	4540.3
Copper (Cu)	0.74
Total copper (Total Cu)	1.52
Potassium (K)	34.92
Iron (Fe)	0.42
Mg as CaCo$_3$	257.8
Magnesium (Mg)	54.52

at wavelengths of 452, 644, and 633 using the spectrophotometer. Chlorophyll a, chlorophyll b, and total carotenoid concentrations (mg/mL) were calculated using the following equations. (2-4) (Frank and Wegmann, 1979).

$$C_{chla}=(10.3 \times E_{633}) - (0.918 \times E_{644}) \quad (2)$$

$$C_{chl\,b}= (19.7 \times E_{644}) - (3.87 \times E_{633}) \quad (3)$$

$$C_{car}=(4.20 \times E_{452}) - (0.0264 \times C_{chl\,a}) - (0.496 \times C_{chl\,b}) \quad (4)$$

Measurement of nutrients (Ammonia, nitrate, and phosphate)

The concentrations of phosphate, ammonia, and nitrate were measured every five days throughout the experiment. On day one, after mixing the designated ratios of distilled water, culture medium, and dairy wastewater, the initial concentrations of nitrate, ammonia, and phosphate were measured using standard reagent tablets and a photometer (Palintest 8000). Subsequent measurements were taken every five days. For each time point, a portion of the sample was transferred into a test tube using a pipette. After centrifugation, the algal biomass was separated, and the supernatant was used to determine nutrient concentrations. To assess nutrient removal efficiency, equation (5) was used (Hen et al., 2015).

$$W\% = (C_i - C_o)/C_o \times 100\% \quad (5)$$

where W% represents the nutrient removal percentage, C_0 is the initial concentration, and C_i is the concentration at the time of measurement.

Statistical analysis

All data were analyzed using SPSS software version 22.0 (SPSS Inc., Chicago, IL, USA). One-way analysis of variance (One-Way ANOVA) was applied to determine statistical differences among treatments.

Mean comparisons were performed using Duncan's multiple range test at a 95% confidence level. Graphs were generated using Microsoft Excel 2016.

Results

Cell counting

According to Table 2, the treatment with 25% wastewater (T2) showed a significant increase in cell density from day 3 to day 12 compared to the other treatments (p <

Table 2. Growth rate of *D. tertiolecta* algae under different treatments

Day	Treatment (mg/L)				
	T₁	T₂	T₃	T₄	T₅
1st	2.93 ± 0.12 [J]	3.07 ± 0.31 [F]	3.13 ± 0.31 [FJ]	2.73 ± 0.61 [E]	3.40 ± 0.20 [D]
3rd	5.87 ± 0.50 [dF]	9.73 ± 0.31 [bE]	8.47 ± 0.31 [cE]	12.87 ± 0.42 [aB]	5.47 ± 0.23 [dC]
6th	10 ± 0.20 [dE]	30.13 ± 0.50 [aC]	30.80 ± 0.40 [aC]	17.07 ± 0.31 [bA]	12.53 ± 0.50 [cA]
9th	16.73 ± 0.12 [cD]	50.20 ± 2.40 [aAB]	43.07 ± 1.70 [bA]	11 ± 1.22 [dC]	7.80 ± 0.40 [eB]
12th	26.87 ± 0.70 [cC]	54.20 ± 1.10 [aA]	36.87 ± 0.42 [bB]	7.13 ± 0.70 [dD]	3.87 ± 2.23 [eD]
15th	32.53 ± 0.64 [bB]	47.40 ± 0.60 [aB]	16.07 ± 1.10 [cD]	3.67 ± 0.23 [dE]	2.47 ± 0.23 [eE]
18th	32.93 ± 0.83 [aB]	20.27 ± 1.22 [bD]	3.87 ± 0.42 [cF]	1.67 ± 0.12 [dF]	-
21th	33.87 ± 0.61 [aA]	11.67 ± 7.10 [bE]	2.20 ± 0.40 [cJ]	-	-

0.05), reaching the highest value of 54.2 × 10^4 cells/mL on day 12. The treatment with 50% wastewater (T3) also exhibited a significant upward trend from day 3 (8.47 × 10^4 cells/mL) to day 9 (43.10 × 10^4 cells/mL) (p < 0.05); however, a decline in cell density was observed in both T2 and T3 treatments thereafter. In contrast, the 75% (T4) and 100% (T5) wastewater treatments showed only a slight increase in cell density on day 6, reaching 17.07 × 10^4 and 12.53 × 10^4 cells/mL, respectively, followed by a continuous decrease that approached zero by day 18. Interestingly, the control treatment (T1) exhibited a delayed but steady increase in cell density from day 6 (10 × 10^4 cells/mL) to day 21 (33.87 × 10^4 cells/mL), with statistically significant differences compared to the other treatments from day 18 to day 21 (p < 0.05).

Chlorophyll a and b analysis

Based on Figures 1 and 2, the highest levels of chlorophyll a and b were observed in treatment T_2 on day 12, with mean values of 2.76 ± 0.04 mg/mL and 7.24 ± 0.06 mg/mL, respectively, compared to other treatments. Similarly, treatment T_3 showed peak concentrations on day 9, with chlorophyll a at 2.45 ± 0.10 mg/mL and chlorophyll b at 7.05 ± 0.05 mg/mL. Following these peak values, both pigments exhibited a declining trend. The lowest concentrations of chlorophyll a and b were recorded in treatments T_4 and T_5.

Carotenoid analysis

According to Figure 3, different concentrations of wastewater had a significant effect on carotenoid content. On day 18, treatment T_2 exhibited the highest carotenoid concentration (4.24 ± 0.06 mg/mL), significantly exceeding the values observed in the other treatments. In contrast, the lowest carotenoid level was recorded in treatment T_5.

Phosphate analysis

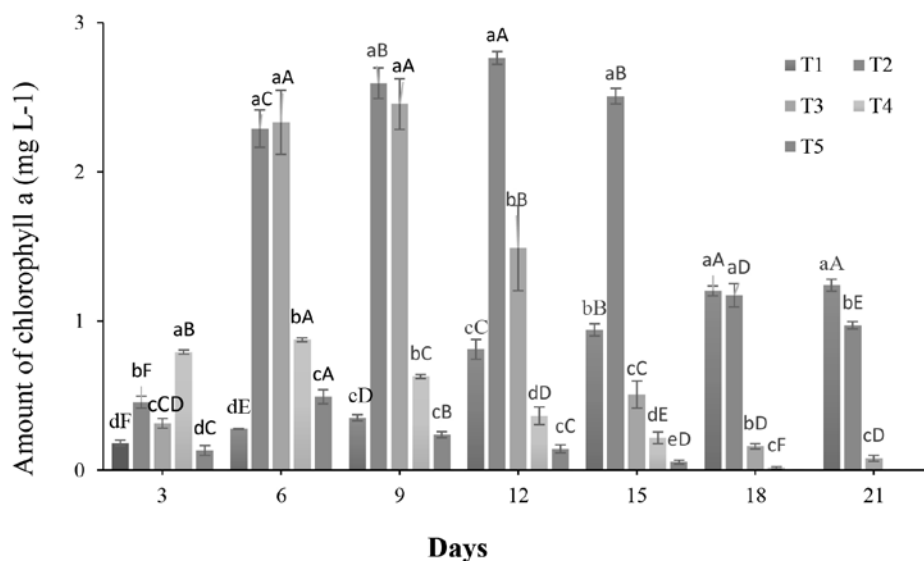According to Table 3, increasing the dilution of wastewater led to a decrease in the initial

Fig. 1. Chlorophyll a content of microalgae *D. tertiolecta* in different treatments (lowercase and uppercase letters indicate significant differences (p< 0.05) on one and different days between treatments, respectively))
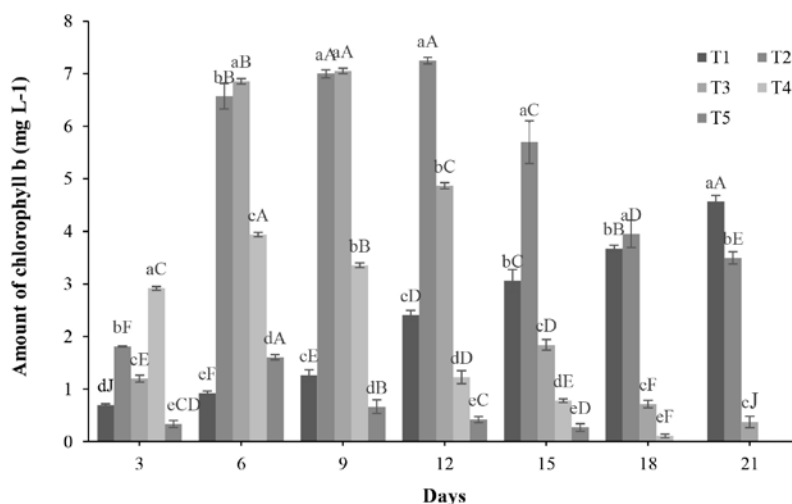
Fig. 2. Chlorophyll b content of microalgae *D. tertiolecta* in different treatments (lowercase and uppercase letters indicate significant differences (p< 0.05) on one and different days between treatments, respectively)

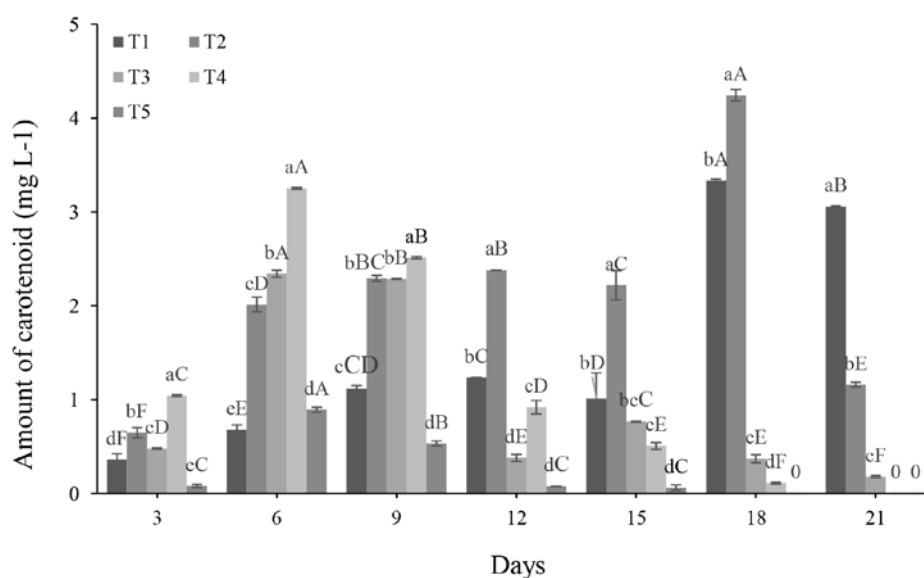**Fig. 3.** Total carotenoid content of microalgae *D. tertiolecta* in different treatments (lowercase letters indicate significant differences (p<0.05) on one day between different treatments, and uppercase letters indicate significant differences (p<0.05) between each treatment on different days)

Table 3. Phosphate concentrations (mg L^{-1}) in different treatments

Phosphate	Day				
	1st	5th	10th	15th	20th
T_2	368.2 ± 0.4 [dA]	272.1 ± 0.3 [cB]	234.8 ± 0.5 [dC]	198.8 ± 0.4 [dD]	176.6 ± 0.3 [bE]
T_3	387.8 ± 0.4 [cA]	264.5 ± 0.4 [dB]	249.3 ± 0.4 [cC]	228.4 ± 0.3 [cD]	219.4 ± 0.5 [aE]
T_4	394.3 ± 0.5 [bA]	320.8 ± 0.4 [bB]	310.9 ± 0.4 [bC]	308.2 ± 0.3 [bD]	-
T_5	405.7 ± 0.5 [aA]	382.4 ± 0.3 [aB]	368.4 ± 0.5 [aC]	361.5 ± 0.4 [aD]	-

(Uppercase letters indicate significance (p< 0.05) in each row, and lowercase letters indicate significance (p< 0.05) in each column)

42

phosphate concentration. The highest initial phosphate level was observed in the treatment with 100% wastewater (T5), measuring 405.7 mg/mL.There were only slight changes in phosphate removalafter day 10 in treatments T4 and T5. However, treatments T2 (234.8 mg/mL) and T3 (249.3 mg/mL) demonstrated a greater capacity for phosphate reduction compared to the other treatments. Overall, the results indicate that phosphate concentrations significantly decreased over time across all treatments ($p < 0.05$).

Nitrate analysis

Nitrate concentrations across the different treatments during the experimental period are presented in Table 4. The results indicated a decreasing trend in nitrate levels over time in all treatments. The highest initial nitrate concentration was recorded in treatment T5 on day 1, with a value of 53.4 mg/mL. All treatments, except T3, showed statistically significant differences in nitrate levels on days 10, 15, and 18 ($p < 0.05$).

Ammonia analysis

According to Table 5, the ammonia levels in all experimental treatments exhibited a significant reduction from day 1 to day 10. Following day 10, the ammonia removal rate declined. Statistically significant differences ($p < 0.05$) were observed in all treatments except T_3 on days 10 and 15, as well as treatments T_2 and T_3 on day 20.

Phosphate, nitrate, and ammonia removal

Table 4. Nitrate concentrations (mg L^{-1}) in different treatments

Nitrate	Day				
	1st	5th	10th	15th	20th
T_2	28.6 ± 0.8 [dA]	19.7 ± 0.3 [cB]	14.8 ± 0.4 [dC]	12.6 ± 0.4 [dD]	11.8 ± 0.6 [bD]
T_3	32.8 ± 0.4 [cA]	18.7 ± 0.5 [dB]	17.2 ± 0.3 [cC]	16.8 ± 0.3 [cD]	16.2 ± 0.5 [aC]
T_4	48.2 ± 0.5 [bA]	36.8 ± 0.5 [bB]	32.4 ± 0.3 [bC]	30.8 ± 0.3 [bD]	-
T_5	53.4 ± 0.5 [aA]	46.2 ± 0.4 [aB]	44.7 ± 0.4 [aC]	41.5 ± 0.4 [aD]	-

(Uppercase letters indicate significance ($p < 0.05$) in each row, and lowercase letters indicate significance ($p < 0.05$) in each column)

Table 5. Ammonia concentrations (mg L^{-1}) in different treatments

Ammonia	Day				
	1st	5th	10th	15th	20th
T_2	14.2 ± 0.4 [dA]	12.4 ± 0.5 [dB]	8.9 ± 0.3 [dC]	6.6 ± 0.3 [dD]	5.8 ± 0.4 [aE]
T_3	18.6 ± 0.3 [cA]	15.2 ± 0.3 [cB]	11.6 ± 0.3 [cC]	10.2 ± 0.3 [cC]	7.1 ± 2.2 [aD]
T_4	26.4 ± 0.3 [bA]	23.6 ± 0.3 [bB]	20.8 ± 0.4 [bC]	19.4 ± 0.5 [bD]	-
T_5	29.8 ± 0.4 [aA]	25.9 ± 0.3 [aB]	24.6 ± 0.3 [aC]	23.8 ± 0.4 [aD]	-

(Uppercase letters indicate significance ($p < 0.05$) in each row, and lowercase letters indicate significance ($p < 0.05$) in each column)

Table 6 indicates that the highest nitrate removal rate (58.75%) was observed in the 25% wastewater treatment (T2), while the lowest rate (22.28%) was recorded in the 75% treatment (T5). A statistically significant difference was observed among all treatments. Phosphate removal percentages also showed significant differences across treatments ($p < 0.05$), with the highest and lowest removal rates corresponding to T2 (52.3%) and T5 (10.89%), respectively. Regarding ammonia, the highest removal rates were observed in T3 (61.54%) and T2 (59.18%). However, no significant differences were found between T2 and T3, nor between T4 and T5.

Discussion

Biomass Production

The growth of microalgae and biomass productivity is significantly influenced by environmental parameters, including salinity, light intensity, temperature, pH, total dissolved solids (TDS), and nutrient availability. These factors play a crucial role in regulating photosynthetic efficiency and cellular metabolism, ultimately determining the success of algal cultivation systems (Peralta, 2023). In the present study, the highest biomass yield was observed in the treatment containing 25% dairy wastewater. This dilution appears to strike an optimal balance between nutrient availability and the mitigation of potential toxicity. At higher concentrations (75% and 100%), growth declined earlier, likely due to excessive organic load, oxygen depletion, pH fluctuations, and nutrient exhaustion. These findings align with those of Khalaji et al. (2019), who reported enhanced biomass production of *Chlorella vulgaris* in 25% dairy wastewater. Similarly, Salla et al. (2016) found that supplementing *Spirulina* cultures with whey protein concentrate significantly boosted biomass. Salgueiro et al. (2016) observed that *C. vulgaris* initially underwent an adaptation phase in wastewater, followed by exponential growth, and biomass increased from 0.05 g/L to 0.75 g/L within 9 days before declining due to environmental limitations. Lu et al. (2017) studied *Spirulina platensis* in brewery wastewater and reported that a 50% concentration caused excessive turbidity, reducing light penetration and photosynthetic efficiency. This is consistent with the reduced growth observed in treatments T4 and T5 of the present study. They also noted that while 10% dilution limited growth due to insufficient nutrients, a 20% concentration provided optimal conditions—closely mirroring the performance of the 25% treatment in this research.

Pigment Dynamics

Chlorophyll a and chlorophyll b are the primary photosynthetic pigments in algae, essential for capturing light energy and driving the photosynthetic process (Robertson, 2021; Nave, 2023). Chlorophyll b serves not only as an accessory pigment that broadens the spectrum of light absorption in photosynthetic organisms, but also plays a regulatory role in modulating the activity of other photoreceptors. Under environmental stress conditions, such as reduced light intensity, chlorophyll b contributes to cellular defense mechanisms by minimizing oxidative damage through enhanced energy dissipation and photoprotection (Nave, 2023).

Chlorophyll is a nitrogen-rich pigment, with each molecule containing four nitrogen atoms embedded within the porphyrin ring. Under nitrogen-deficient conditions, plants mobilize internal nitrogen reserves to sustain essential processes such as cell division and photosynthesis. This limitation reduces photosynthetic efficiency and modifies the relative concentrations of chlorophyll a and b. Conversely, elevated levels of nitrogen and magnesium—such as those found in dairy wastewater—can promote chlorophyll biosynthesis and enhance photosynthetic performance through facilitating enzyme activation and pigment production (Chen, 2024). In this study, chlorophyll levels initially increased due to elevated nitrogen and magnesium in the dairy wastewater, which promote chlorophyll biosynthesis and enzymatic activity However, as cultivation progressed, nutrient depletion, temperature stress, and increased turbidity from biomass accumulation led to a decline in chlorophyll a. Dickinson et al. (2014) reported that *Scenedesmus* sp. grown in municipal wastewater exhibited chlorophyll a levels 2.5 times higher in nutrient-rich treatments, but light limitation due to biomass build-up eventually reduced pigment content. De Francisci et al. (2017) found that *C. sorokiniana* cultivated in mixed municipal-industrial wastewater produced average pigment levels of 0.44 mg/g β-carotene and 11.82 mg/g chlorophyll (dry weight), indicating wastewater can enhance pigment synthesis. Carotenoids absorb light in the 400–550 nm range and protect cells from oxidative stress and high radiation. *Dunaliella tertiolecta* is particularly adept at increasing carotenoid

synthesis under stress conditions such as high salinity, nutrient deficiency, and intense lightup to 42 pg/cell (Trenkenshu, 2005). In the present study, the highest carotenoid content was observed in the 25% wastewater treatment, significantly higher than the control (p < 0.05). Seo et al. (2024) observed that *Halochlorella rubescens* grown in pig wastewater exhibited elevated chlorophyll and carotenoid levels on day 4, with carotenoids doubling compared to initial values. Additionally, Zhang et al. (2017) demonstrated that *C. vulgaris* increases carotenoid synthesis under gradual nitrogen depletion. These findings reinforce the stress-induced pigment dynamics observed in *D. tertiolecta*. Microalgae's ability to absorb nutrients from dairy wastewater makes it a cost-effective medium for biomass production and wastewater treatment (Costa et al., 2021). In this study, nutrient removal efficiency varied by dilution level. The 25% wastewater treatment achieved the highest nitrate and phosphate removal by the end of cultivation, while the 50% treatment showed the highest ammonia removal. These results suggest that moderate dilution optimizes nutrient uptake by reducing toxicity and maintaining sufficient nutrient levels. Khalaji et al. (2019) conducted a study on *Chlorella* at two different cell densities (13 and 26 million cells/mL) and three varying wastewater concentrations (25%, 50%, 75%). At the lower cell density, they observed a phosphate removal rate of 51.84% in 25% wastewater, a nitrate removal of 57.01% in 50%, and an ammonia removal rate of 44.25% in 50%, which closely matches the present findings. At lower cell density, Brar et al. (2019) compared

Chlorella, *Scenedesmus*, and *Anabaena* in the context of dairy wastewater, revealing that nitrate removal efficiencies of 88.91%, 84.72%, and 89.52%, respectively, alongside phosphate removal rates of 86.51%, 79.02%, and 87.83%. Interestingly, it was observed that higher wastewater concentrations improved phosphate removal, which stands in contrast with the current study. This discrepancy may stem from differences in algal species, wastewater composition, or experimental conditions. Ahmed et al. (2014) reported that *Spirulina* removed 72% phosphate and 80% nitrate from dairy wastewater, with nitrate removal consistently outperforming phosphate, similar to the trend observed in this study. Khemka & Safraf (2017) found that *Desertifilum tharense* removed up to 98% phosphate and 94% nitrate, significantly higher than the rates in this study, likely due to species-specific traits and optimized conditions.

Conclusion

The results demonstrated that the highest cell density was achieved in the 25% wastewater treatment (T2) on day 12, reaching $54.20 \times 10^4 \pm 1$ cells/mL. Similarly, the highest concentrations of chlorophyll a (2.76 ± 0.04 mg/mL), chlorophyll b (7.24 ± 0.06 mg/mL), and carotenoids (2.24 ± 0.06 mg/mL) were also observed in T2. Regarding nutrient removal, T2 showed the most effective reduction in phosphate (0.052 ± 0.02 mg/mL) and nitrate (0.059 ± 0.94 mg/mL), while the highest ammonia removal (0.062 ± 2.23 mg/mL) was recorded in the 50% wastewater treatment (T3). Subsequently, the findings of this study highlight *Dunaliella tertiolecta* as a promising candidate for integrated wastewater treatment and biomass production. Its superior performance in the 25% dairy wastewater treatment, reflected in biomass yield, pigment synthesis, and nutrient removal, demonstrates its resilience and adaptability to semi-stressful environments. The 25% dilution level provides a strategic balance: it minimizes toxicity from organic overload while maintaining sufficient nutrient concentrations and light penetration. This balance supports robust growth and metabolic activity, making it ideal for scalable applications. Compared to other species such as *Chlorella vulgaris* and *Spirulina*, *D. tertiolecta* exhibits enhanced carotenoid synthesis and efficient nutrient uptake under moderate stress. These traits underscore its potential for use in photobioreactors, biofuel production, and eco-friendly wastewater remediation.

Acknowledgement

References

Al-Tayawi, A. N., Sisay, E. J., Beszédes, S., & Kertész, S. 2023. Wastewater treatment in the dairy industry from classical treatment to promising technologies: An overview. Processes, 11(7), 2133. DOI: https://doi.org/10.3390/pr11072133.

Ahmad, F., Khan, A.U., and Yasar, A., 2014. The potential of *Chlorella vulgaris* for wastewater treatment and biodiesel pro-

duction. *Pakistan Journal of Botany*, 45, pp. 461-65.

Babuji, P., Thirumalaisamy, S., Duraisamy, K., & Periyasamy, G. 2023. Human health risks due to exposure to water pollution: A review. Water, 15(14), 2532. DOI: https://doi.org/10.3390/w15142532.

Barbosa, M., Inácio, L. G., Afonso, C., & Maranhão, P. 2023. The microalga *Dunaliella* and its applications: a review. *Applied Phycology*, 4(1), 99–120. DOI: https://doi.org/10.1080/26388081.2023.2222318.

Brar, A., Kumar, M. and Pareek, N., 2019. Comparative Appraisal of Biomass Production, Remediation, and Bioenergy Generation Potential of Microalgae in Dairy Wastewater. *Frontiers in Microbiology,* 10, pp. 678. DOI: https://doi.org/10.3389/fmicb.2019.00678.

Celente, G. S., Schneider, R. C. S., Julich, J., Rizzetti, T. M., Lobo, E. A., & Sui, Y. 2024. Life cycle assessment of microalgal cultivation medium: biomass, glycerol, and beta-carotene production by *Dunaliella salina* and *Dunaliella tertiolecta*. The International *Journal of Life Cycle Assessment*, 29, 2269–2282. DOI: https://doi.org/10.1007/s11367-023-02209-2.

Chen, L.-H., Xu, M., Cheng, Z., & Yang, L.-T. 2024. Effects of nitrogen deficiency on the photosynthesis, chlorophyll a fluorescence, antioxidant system, and sulfur compounds in Oryza sativa. International *Journal of Molecular Sciences*, 25(19), 10409. DOI: https://doi.org/10.3390/ijms251910409.

Costa, J.A.V., Gonzalescruz, C. and Rosa, P.C., 2021. Insights into the technology utilized to cultivate microalgae in dairy effluents. *Biocatalysis and Agricultural Biotechnology,* 35, pp. 102106. DOI: https://doi.org/10.1016/j.bcab.2021.102106.

De Francisci, D., Su, Y., Iital, A. and Angelidaki, I., 2018. Evaluation of microalgae production coupled with wastewater treatment. *Environmental technology*, *39*(5), pp.581-592. DOI: https://doi.org/10.1080/09593330.2017.1308441.

Demmig-Adams, B., López-Pozo, M., Stewart, J. J., & Adams III, W. W. 2020. Zeaxanthin and lutein: Photoprotectors, anti-inflammatories, and brain food. Molecules, 25(16), 3607. DOI: https://doi.org/10.3390/molecules2516360.

Dickinson, K.E., Bjornsson, W.J., Garrison, L.L., Whitney, C.G., Park, K.C., Banskota, A.H., and McGinn, P.J., 2014. Simultaneous remediation of nutrients from liquid anaerobic digestate and municipal wastewater by the microalga *Scenedesmus* sp. AMDD grown in continuous chemostats. *Journal of Applied Microbiology*. 118: pp. 75-83. DOI: https://doi.org/10.1111/jam.12681.

Frank, G. and Wegmann, K., 1979. Physiology and biochemistry of glycerol biosynthesis in *Dunaliella. Biologisches zentralblatt*, 93, pp. 707-723.

Hen, L., Pei, H., Hu, W., Jiang, L., Ma, G., Zhang, S. and Han, F., 2015. Integrated campus sewage treatment and biomass production by *Scenedesmus quadricauda* SDEC-13. *Bioresource technology* 175, pp. 262-268. DOI:10.1016/j.biortech.2014.10.100.

Jayaswal, K., Sahu, V., & Gurjar, B. R. 2017.

Water pollution, human health and remediation. In B. R. Gurjar (Ed.), Air pollution and health impacts in South Asia (pp. 19–34). Springer. DOI: https://doi.org/10.1007/978-981-10-7551-3_2.

Jimeto, K. I., Ajibade, F. O., Ajibade, T. F., John, C. K., Lasisi, K. H., Ojo, A. O., & Adewumi, J. R. 2025. Strategic management of dairy wastewater. In F. O. Ajibade (Ed.), Strategic Management of Wastewater from Intensive Rural Industries (pp. 73–102). Springer. DOI: https://doi.org/10.1007/978-3-031-90314-43.

Khalaji, M., Hosseini, S. A., Ghorbani, R., Agh, N., Rezaei, H., Kornaros, M. and Koutra, E., 2021. Treatment of dairy wastewater by microalgae *Chlorella vulgaris* for biofuels production. *Biomass Conversion and Biorefinery*, pp. 1-7. DOI: https://doi.org/10.1007/s13399-021-01287-2.

Khemka, A. and Saraf, M., 2017. Strategic enhancement of *Desertifilum tharense* MSAK01 on dairy wastewater: An integrated approach for remediation and biomass production. *Applied Water Science*, 7, pp. 2779–2785. DOI: https://doi.org/10.1007/s13201-017-0525-5.

Lin, L., Yang, H., & Xu, X. 2022. Effects of water pollution on human health and disease heterogeneity: A review. Frontiers in Environmental Science, 10, 880246. DOI: https://doi.org/10.3389/fenvs.2022.880246.

Lu, B., Du, X., and Huang, S., 2017. The economic and environmental implications of wastewater management policy in China: from the LCA perspective. *Journal of Cleaner Production,* 142, pp. 3544–3557.

DOI: 10.1016/j.jclepro.2016.10.113.

Martínez-Ruiz, F.E., Andrade-Bustamante, G., Holguín-Peña, R.J., 2025. Microalgae as Functional Food Ingredients: Nutritional Benefits, Challenges, and Regulatory Considerations for Safe Consumption. Biomass, 5(2), 25. Available on MDPI

Martınez, M., Sánchez, S., Jimenez, J., El Yousfi, F. and Mu-noz, L., 2000. Nitrogen and phosphorus removal from urban wastewater by the microalga *Scenedesmus obliquus. Bioresource Technology*,73(3), pp. 263-72. DOI: https://doi.org/10.1016/S0960-8524(99)00121-2.

Mishra, A., Mandoli, A., & Jha, B. 2008. Physiological characterization and stress-induced metabolic responses of *Dunaliella salina* isolated from the salt pan. *Journal of Industrial Microbiology & Biotechnology*, 35(10), 1093–1101. DOI: https://doi.org/10.1007/s10295-008-0387-9.

Mokhberi, R., Rezaei, A., and Kordenaeej, A., 2015, Increased Production of Beta-Carotene and Glycerol in *Dunaliella Salina* Cell Culture by Ultrasound. *Journal of Cell & Tissue*, 6 (3), pp. 397-408.

Nave, R. 2023. Pigments for photosynthesis. HyperPhysics, Georgia State University. Retrieved from http://hyperphysics.phy-astr.gsu.edu/hbase/Biology/pigpho.html

Neczaj, E., Okoniewska, E. and Kacprzak, M., 2005.Treatment of landfill leachate by a sequencing batch reactor. Desalination. 185(1), pp. 357-62. DOI: https://doi.org/10.1016/j.desal.2005.04.044.

Peralta, H. M. 2023. An overview of environmental factor's effect on the growth

of microalgae. Academia.edu. Retrieved from the Academia.edu publication page.

Radwan, M. 2020. A short review of effective dairy wastewater treatment techniques. International *Journal of Engineering Research & Technology* (IJERT), 9(7), Article IJERTV9IS070456. DOI: https://www.ijert.org/a-short-review-on-effective-dairy-wastewater-treatment-techniques.

Richmond, A., 2003. Handbook of Microalgal Mass Culture: Biotechnology and Applied Phycology. *Blackwell Publishing Ltd*., pp. 212–230. DOI:10.1002/9780470995280.

Robertson, D. E. 2021. Algal pigments. The Robertson Laboratory, Clark University. Retrieved from https://wordpress.clarku.edu/debrobertson/laboratory-protocols/algal-pigments.

Rodrigues-Sousa, A.E., Nunes., V.O.I. Muniz-Junior, A.B., Carvalho, J.C.M., Mejia-da-Silva, L.C., Salla, A. C. V., Margarites, A. C., Seibel, F. I., Holz, L. C., Brião, V. B., Bertolin, T. E. and Costa, J. A. V., 2016. Increase in the carbohydrate content of the microalgae *Spirulina* in culture by nutrient starvation and the addition of residues of whey protein concentrate. *Bioresource technology*, 209, pp. 133-141. DOI: https://doi.org/10.1016/j.biortech.2016.02.069.

Salgueiro, J. L., Perez, L., Maceiras, R., Sanchez, A. and Cancela, A., 2016. Bioremediation of wastewater using *Chlorella vulgaris* microalgae: Phosphorus and organic matter. *International Journal of Environmental Research*, 10(3), pp. 465-470. DOI: 10.22059/IJER.2016.58766.

Seo, Y. H., Do, J. M., Suh, H. S., Park, S.

B., and Yoon, H. S., 2024. Treatment of Swine Wastewater Using the Domestic Microalga *Halochlorella rubescens* KNUA214 for Bioenergy Production and Carotenoid Extraction. *Applied Sciences*, 14(24), pp. 11650. DOI: https://doi.org/10.3390/app142411650.

Sudhanthiran, M. C., & Perumalsamy, M. 2022. Bioremediation of dairy industry wastewater and assessment of nutrient removal potential of *Chlorella vulgaris*. Biomass Conversion and Biorefinery, 14, 10335–10346. DOI: https://doi.org/10.1007/s13399-022-03068-x.

Tayawi, A., Sisay, E., Beszédes, S., & Kertész, S. 2025. Wastewater treatment in the dairy industry from classical treatment to promising technologies: An overview. MDPI. Retrieved February 18, 2025, from Wikipedia summary.

Trenkenshu, R.P., 2005. Simplest models of microalgae growth, 2 queasy continuous culture. *Ecologia moray*, 67, pp. 98-110.

Yang, C., Liu, H., Li, M., Yu, C., and Yu, G., 2011. Treating urine by *Spirulina platensis*. *Acta Astronautica*. 63(7-10), pp. 1049–1054. DOI: https://doi.org/10.1016/j.actaastro.2008.03.008.

Zhang, P., Li, Z., Lu, L., Xiao, Y., Liu, J., Guo, J., and Fang, F., 2017. Effects of Stepwise Nitrogen Depletion on Carotenoid Content, Fluorescence Parameters, and the Cellular Stoichiometry of *Chlorella vulgaris*. *Spectrochimica Acta Part A: Molecular and Biomolecular Spectroscopy*, 181, pp. 30–38. DOI: https://doi.org/10.1016/j.saa.2017.03.022.

Production of Phycocyanin Natural Blue Dye of Algal Origin and Evaluation of Different Extraction and Purification Methods

Fariba Hokmollahi[1], Maryam Sadat Mirbagheri Firoozabad[2]* , **Hamid Sodaeizadeh[1], Amirhossein Nateghi[3]**

Abstract

Phycocyanin's potential as a natural dye is indeed promising, especially considering the harmful side effects associated with artificial food colors. Its high antioxidant properties make it a valuable ingredient in various industries, including food, pharmaceutical, and beauty. Phycocyanin, a blue pigment extracted from *Spirulina platensis*, is a phycobiliprotein known for its diverse pharmacological benefits. Its natural origin and functional properties make it a promising alternative to synthetic food colorants, and continued research into its applications may provide safer and healthier options for consumers. The comparison of the freeze-thaw and phosphate buffer extraction methods in this study sheds light on the efficiency and effectiveness of different extraction techniques for obtaining phycocyanin. The exploration of salt concentrations as a means to enhance purity index and product yield provides valuable insights into optimizing extraction processes. Additionally, the use of chitosan, activated charcoal, and sodium citrate for purification further demonstrates the importance of refining and purifying phycocyanin for various applications. Overall, the study's findings contribute to the understanding of extraction and purification methods for phycocyanin, offering potential strategies for improving the quality and yield of this natural pigment.

The outcomes of this research project indicate that the purity index of phycocyanin obtained through the freeze-thaw method surpasses that achieved via the phosphate buffer method. Moreover, the results from the sodium chloride salt method, when compared to the control, demonstrate that the purity of phycocyanin can be enhanced with increasing concentrations of salt, reaching up to1 M. Furthermore, activated charcoal has been identified as the most effective substance for phycocyanin purification, significantly enhancing the purity of the blue color among three purification methods evaluated, which include chitosan, activated charcoal, and sodium citrate. Under optimal conditions, the extracted phycocyanin exhibits the highest concentration of 5.12 mg/mL, a purity index of R: 1.17, and a production efficiency of 11.8%. Future studies should aim to scale up the optimized extraction and purification processes, eval-

Fariba Hokmollahi1, Maryam Sadat Mirbagheri Firoozabad2*, Hamid Sodaezade1, Amirhossein Nateghi3
1-Faculty of Natural Resources and Desert Study, Yazd University, Yazd, Iran
2-Department of Biology, Yazd University, Yazd, Iran
3-Department of Electrical Engineering, Cambridge University, Cambridge, UK
*Corresponding author email address: m.mirbagheri@yazd.ac.ir

uating the economic feasibility for industrial production, and evaluate the stability and functionality of the purified phycocyanin within specific food and cosmetic applications.

Keywords: Blue-green algae, *Spirulina platensis*, Purity index, Production efficiency

Introduction

The growing demand for natural ingredients has spurred the food, pharmaceutical, and cosmetic industries to seek alternatives to synthetic colorants (Ghosh et al., 2022). Microalgae represent a sustainable source of valuable natural pigments, including phycocyanin, astaxanthin, chlorophyll, and carotenoids. These pigments are not only safer but also offer enhanced health benefits derived from their antioxidant and anti-inflammatory properties, unlike their synthetic counterparts (Vinothkanna and Sekar, 2020; Mirbagheri Firoozabad and Nateghi, 2025). Furthermore, microalgae cultivation requires less water and land compared to conventional agriculture and can contribute reduce greenhouse gas emissions, positioning it as an environmentally friendly platform for producing high-value compounds (Omokaro et al., 2025). Among microalgae, the cyanobacterium *Spirulina platensis* is the primary commercial source of the natural blue pigment, C-phycocyanin (C-PC). *Spirulina* is a nutrient-dense organism, with a high protein content (up to 70% dry weight) and a rich profile of vitamins, minerals, and essential fatty acids, making it a popular

dietary supplement (Matufi et al., 2020). Beyond its nutritional value, *Spirulina* and its predominant pigment, C-PC, have been investigated for their therapeutic potential in treating chronic conditions such as cancer and immune diseases, largely due to their potent antioxidant and anti-inflammatory activities (Subramaiam et al., 2021; Vilahur et al., 2022).

C-PC is a phycobiliprotein, a class of brightly colored, fluorescent pigment proteins that constitute the light-harvesting phycobilisomes in cyanobacteria and red algae. These complexes are crucial for photosynthesis, as they absorb light energy and transfer it to reaction centers (Hsieh-Lo et al., 2019). Phycobiliproteins are categorized based on spectral properties; C-PC, the major phycobiliprotein in *Spirulina*, has a maximum absorbance between 610 and 620 nm (Payne et al., 2025) and can constitute up to 20% of the dry weight under optimal growth conditions (Chini Zittelli et al., 2022). This high abundance, combined with its unique color and fluorescence, makes C-PC highly valuable for applications in biotechnology, medicine, and as a natural colorant.

However, the commercial use of C-PC is limited by challenges in downstream processing. Efficient extraction and purification are crucial steps that directly influence the yield, purity, and cost of the final product. The tough cell wall of Spirulina requires effective disruption methods to release C-PC. Common techniques include freeze-thaw cycles, bead milling, homogenization, and chemical extraction. Each method has trade-offs: while freeze-thaw often produc-

es high-purity extracts, it is time-consuming and energy-intensive (Jaeschke et al., 2021). Mechanical methods such as bead milling, are quick but can co-extract impurities such as chlorophyll and cell debris, making subsequent purification more chalenging. Chemical extraction with buffers is simple but may yield dilute extracts with lower initial purity (Soto-Sierra et al., 2018; Ferreira-Santos et al., 2020; Zhang et al., 2015). Therefore, a purification step is necessary to achieve the high purity required for sensitive applications like pharmaceuticals. Techniques such as ammonium sulfate precipitation, chitosan treatment, and activated charcoal adsorption are used, but there is no consensus on their relative effectiveness. Importantly, no standardized protocol exists for extracting and purifying C-PC, as the best methods depend on the algal strain and product specifications. Thus, systematic comparisons are essential to develop efficient and scalable processes. This study aims to fill this gap by comparing the efficiency of freeze-thaw and phosphate buffer extraction methods for

obtaining C-PC from *Spirulina platensis*. It also evaluates three purification strategies—chitosan, activated charcoal, and sodium citrate treatment—to improve the purity and yield of the final product. The results will provide valuable insights for optimizing the downstream processing of C-PC, thereby facilitating its broader application as a natural blue colorant and nutraceutical.

Material and methods
Growth and culture conditions
Spirulina platensis was obtained from the Yazd University̓s algae bank and cultivated to generate sufficient biomass for analysis. The cyanobacterium was grown in a modified Zarrouk medium (pH ~9.5) with the following composition of the medium per liter of distilled water: 1.0 g $NaHCO_3$, 1.5 g K_2HPO_4, 1.5 g $NaNO_3$, 1.1 g urea, 1.15 g $FeSO_4$, 1.1 g $MgSO_4 \cdot 7H_2O$, 1.0 g NaCl, and 1.5 g K_2SO_4. For initial culture, 20–25 mL of *S. platensis* stock culture was inoculated into 1 L Erlenmeyer flasks containing autoclaved Zarrouk liquid medium (sterilized at

Fig. 1. Layers in freeze-thaw cycles

120 °C for 20 min) (Vonshak et al., 1982). Cultures were incubated at room temperature under a 12 hours' light to 12 hours' dark cycle. For large-scale biomass production, the culture was scaled up to a 70 L aquarium maintained under the same conditions. Biomass was harvested during the final growth phase for subsequent extraction procedures.

Optimization of extraction procedures

Freeze-Thaw extraction

The efficacy of repeated freeze–thaw cycles for extracting C-phycocyanin (C-PC) from *S. platensis* was investigated. This method disrupts cells through the formation and melting of intracellular ice crystals (D'hondt et al., 2017). Harvested biomass was mixed with distilled water at a 5:1 water-to-biomass ratio (w/w). To determine the optimal freezing duration, two freezing times were tested: 3 h and 24 h. Based on the results of this initial test, a 3-hour freezing period was selected for further optimization. Subsequently, the impact of adding salt to the slurry was evaluated by testing 0.7 M and 1 M salt concentrations, alongside a salt-free control. Following the cycles, samples were centrifuged at 5,000 rpm for 15 min to pellet cell debris (Figure 1). The supernatant was then collected, and its absorbance was measured spectrophotometrically within a range of 200–700 nm using a spectrophotometer (Analytik Jena 210, Germany) to determine C-PC concentration and purity. The optimal freeze–thaw condition was selected based on the highest yield and purity of C-PC (Figure 1).

Phosphate buffer extraction

C-PC was also extracted using phosphate buffer, which facilitates cell wall disruption and dissolution of water-soluble phycobilins. A sterile phosphate buffer solution was prepared and autoclaved. Subsequently, 3 g of dry *S. platensis* powder was dissolved in 100 mL of this buffer. The mixture was agitated at 150 rpm for three hours to facilitate extraction (Oliveira et al., 2008).

Purification

Crude extracts from both methods were clarified by filtration through 20-μm filter paper followed by centrifugation at 14,000 rpm for 20 minutes. The clarified extracts were then purified using one of three methods: chitosan flocculation, activated charcoal, and sodium citrate precipitation (Figure 2).

Fig. 2. Removing cell debris via filter paper

Chitosan flocculation

Chitosan was added to the clarified extract at a final concentration of 0.5% (v/v) and incubated for 20 min. The mixture was magnetically stirred at 4 °C for 20 min and then centrifuged at 8,000 rpm for 15 min at 4 °C. The resulting supernatant was analyzed by spectrophotometry between 200–700 nm (Fekrat et al., 2019).

Activated charcoal treatment

This procedure mirrored the chitosan method. but it used 10 mL of extract with 5% (w/v) activated carbon. This treatment was noted to enhance the chromatic properties of the solution (De Matos Fernandes et al., 2010).

Sodium citrate precipitation

Sodium citrate was added to a phycocyanin solution at a concentration of 0.5 g per 100 mL. Acting as a stabilizer and chelating agent, sodium citrate enhances the refinement of phycocyanin. The mixture was centrifuged at 4,500 rpm to remove impurities, resulting in a concentrated and purified product in the supernatant (Mogany et al., 2019).

Drying methods

Purified phycocyanin was subjected to three drying methods to assess their impact on stability and yield. These methods included freeze-drying, cold drying (conducted in a refrigerated, dark setting), and oven drying at 35 °C. The phycocyanin content and purity index of each dried sample were measured and compared. The cold-drying process required approximately two days to achieve complete desiccation (Kuhnholz et al., 2024).

Analytical procedures

The concentration and purity of phycocyanin during all extraction and purification stages were measured using a spectrophotometer scanning from 200-700 nm. The C-PC concentration (mg/mL) was calculated using the equations below (Bennett et al., 1973):

$$C - PC = \frac{OD_{620} - 0.474\, OD_{652}}{5.34}$$

The purity index was calculated as the ratio of the absorbance at 620 nm to that at 280 nm.

Purity= OD_{620} /OD_{280}

The extraction yield of phycocyanin (mg/g dry biomass) is calculated using the formula stablished by Silveira et al. (2007).

$$Yield = \frac{(C - PC)V}{DB}$$

Where V represents the volume of the solvent (mL) and DB is the mass of the dry biomass (g).

Results

The optimization of the freeze-thaw extraction process identified a three-hour freezing period combined with three complete freeze-thaw cycles in the presence of sodium chloride (NaCl) as the most effective protocol. This study evaluated the impact of NaCl concentration on phycocyanin purity by comparing 1 M and 0.7 M solutions to a salt-free control. The results show that the inclusion of salt significantly enhanced phycocyanin purity compared to the control. Furthermore, a higher NaCl concentration (1 M) yielded a product with greater purity of phycocyanin compared to the lower concentration (0.7 M), which has a purity index of 0.94. The extract obtained using the 1 M NaCl protocol exhibited an intense blue col-

or and achieved the highest purity index of 1.17 (Fig. 3). The control showed a purity index of 0.77.

Comparison of salt concentrations

The optimal process involved three freeze-thaw cycles (freezing at -20°C and thawing at 4°C) using a 1 M NaCl solution, which yielded the highest purity index (Figure 4). The purity of phycocyanin extracted under different conditions is detailed in Figure 5.

Comparison of phycocyanin purification methods

Three purification methods activated charcoal, sodium citrate, and chitosan- were evaluated. Among these, activated charcoal treatment was the most effective, resulting in the greatest increase in phycocyanin pu-

rity (Fig. 5).

A comprehensive summary of all techniques is shown in Table 1. The combined freeze–thaw and sodium citrate purification method achieved a high purity index of 1.03. However, the most effective method for obtaining high-purity phycocyanin was freeze-thaw with 1 M NaCl solution, which yielded a purity index of 1.17 at a concentration of 3.8 mg/mL, though with an extraction efficiency of 6%. In terms of production yield, the phosphate buffer extraction method followed by a combined chitosan and activated charcoal purification step was most effective. This method achieved a higher concentration (3.54 mg/mL) and extraction efficiency (11.8%), although with a lower purity
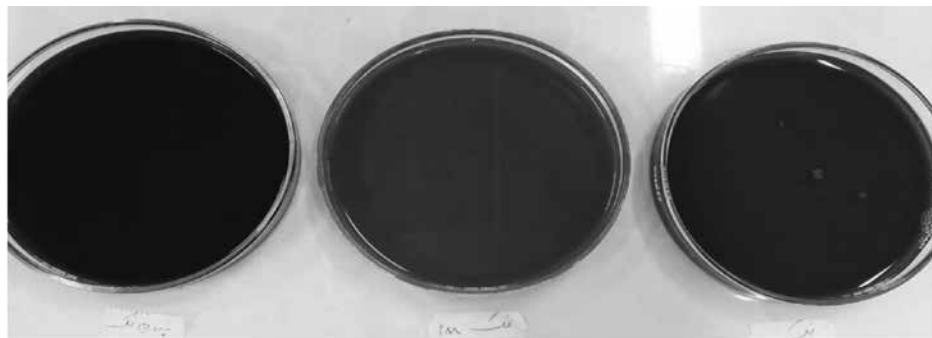

Fig. 3. A: Phycocyanin extraction without salt, B: Extraction with 1M salt, and C: extraction with 0.7M salt
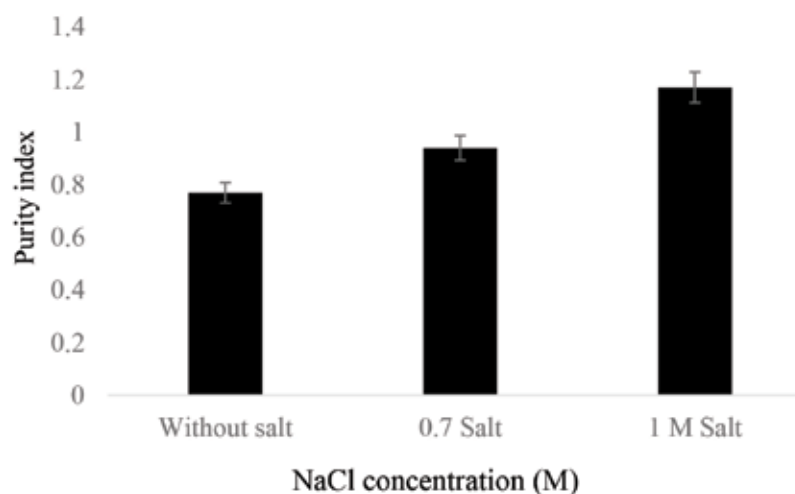

Fig. 4. Purity index of phycocyanin after centrifugation in different NaCl concentrations by the freeze-thaw method

index of 0.64. This finding is consistent with previous studies indicating that chitosan and activated charcoal can enhance phycocyanin purity index (Fekrat et al., 2019).

Comparison of drying methods

Analysis of the purity index showed that freeze-drying (vacuum lyophilization) was the most effective method, producing the highest quality powder with an R-value of 0.60. Refrigeration and oven drying resulted in lower purity levels, with R-values of 0.51 and 0.41, respectively (Fig. 6). Therefore, for optimal dry powder production, lyophilization is the preferred method.

In summary, the most effective protocol identified was a triple freeze-thaw extraction using a 1 M sodium chloride solution, which achieved a purity index of 1.17. The purity of phycocyanin can be further improved after extraction with activated charcoal, with the optimal treatment (5% w/v) resulting in a purity index of 1.06. For final powder
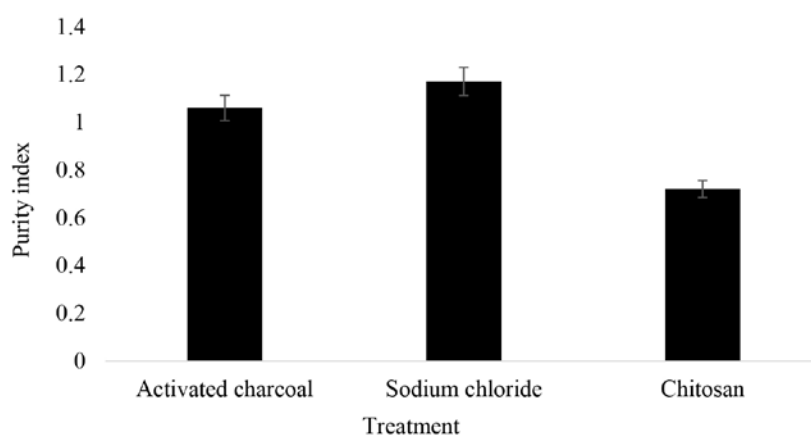

Fig. 5. Purity index of results of three phycocyanin purification methods, including activated charcoal, sodium citrate, and chitosan

Table 1. Evaluating the purity index, concentration, and production efficiency of different extraction and purification methods

Extraction	Purification	Purity Index	Concentration (mg/ml)	Product (Yield)
Freeze-thaw	–	0.77	3.6	45 mg/g Efficiency: 4.5%
Freeze-thaw	Activated charcoal and chitosan	0.78	5.12	80 mg/g Efficiency: 8%
Freeze-thaw	Sodium chloride	1.17	3.8	60 mg/g Efficiency: 6%
Freeze-thaw without sodium chloride	Chitosan	0.72	3.8	76 mg/g Efficiency: 7.6%
Freeze-thaw without sodium chloride	Activated charcoal	1.06	3.8	76 mg/g Efficiency: 7.6%
Freeze-thaw without sodium chloride	Sodium citrate	1.03	3.8	45 mg/g Efficiency: 7.6%
Phosphate buffer	–	0.58	1.69	33.56 mg/g Efficiency: 5.63%
Phosphate buffer	Activated charcoal and chitosan	0.64	3.54	118 mg/g Efficiency: 11.8%

production, lyophilization is recommended. This study successfully established a method to achieve a high purity index (R: 1.06), though further studies could potentially improve color purity even more.

Discussion

Phycocyanin, a blue pigment derived from blue-green algae like *Spirulina*, is well-known for its fluorescence and antioxidant properties. This phycobiliprotein can be extracted using various cell wall disruption techniques, but the cost of obtaining and purifying phycocyanin remains a significant challenge due to the complex purification processes involved. Currently, there is no universally accepted method for isolating and purifying phycocyanin, which highlights the need for cost-effective techniques that can produce sufficient quantities of phycocyanin for various applications in healthcare and manufacturing.

Numerous extraction techniques have been used in both industrial and laboratory settings, including ultrasound, high hydrostatic pressure, ultracentrifugation, ultra-homogenization, and extraction with water, organic solvents, and inorganic solvents. Among these methods, the use of water for separation of the cell membrane is widely practiced in global industries. This process involves sequential freezing and thawing of *Spirulina* in a liquid solution to disrupt the cell membrane (Mirbagheri Firoozabad and Nateghi, 2025). The most effective method for extracting and purifying phycocyanin, in terms of achieving the highest concentration and purity index, was found to be the freeze–thaw technique combined with a 1 M sodium chloride solution. This method yielded a purity index of 1.17, a concentration of 3.8 mg/ml, and an extraction efficiency of 6%, outperforming other techniques and therefore recommended for obtaining high-quality phycocyanin. This research is comparable to that of Ameri et al. (2018), and the purity of phycocyanin obtained by the freeze-thaw method is very similar in both studies, with the yield increasing to 60 mg/g in this study. Further research shows that the freeze-thaw technique, combined with a 1 M Tris-HCl buffer, yields about 11.34% of dry cell weight in phycocyanin, which is a significantly higher amount compared to previous
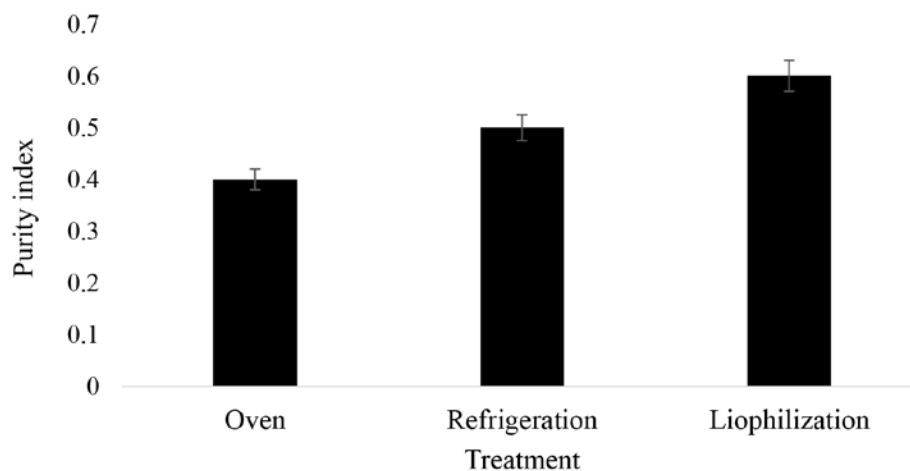

Fig. 6. Purity index of results of phycocyanin drying methods

studies (Pispas et al., 2024). It is recommended that this buffer be used as a lysis buffer for extracting of phycocyanin from Spirulina. Additionally, research suggests that enzyme treatment may be more effective than freeze-thaw methods or mineral solvents for extracting phycocyanin, and its use is recommended for future studies (Safari et al., 2020). Based on the research by Kumar et al. (2014), it is also suggested to use dialysis membranes and anion exchange chromatography to increase the purity to 2.93 and 4.58, respectively. Future studies should focus on scaling up the optimized extraction and purification process, evaluating the economic feasibility for industrial production, and assessing the stability and functionality of the purified phycocyanin in specific food and cosmetic matrices.

References

Ameri, M., Gord-Noshahri, N., Ghazi-Birgandi, R. and Jalali Ghassam, B., 2018. Evaluation of different extraction methods for phycocyanin extraction from *Spirulina platensis*. *Plant, Algae, and Environment*, *2*(2), pp.211-217. https://plagen.sbu.ac.ir/article_99092_8c00b-9b1983eb9f07bee5c9c25c92ccd.pdf.

Bennett, A. and Bogorad, L., 1973. Complementary chromatic adaptation in a filamentous blue-green alga. *The Journal of Cell Biology*, *58*(2), pp.419-435. DOI: 10.1083/jcb.58.2.419.

Chini Zittelli, G., Mugnai, G., Milia, M., Cicchi, B., Benavides, A. S., Angioni, A., & Torzillo, G. 2022. Effects of blue, orange, and white lights on growth, chlorophyll fluorescence, and phycocyanin production of *Arthrospira platensis* cultures. *Algal Research*, 61, 102583. DOI: org/10.1016/j.algal.2021.102583.

Posadas, E., Alcántara, C., García-Encina, P.A., Gouveia, L., Guieysse, B., Norvill, Z., Acién, F.G., Markou, G., Congestri, R., Koreiviene, J. and Muñoz, R., 2017. Microalgae cultivation in wastewater. In *Microalgae-based biofuels and bioproducts* (pp. 67-91). Woodhead Publishing. DOI: 10.1016/B978-0-08-101023-5.00006-6.

De Matos Fernandes SC. 2010. Novel materials based on chitosan, its derivatives, and cellulose fibres. PhD thesis. Universidade de Aveiro (Portugal).

Doke Jr, J.M., 2005. An improved and efficient method for the extraction of phycocyanin from *Spirulina* sp. *International Journal of Food Engineering*, *1*(5). Doi: 10.2202/1556-3758.1037.

Fekrat, F., Nami, B., Ghanavati, H., Ghaffari, A. and Shahbazi, M., 2019. Optimization of chitosan/activated charcoal-based purification of *Arthrospira platensis* phycocyanin using response surface methodology. *Journal of Applied Phycology*, *31*(2), pp.1095-1105. DOI: 10.1007/s10811-018-1626-8.

Ferreira-Santos, P., Nunes, R., De Biasio, F., Spigno, G., Gorgoglione, D., Teixeira, J.A. and Rocha, C.M., 2020. Influence of thermal and electrical effects of ohmic heating on C-phycocyanin properties and biocompounds recovery from *Spirulina platensis*. *Lwt*, *128*, p.109491. Doi: 10.1016/j.lwt. 2020.109491.

Ghosh, S., Sarkar, T., Pati, S., Kari, Z. A., Edinur, H. A., and Chakraborty, R. 2022. Novel bioactive compounds from marine sources as a tool for functional food development. *Frontiers in Marine Science*, 9, 832957. DOI: 10.1016/j. lwt.2021.112527.

Hsieh-Lo, M., Castillo, G.; Ochoa-Becerra, M.A.; Mojica, L. 2019. Phycocyanin and phycoerythrin: Strategies to improve production yield and chemical stability. *Algal Research*, 42, 101600. DOI: 10.1016/j.algal.2019.101600.

Jaeschke DP, Teixeira IR, Marczak LDF, Mercali GD. 2021. Phycocyanin from *Spirulina*: A review of extraction methods and stability. *Food Research International,* 143:110314. Doi: 10.1016/j. foodres. 2021.110314.

Kuhnholz J, Glockow T, Siebecke V, Le AT, Tran L-D, Noke A. 2024. Comparison of different methods for the extraction of phycocyanin from the cyanobacterium *Arthrospira maxima* (*Spirulina*). *Journal of Applied Phycology*, 1-11. DOI: 10.1007/s10811-024-03224-y.

Kumar, D., Dhar, D.W., Pabbi, S., Kumar, N. and Walia, S., 2014. Extraction and purification of C-phycocyanin from *Spirulina platensis* (CCC540). *Indian Journal of Plant Physiology*, *19*(2), pp.184-188. Doi: 10.1007/s40502-014-0094-7.

Matufi F., and Choopani A. 2020. *Spirulina*, food of the past, present, and future. *Health Biotechnology and Biopharma*, 3(4): 1-20. DOI: 10.22034/HBB.2020.26.

Mirbagheri Firoozabad, M.S., and Nateghi, A.H., 2025. Microbial Production of Phycocyanin. In *Microbial Production of Food Bioactive Compounds* (pp. 1-19). Cham: Springer Nature Switzerland. DOI: 10.1007/978-3-030-81403-8_61-1.

Mogany, T., Kumari, S., Swalaha, F.M., and Bux, F., 2019. Extraction and characterisation of analytical grade C-phycocyanin from *Euhalothece* sp. *Journal of Applied Phycology*, *31*(3), pp.1661-1674. Doi: 10.1007/s10811-018-1661-5.

Oliveira EGd, Rosa GSd, Moraes MAd, Pinto LAdA. 2008. Phycocyanin content of *Spirulina platensis* dried in a spouted bed and thin layer. *Journal of Food Process Engineering*; 31(1):34-50. DOI: 10.1111/j.1745-4530.2007.00143.x.

Omokaro, G.O., Nafula, Z.S., Iloabuchi, N.E., Chikukula, A.A., Osayogie, O.G., and Nnoli, E.C., 2025. Microalgae as Biofactories for Sustainable Applications: Advancing Carbon Sequestration, Bioenergy, and Environmental Remediation. *Sustainable Chemistry for Climate Action*, p.100098. DOI: 10.1016/j. scca.2025.100098.

Payne, E.J.R., Griffiths, M., Harrison, S.T.L., and FaganEndres, M.A. 2025. A summary and critique of the various spectrophotometric methods used to quantify C-phycocyanin concentration. *Journal of Applied Phycology*, 37, 727–734. DOI: 10.1007/s10811-025-03474-4.

Pispas, K.; Manthos, G.; Sventzouri, E.; Geroulia, M.; Mastropetros, S.G.; Ali, S.S.; Kornaros, M. 2024. Optimizing phycocyanin extraction from cyanobacterial biomass: a comparative study of freeze–thaw cycling with various solvents. *Marine Drugs,* 22, 246. DOI: 10.3390/md22060246.

Safari R., Raftani Amiri Z., and Esmaeilzadeh Kenari R. 2020. Antioxidant and antibacterial activities of C-phycocyanin from the common name *Spirulina platensis*. *Iranian Journal of Fisheries Sciences*, 19(4) 1911-1927. Doi: 10.22092/ijfs.2019.118129.

Silveira ST, Burkert JFdM, Costa JAV, Burkert CAV, Kalil SJ. 2007. Optimization of phycocyanin extraction from *Spirulina platensis* using factorial design. *Bioresource Technology*, 98: 1629-1634. DOI: 10.1016/j.biortech.2006.05.050.

Soto-Sierra, L., Stoykova, P. and Nikolov, Z.L., 2018. Extraction and fractionation of microalgae-based protein products. *Algal research*, 36, pp.175-192. DOI 10.1016/j.algal.2018.10.023.

Subramaiam, H., Chu, W.L., Radhakrishnan, A.K., Chakravarthi, S., Selvaduray, K.R. and Kok, Y.Y., 2021. Evaluating anticancer and immunomodulatory effects of spirulina (Arthrospira) platensis and gamma-tocotrienol supplementation in a syngeneic mouse model of breast cancer. *Nutrients*, 13(7), p.2320. DOI: 10.3390/nu13072320.

Vilahur, G., Sutelman, P., Ben-Aicha, S., Mendieta, G., Radiké, M., Schoch, L., Casaní, L., Borrell-Pagés, M., Padro, T. and Badimon, L., 2022. Supplementation with spirulina reduces infarct size and ameliorates cardiac function in a pig model of STEMI. *Frontiers in Pharmacology*, 13, p.891801.

Vinothkanna, A. and Sekar, S., 2020. Diagnostic applications of phycobiliproteins. In *Pigments from microalgae handbook* (pp. 585-610). Cham: Springer International Publishing.

Vonshak, A., Abeliovich, A., Boussiba, S., Arad, S. and Richmond, A., 1982. Production of Spirulina biomass: effects of environmental factors and population density. *Biomass*, 2(3), pp.175-185. DOI: 10.1016/0144-4565(82)90028-2.

Zhang, X., Zhang, F., Luo, G., Yang, S. and Wang, D., 2015. Extraction and separation of phycocyanin from Spirulina using aqueous two-phase systems of ionic liquid and salt. *Journal of Food and Nutrition Research*, 3(1), pp.15-19. DOI: 10.12691/jfnr-3-1-3.

Differential Modulation of Biomass Productivity and Fatty Acid Composition in *Dunaliella salina* by Salinity and Nutrient Stress

Mohammad Roozitalab[1], Gilan Attaran-Fariman*[1] ⬤ **, Hasan Zadabbas Shahabadi[1,2]**

Abstract

Dunaliella salina, a microalga renowned for its production of bioactive compounds, holds significant potential for biofuel generation. This study investigated the interactive effects of salinity and nutrient availability on the growth kinetics, biomass yield, total lipid content, and fatty acid composition of a *D. salina* strain isolated from the southern coast of Iran. The microalga was cultivated under three distinct salinity levels (35, 70, and 105 g/L), each supplemented with varying concentrations of nitrate (100%, 50%, 25%) and glucose (1, 2, and 3 g/L). The highest biomass yield (1449 mg/L) was achieved at the lowest salinity (35 g/L) when supplemented with 3 g/L glucose. Notably, the average biomass production across various nutrient treatments at 70 g/L salinity surpassed that observed at the other salinities. While alterations in nutrient concentrations did not significantly impact the overall lipid content ($P \geq 0.05$), the highest lipid accumulation was observed at the highest salinity (105 g/L). However, the lipid productivity at 35 g/L with 3 g/L glucose was superior due to the substantially higher biomass yield. Saturated Fatty Acids (SFAs) dominated the fatty acid profiles, ranging from 41% to 73% of the total fatty acids, whereas Polyunsaturated Fatty Acids (PUFAs) varied between 2% and 40%. Palmitic acid (C16:0) consistently represented the most abundant individual fatty acid (13-44%) across all treatments. The maximum accumulation of SFAs was observed at 70 g/L salinity. The findings of this study demonstrate the significant influence of salinity and nutrient regimes on the biomass and lipid characteristics of the Iranian *D. salina* isolate, suggesting its potential as a promising feedstock for biofuel production.

Keywords: *Dunaliella salina,* Biomass Production, Biofuel Feedstock, Fatty acids, Salinity Stress, Nutrients, Glucose Supplementation

Introduction

Microalgae represent a promising and abundant source of diverse biogenic materials, attracting significant attention across various biotechnology research domains. The inceasing global production of carbon dioxide, as represent by the Intergovernmental Panel on Climate Change

(IPCC) indicated that fossil fuel and industrial CO_2 emissions averaged approximately 36 ± 2.9 $GtCO_2$ per year from 2010 to 2019, reaching in around 38 ± 3 $GtCO_2$ in 2019 (IPCC, 2022). More recent estimates from the International Energy Agency (IEA) indicate that energy-related CO_2 emissions reached a record 37.4 $GtCO_2$ in 2023 and approximately 37.8 $GtCO_2$ in 2024 (IEA, 2024a; IEA, 2025), posing a critical environmental challenge. Furthermore, the absorption of approximately 30% of anthropogenic carbon dioxide by ocean waters leads to detrimental ocean acidification, with devastating consequences for marine ecosystems, including coral reef degradation and biodiversity loss (Mata et al., 2010). In this context, biofuels derived from renewable sources offer a compelling alternative to fossil fuels due to their lower environmental impact (Scragg et al., 2003; Deora et al., 2023). Microalgae have the potential to absorb approximately 513 tons of CO_2 per hectare per year, corresponding to an annual yield of around 280 tons of dry biomass per hectare, under optimal solar conditions as reported by Bhola et al. (2014). Given that flue gases contain CO_2 concentrations ranging from 3% to 30%, a critical factor for successful biofixation is the precise selection of algae species capable of thriving and efficiently absorbing CO_2 at such elevated levels (Iglina et al., 2022).

The key factor governing the economic viability of biodiesel production from microalgae is the efficiency of lipid accumulation (Pacheco et al., 2017). While certain microalgal species exhibit high intracellular lipid content, their slow growth rates can result in overall low lipid productivity (Chu, 2012). Notably, the growth rate, biomass yield, and the qualitative and quantitative composition of fatty acids in microalgae are species-specific and are also significantly modulated by prevailing environmental conditions (Mata et al., 2013; Rios et al., 2016; Pacheco et al., 2017; Hopkins et al., 2019; Morales et al., 2020). Some microalgal taxa are rich in polyunsaturated fatty acids (PUFAs), valuable for various applications, while others accumulate significant amounts of triglycerides, readily convertible to biofuel (Bougaran et al., 2012). Enhancing the overall efficiency of fatty acid production necessitates optimizing both biomass accumulation and cellular lipid content (Mairet et al., 2011; Shokravi et al., 2020).

The genus *Dunaliella* comprises halotolerant microalgae capable of thriving in high salinity environments through sophisticated physiological mechanisms involving glycerol production and ion regulation (Thompson Jr., 1996). Within this genus, species exhibit considerable variability in lipid content and biomass production in response to diverse environmental cues (Hopkins et al., 2019). Specifically, *Dunaliella salina* (Dunal) Teodoresco is recognized as a promising source for the production of various bioactive compounds (Truc et al., 2017).

This study aimed to elucidate the combined effects of varying salinity levels and nitrate concentrations, as well as glucose supplementation (to induce mixotrophic growth), on the growth rate, biomass yield, total lipid content, and fatty acid profile of *Dunaliella salina* over a defined cultivation period.

The findings of this research contribute to a better understanding of the physiological responses of this microalgal species to key environmental factors relevant for optimizing its potential in biofuel and other biotechnological applications.

Material and methods

Microalgal strain and culture maintenance

The microalgal strain *Dunaliella salina* (=*Dunaliella bardawil*) used in this study was obtained from the culture collection of Chabahar Maritime University, Iran. This isolate was originally sourced from the northern coast of the Oman Sea (Iranian coast, Lipar region; pink lagoon) and identified through gene sequencing, with its sequence data deposited in GenBank under the accession number JX524863. Stock cultures were maintained axenically in f/2 culture medium (Guillard and Ryther, 1962) under controlled laboratory conditions, including a temperature of 25 ± 1 °C, a light intensity of 100 µmol photons m^{-2} s^{-1} with a photoperiod of 12:12 h light: dark, and continuous aeration with filter-sterilized air.

Experimental design and culture conditions

This study employed a factorial experimental design to investigate the individual and interactive effects of three salinity levels, three nitrate concentrations, and three glucose concentrations on the growth, biomass yield, total lipid content, and fatty acid composition of *D. salina*. Each treatment combination was conducted in triplicate over a 14-day cultivation period.

Three salinity levels were established by adjusting the f/2 culture medium to 35 g/L (representing standard seawater salinity), 70 g/L (two-fold seawater salinity), and 105 g/L (three-fold seawater salinity). Natural sea salt sourced from the Oman Sea was utilized to elevate the salinity of the base f/2 medium. To examine the effects of nitrate availability, sodium nitrate ($NaNO_3$) in the f/2 culture medium was adjusted to 25%, 50%, and 100% of the standard protocol, and these treatments were applied under all salinity conditions. For the mixotrophic growth conditions, glucose ($C_6H_{12}O_6$) was supplemented at concentrations of 1, 2, and 3 g/L to the culture medium at each salinity level and nitrate concentration.

All microalgal cultures were maintained in 250 mL Erlenmeyer flasks under controlled *in vitro* conditions, including a 12:12 h light: dark photoperiod, a constant temperature of 24 ± 1 °C, and continuous aeration with filter-sterilized air.

Statistical analyses were performed using SPSS software. The normality of the data was assessed using the Shapiro-Wilk test. Significant differences between treatment groups were determined using one-way and two-way Analysis of Variance (ANOVA), followed by Duncan's post-hoc test for pairwise comparisons. A significance level of $P < 0.05$ was used for all statistical analyses.

Assessment of Growth

Microalgal growth was monitored every 48 hours throughout the 14-day cultivation period. This 14-day duration was chosen because the growth curve observed in the preliminary assessment suggested that growth would plateau after this point. For the experimental setups, cultures were initiated by inoculating the stock culture at a 1:10 dilution. This dilution ratio was adjusted according to

the initial cell density of each treatment.

At each sampling time, aliquots were aseptically withdrawn from the culture flasks and initially assessed microscopically (Nikon ECLIPSE 50i light microscope) to verify cell viability and overall culture health. Subsequently, the samples were fixed with a 2% (w/v) Lugol's iodine solution to immobilize the cells for enumeration. Cell density was determined using a Neubauer counting chamber (Marienfeld GMBH and Co., Germany) following standard hemocytometry procedures. Cell counts were performed in triplicate for each culture flask at each time point, and the average cell density (cells/mL) was calculated. During the exponential growth phase an increase in cell density, from N_0 to N_1, can be utilized to determine the specific growth rate (μ). The specific growth rate is defined as below.

$$\mu \ (day^{-1}) = Ln \ N_1 - Ln \ N_0 / t_1 - t_0$$

N_0 represents the initial cell density at time t_0, and N_1 represents the cell density at a later time (Moheimani et al., 2013). Growth curves were then generated by plotting cell density against time.

Evaluation of biomass, total lipid content, and fatty acid composition

Biomass determination

At the termination of the 14-day cultivation period, biomass production was determined gravimetrically. Aliquots of the microalgal cultures were transferred to pre-weighed centrifuge tubes (W_1) and centrifuged at 4000 rpm for 15 minutes to pellet the cells. The resulting microalgal pellets were washed twice with distilled water to remove residual salts from the culture medium. The centrifuge tubes containing the washed bio-

mass were then transferred to a freeze dryer (JFD 2L, JAL TEB, Iran) and lyophilized at -30 °C for 24 hours to ensure complete removal of moisture (Talebi et al., 2013). Following lyophilization, the tubes were re-weighed (W_2), and the dry weight biomass concentration (mg/L) was calculated by subtracting the initial weight of the tube (W_1) from the final weight (W_2) and normalizing to the volume of the initial culture sample.

Total lipid extraction

Total lipids were extracted from the freeze-dried algal biomass using a modified Bligh and Dyer method (Bligh and Dyer, 1959; Nigam et al., 2011). Briefly, approximately 100 mg of lyophilized algal biomass was transferred to a glass vial, and 3 mL of a 1:2 (v/v) methanol/chloroform solution was added. The mixture was then agitated on a magnetic stirrer at 25 °C for 18 hours to facilitate lipid solubilization. Subsequently, the mixture was centrifuged at 2000 rpm for 3 minutes to separate the phases. The chloroform layer, which contains the extracted lipids, was carefully transferred to a pre-weighed glass test tube. The solvent was then evaporated under a gentle stream of nitrogen gas within a fume hood, and the sample was dried in an oven at 80 °C for 2 hours to ensure complete solvent removal. After drying, the test tubes containing the total lipids were re-weighed, and the total lipid content was expressed as a percentage of the dry weight biomass.

Fatty acid methyl ester (FAME) preparation and analysis

The fatty acid composition of the *D. salina* biomass was determined using a direct trans-esterification method to yield fatty

acid methyl esters (FAMEs) (Talebi et al., 2013). Briefly, approximately 8 mg of lyophilized algal biomass was placed in a glass vial, and 300 µl of extract buffer was added. The mixture was then incubated at 75 °C for 2 hours to facilitate the trans-esterification reaction. Following incubation, 300 µL of a 0.9% (w/v) sodium chloride (NaCl) aqueous solution and 300 µL of n-hexane were added to the mixture, and the resulting solution was vigorously vortexed. The samples were then centrifuged at 5000 rpm at 20 °C for 3 minutes to achieve phase separation. The upper hexane layer, containing the extracted FAMEs, was carefully transferred to a clean gas chromatography (GC) vial for analysis. FAME analysis was performed using a Shimadzu GC-2014 gas chromatograph equipped with a flame ionization detector (FID) and a BPX70 capillary column (25 m × 0.22 mm internal diameter, 0.25 µm film thickness). Nitrogen was used as the carrier gas at a constant flow rate of 1.0 mL/min. Fatty acid methyl esters were identified by comparing their retention times to those of a commercially available fatty acid methyl ester standard (FAMQ-005, Accu Standard, USA). The relative abundance of each fatty acid was expressed as a percentage of the total identified fatty acids.

Results

Growth rate analysis

Figure 1 illustrates the growth curves of *Dunaliella salina* cultivated at three salinity levels (35, 70, and 105 g/L) under varying nitrate and glucose concentrations over a 14-day culture period. At the lowest salinity of 35 g/L (Fig. 1A), the highest cell density (6.42 × 10^6 cells/mL) was observed in cultures supplemented with 3 g/L glucose, surpassing those with lower glucose concentrations. A notable increase in cell density was observed after 4 days of cultivation across all nutrient treatments at this salinity. At 70 g/L salinity (Fig. 1B), the maximum cell density achieved was 6.49 × 10^6 cells/mL in the culture containing 2 g/L glucose on day 8. Furthermore, at this salinity, no statistically significant differences (P ≥ 0.05) were observed in the maximum cell densities achieved across the different nitrate concentrations when glucose was held constant. In contrast, growth was significantly inhibited at the highest salinity of 105 g/L (Figure 1C). The maximum cell density observed at this salinity level (1.54 × 10^6 cells/mL) was recorded in the treatment that included 1 mg/L nitrate. Notably, at a concentration of 105 g/L, the addition of glucose did not significantly alter cell density when compared to cultures with varying nitrate concentrations. Moreover, microalgal growth was minimal during the initial 4 days of cultivation at this high salinity, followed by a gradual increase in cell density.

Biomass production

The highest biomass yield (1449 mg/L) across all treatments was observed at a salinity of 35 g/L in the mixotrophic cultures supplemented with 3 g/L glucose. However, the average biomass production across all nutrient treatments was higher at a salinity of 70 g/L compared to both 35 g/L and 105 g/L (Fig. 2). At 70 g/L, the maximum biomass yield (1150 mg/L) was achieved with 1 g/L glucose supplementation. In contrast, biomass production was significantly re-

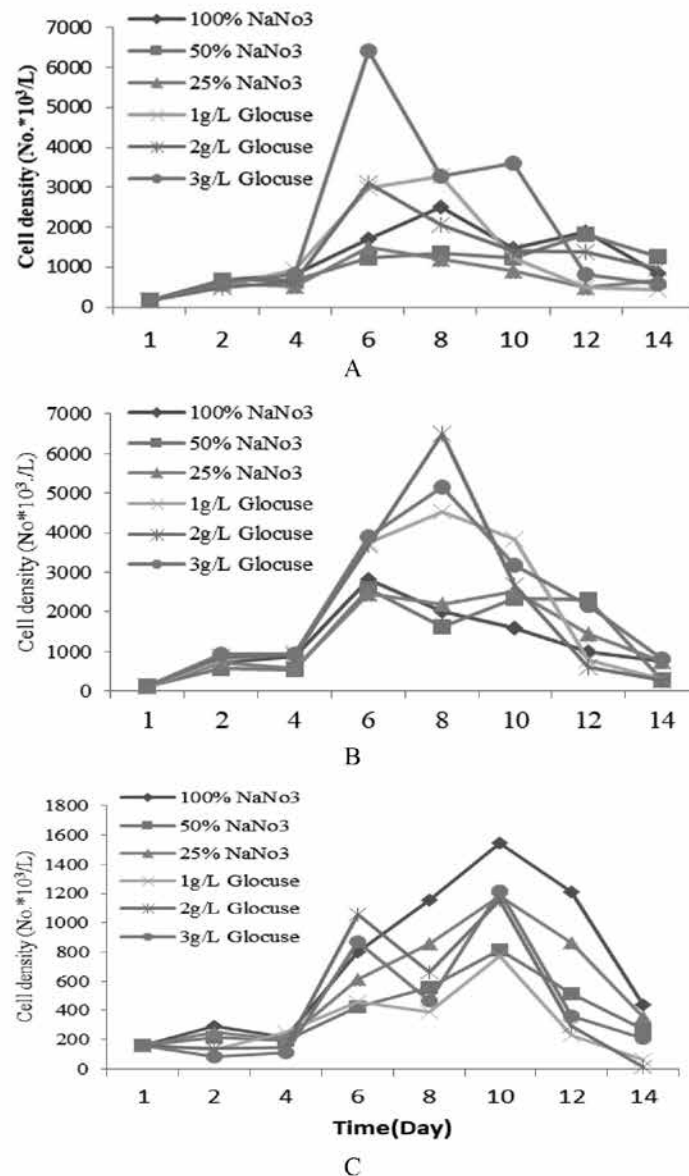**Fig. 1** Growth rate of *D. salina* at salinities; (A) 35 g/L, (B) 70 g/L, and (C) 105 g/l affected by nutrients
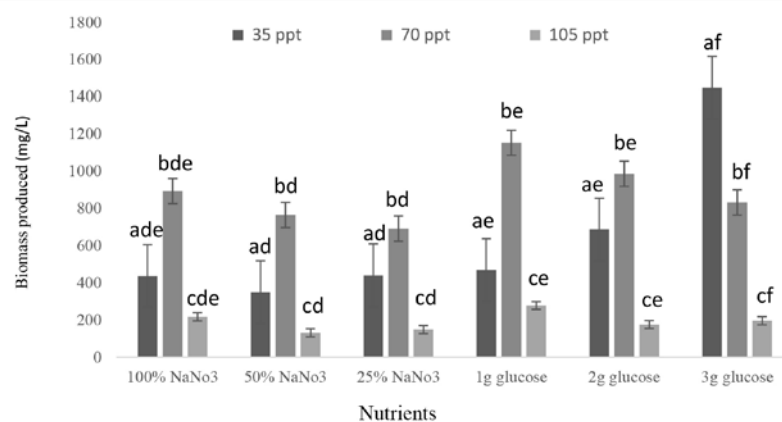

Fig. 2. Biomass yield (mg/L) of *D. salina* after 14 days of cultivation under varying salinity and nutrient concentrations; (Similar letters indicate no significant difference. (Duncan 0.05); a,b,c: represents the salinity effect; d,e,f: represents the effect of nutrients)

duced at the highest salinity of 105 g/L. Two-way ANOVA revealed a statistically significant effect of both nutrient composition and salinity on the biomass yield of *D. salina*. Furthermore, a significant interaction between nutrient composition and salinity was observed, indicating that the effect of nutrients on biomass yield varied depending on the salinity level (Supp. Table 1)

The average biomass yield at 70 g/L (912.5 mg/L) was notably higher than at 35 g/L (638 mg/L) and 105 g/L (191 mg/L). While a slight decrease in biomass was observed with decreasing nitrate concentrations (Fig. 3), this trend was not statistically significant (P ≥ 0.05). Conversely, in cultures supplemented with glucose, biomass yield increased from an average of 616 mg/L at 1 g/L glucose to 825 mg/L at 3 g/L glucose. This increase was statistically significant only at the 3 g/L glucose concentration (P ≤ 0.05).

One-way ANOVA further elucidated the effect of glucose at each salinity level. At 35 g/L, biomass production varied significantly with different glucose concentrations (P = 0), with the highest average biomass (1449 mg/L) observed at 3 g/L glucose (supp. Table 1). At 70 g/L, the average biomass produced in glucose-supplemented treatments (1044

mg/L) did not differ significantly (P ≥ 0.05) from the average biomass produced in treatments with varying nitrate concentrations (785 mg/L), suggesting that nutrient changes had a minimal impact on biomass yield at this salinity. At 105 g/L, a significant difference in biomass production was observed between nitrate and glucose treatments (P = 0). The highest biomass yield (278 mg/L) at this salinity was achieved with 1 g/L glucose. Furthermore, when comparing only the glucose-supplemented treatments at 105 g/L, significant differences in mean biomass production were found (P ≤ 0.05), indicating that glucose concentration did influence biomass yield at this high salinity.

Total Lipid Content

The percentage of total lipid content based on the dry weight of *D. salina* biomass under different salinity and nutrient treatments is presented in Table 1. . The highest rate of total lipid (26.17%) was observed at a salinity of 70 g/L in cultures supplemented with 3 g/L glucose. Conversely, the lowest lipid percentage (16.77%) was recorded at a salinity of 35 g/L with 50% nitrate. Notably, the total lipid content was not determined for glucose-supplemented cultures at the highest salinity (105 g/L) due to the limited biomass yield obtained under these condi-

Table 1. Average lipid level (%) of *D. salina* in different culture conditions

Salinity	100% NaNO₃	50% NaNO₃	25% NaNO₃	1g glucose	2g glucose	3g glucose
35(ppt)[a]	2.56±19.03	2.53±16.73	3.2±20.4	2.7±18.07	1.4±17.63	3.8±22.67
70(ppt)[b]	3.19±22.67	1.9±26	3±19.93	3.4±24.4	2.9±24.27	1.6±26.17
105(ppt)[b]	0.6±24.43	2±25	2.09±22.07	-	-	-

a, b indicates a significant difference in different salinities (Duncan test)

tions.

The results of two-way ANOVA indicated a statistically significant effect of salinity on the percentage of lipid dry weight (P< 0.001). In contrast, the impact of different nutrient concentrations on the mean lipid percentages was not statistically significant (P ≥ 0.05), suggesting that the tested nutrient variations did not significantly alter the overall percentage of lipid within the biomass. However, the total lipid produced per liter of culture medium exhibited considerable variation across different nutrient and salinity treatments, as represented in Figure 3.

Two-way ANOVA revealed a statistically significant effect of both salinity and nutrient levels on the total lipid produced per liter of culture medium (P ≤ 0.05). Duncan's post-hoc analysis further indicated significant differences in the mean total lipid production across all three tested salinity levels. Conversely, no statistically significant differences were observed in the mean total lipid production in response to varying nitrate concentrations (P ≥ 0.05). A statistically

significant interaction between salinity and nutrient levels (P < 0.001) suggests that the effect of nutrients on total lipid production was dependent on the salinity. Furthermore, treatments supplemented with different glucose concentrations showed significant differences in mean total lipid production (P ≤ 0.05), specifically between the 3 g/L glucose treatment and the 1 g/L and 2 g/L glucose treatments.

Fatty acid profile

Gas chromatography-flame ionization detector (GC-FID) analysis identified 17 distinct fatty acids in the *Dunaliella salina* biomass across the various treatment conditions. The relative abundance of these fatty acids varied significantly with both salinity and nutrient availability. Notably, the proportion of stearidonic acid (SDA, C18:4n-3) at a salinity of 35 g/L was substantially higher compared to the levels observed at 70 g/L and 105 g/L. A significant inverse correlation was found between salinity and SDA content, with increasing salinity leading to a marked decrease in SDA. Furthermore, at 35 g/L salinity, the addition of glucose to the culture
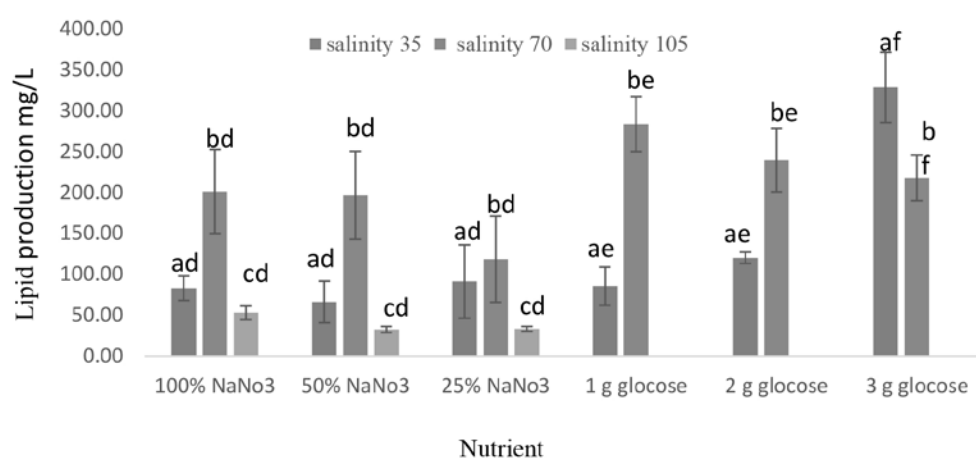

Fig. 3. Lipid production (mg/L) in *D. salina* culture; a, b, c represents the effect of salinity; d, e, f represents the effect of nutrients

medium resulted in a significant reduction in the relative abundance of SDA within the total fatty acid pool.

The specific composition and relative quantities of each identified fatty acid at salinities of 35 g/L, 70 g/L, and 105 g/L are presented in Tables 2, 3, and 4, respectively. These Tables provide a comprehensive overview of the impact that various nutrient regimes (nitrate and glucose concentrations) influenced the fatty acid profiles at each designated salinity level.

The Shapiro-Wilk test confirmed the normality of the saturated fatty acid (SFA) data across the 15 treatment groups and 45 replicates ($P \geq 0.05$). Duncan's post-hoc analysis revealed a statistically significant difference in the mean SFA content at a salinity of 70 g/L compared to both 35 g/L and 105 g/L ($P \leq 0.05$). Specifically, the proportion of SFAs was significantly higher at 70 g/L salinity than at the other two salinity levels, while no significant difference in SFA content was observed between the 35 g/L and 105 g/L salinity conditions. Regarding glucose supplementation, the treatments containing 1 g/L and 2 g/L glucose exhibited a higher percentage of SFAs. However, increasing the glucose concentration to 3 g/L resulted in a statistically significant reduction in the

Table 2. Fatty acid composition of *D. salina* cultivated at a salinity of 35 under various nutrient conditions

Fatty acids	100% NaNO₃	50% NaNO₃	25% NaNO₃	1g /L glucose	2g /L glucose	3g/L glucose
Dodecanoic (C12:0)	1.06±0.58	1.89±0.78	1.31±0.38	0.94±0.39	2.68±0.38	0.60±0.19
Tetradecanoic (C14:0)	0.94±0.53	1.33±0.84	1.43±0.81	8.61±0.66	15.79±1.0	4.2±4.94
pentadecanoic (C15)	1.18±0.39	1.75±0.70	1.53±0.79	0.85±0.59	3.54±4.16	0.43±0.18
Hexadecanoic (C16:0)	25.99±1.30	26.44±1.1	29.5±.54	26.6±5.79	34±2.60	26.33±3.45
Palmitoleic (C16:1)	4.44±0.50	6.27±0.30	4.42±2.76	2.96±0.88	10.3±1.34	6.92±0.27
Octadecanoic (C18:0)	17.49±2.30	23.23±1.0	20.85±1.5	23.07±6.5	12.49±0.7	9.76±0.98
Octadecenoic (C18:1)	5.25±2.90	1.13±1.01	2.09±0.22	2.82±1.53	4.29±0.51	9.70±8.42
Linoleic (C18:2)	12.04±0.75	7.81±0.02	5.23±0.05	8.51±0.76	5.03±0.25	10.58±3.46
Linolenic (C18:3)	0.31±0.54	0.22±0.20	0.22±0.20	.64±0.35	6.10±5.58	16.77±5.42
Stearidonic (C18:4)	22.99±1.42	23.77±0.01	22.78±0.4	16.00±1.2	0.24±0.24	0
Eicosanoic (C20:0)	0.10±0.09	0.05±0	0.04±0.04	0.79±1.38	1.20±1.24	0.24±0.35
Eicosenoic (C20:1)	3.23±1.05	3.23±0.34	2.43±0.35	1.92±1.72	1.10±0.11	1.20±0.29
Eicosatrienoic (C20:4)	1.54±0.18	0	1.01±0.90	1.67±1.42	0	9.10±6.62
Ecisoapentanoic(C20:5)	0	0.78±0.69	0	0	0	0
Behenic (C22:0)	0.08±0.07	0	0.11±0.10	0	0	0.08±0.15
Docosanoic (C22:1)	3.19±0.35	1.99±0.77	6.85±0.46	4.53±1.12	3.12±0.51	3.11±0.81
Docosatetraenoic(C22:4)	0.15±0.13	0.11±0.10	0.15±0.13	0.07±0.11	0	1.72±0.99
SFA	46.76	55.47	54.73	73.52	69.80	41.56
USFA	53.24	44.53	45.27	39.11	30.20	58.44
MUFA	23.02	10.63	9.04	7.69	15.71	17.90
PUFA	40.21	33.90	36.23	31.42	14.49	40.54
SFA/USFA ratio	0.88	1.25	1.21	1.56	2.31	0.71
Degree of unsaturation (DU)	94.45	78.43	81.51	70.54	44.69	98.98

Table 3. *D. salina* fatty acid composition at salinity 70g/L and different nutrients

Fatty acids	100% NaNO3	50% NaNO3	25% NaNO3	1g /L glucose	2g /L glucose	3g /L glucose
Dodecanoic (C12:0)	1.48±0.39	1.2±0.14	40.1±0.30	0.71±0.32	0.94±0.32	1.77±0.40
Tetradecanoic (C14:0)	11.31±2.54	10.39±1.69	8.64±1.99	20.31±4.21	23.3±12.91	5.01±3.12
pentadecanoic (C15)	0.97±0.15	1.96±0.21	89.1±0.20	1.06±0.15	0.72±0.25	1.29±0.37
Hexadecanoic (C16:0)	44.25±0.43	27.54±0.05	27.74±5.18	24.38±0.76	13.34±3.37	36.16±5.28
Palmitoleic (C16:1)	1.04±0.62	2.83±1.08	3.06±0.62	2.08±0.98	3.25±2.73	6.17±1
Octadecanoic (C18:0)	22.63±6.95	19.62±1.21	18.74±5.38	20.86±6.94	18.36±4.17	12.25±11
Octadecenoic (C18:1)	5.87±4.01	3.41±0.26	6.67±4.22	2.75±0.11	2.57±1.90	2.17±2.07
Linoleic (C18:2)	11.12±2.48	12.14±0.45	13.83±4.23	4.89±0.03	6.19±2.78	9.23±3.47
Linolenic (C18:3)	11.16±9.72	17.62±1.06	13.04±4.53	6.68±4.81	6.07±3.91	20.13±0.45
Stearidonic (C18:4)	0	0.11±0.11	0	0	0	0.16±0.05
Eicosanoic (C20:0)	0	0.7±0.7	0.1±0.97	0	0.77±0.83	1.01±0.97
Eicosenoic (C20:1)	1.08±0.98	0.98±0.04	0.87±0.2	2.2±1.66	1.11±0.38	1.51±0.11
Eicosatrienoic (C20:4)	0.8±0.75	0	0	0	0.1±0.09	0
Ecisoapentanoic(C20:5	0	0	0	0	0	0
Behenic (C22:0)	0	0	0	0	0	0.05±0.05
Docosanoic (C22:1)	3.27±0.05	1.87±1.21	2.75±0.15	3.2±0.81	4.81±1.51	2.42±2.39
Docosatetraenoic(C22:4)	0.11±0.12	0	0.26±0.25	0	0.15±0.14	0.22±0.04
SFA	64.83	49.42	68.27	68.27	40.66	54.44
USFA	35.17	45.82	19.22	19.93	19.83	42.06
MUFA	8.71	39.31	28.44	12.09	43.26	9.91
PUFA	26.46	11.27	2.2	8.81	5.4	32.15
SFA/USFA ratio	1.84	1.08	3.55	3.47	2.05	1.29
(DU)	61.64	61.85	32.83	29.71	54.07	74.21

Table 4. *D. salina* fatty acid composition at salinity 105 g/L and different nutrients

Fatty acids	100% NaNO₃	50% NaNO₃	25% NaNO₃
Dodecanoic (C12:0)	1.92±0.54	1.29±0.53	1.04±0.85
Tetradecanoic (C14:0)	6.59±3.73	1.81±0.24	2.54±1.37
pentadecanoic (C15)	2±0.47	0.96±0.42	0.70±0.44
Hexadecanoic (C16:0)	44.83±8.90	35.31±0.66	33.66±5.21
Palmitoleic (C16:1)	4.34±1.32	4.16±0.05	3.91±0.44
Octadecanoic (C18:0)	10.56±1.28	9.38±1.80	7.61±3.73
Octadecenoic (C18:1)	3.75±3.86	4.22±0.34	14.31±8.47
Linoleic (C18:2)	11.82±9.28	28.36±2.45	25.13±3.13
Linolenic (C18:3)	6.70±6.39	6.44±7.33	6.08±5.06
Stearidonic (C18:4)	0	0.08±0.01	0.13±0.04
Eicosanoic (C20:0)	0	0.26±0.30	0.02±0.02
Eicosenoic (C20:1)	2.50±0.94	2.09±0.27	2.07±0.07
Eicosatrienoic (C20:4)	0.07±0.07	0	0.09±0.08
Ecisoapentanoic(C20:5	0.09±0.09	0	0.080.05 ر
Behenic (C22:0)	0	0.08±0.07	0.13±0.03
Docosanoic (C22:1)	4.69±2.22	5.31±0.89	2.26±1.8
Docosatetraenoic(C22:4)	0.15±0.15	0.26±0.01	0.24±0.07
SFA	65.98	49	45.65
USFA	31.51	51	54.35
MUFA	10.59	10.55	20.42
PUFA	33.93	40.45	33.93
SFA/USFA ratio	2.09	0.96	0.84
(DU)	78.45	91.45	88.28

70

percentage of SFAs (P ≤ 0.05). The mean percentage of monounsaturated fatty acids (MUFA) exhibited statistically significant differences across the tested salinity levels (P ≤ 0.05). However, no significant differences in the mean MUFA percentage were observed in response to varying nutrient levels (P ≥ 0.05). In contrast to MUFA, the mean percentage of polyunsaturated fatty acids (PUFA) did not show statistically significant differences across all salinity levels and nutrient conditions (P ≥ 0.05). While the average percentage of PUFA fatty acids was not significantly different across the three salinity levels (P ≥ 0.05), changes in nutrient availability did appear to influence PUFA content (Figure 4). Generally, the proportion of unsaturated fatty acids (USFA), including both MUFA and PUFA, decreased in glucose-supplemented cultures at all tested salinities.
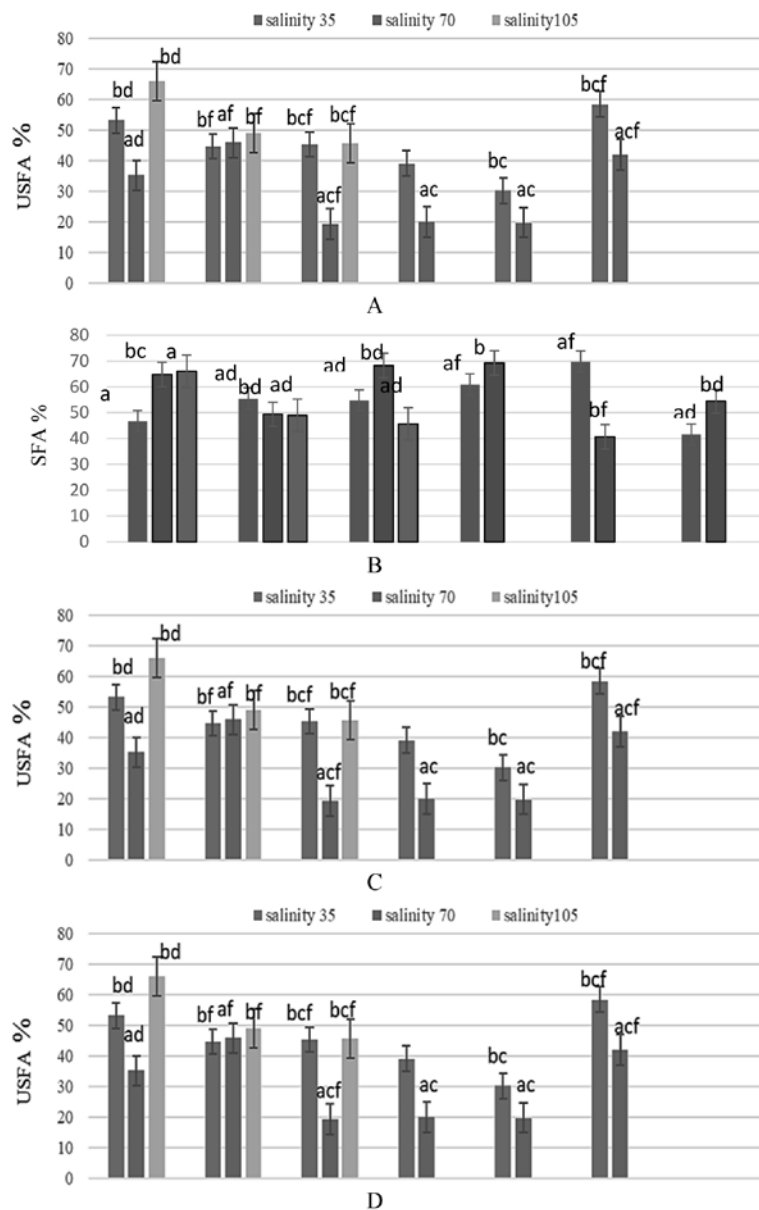

Fig. 4. USFA, SFA, MUFA, PUFA percentage of total fatty acids in *D. salina* under different treatment conditions, a, b. show the effect of salinity and c, d, f; Nutrient. Similar letters indicate no significant difference in mean percentage (Duncana)

Discussion

Effect of salinity on growth and biomass production

The response of microalgae to salinity fluctuations is species-specific, and within the genus *Dunaliella*, varying growth rates have been documented across a range of salinities (Borowitzka and Siva, 2007). Notably, *Dunaliella* species are generally recognized for their capacity to tolerate high salinity environments (Figure 1). In this study, the highest average biomass yield was observed at a salinity of 70 g/L ($P \leq 0.05$). However, the absolute maximum biomass (1449 mg/L) was achieved at 35 g/L in the treatment supplemented with 3 g/L glucose (Fig. 2). Numerous studies have investigated the influence of salinity on the growth rate and biomass accumulation of *Dunaliella* species (Chen et al., 2009; Takagi and Yoshida, 2006; Vo and Tran, 2014; Vo et al., 2017). Chen et al. (2009) reported an optimal salinity range of 1-2 M NaCl for the growth of *D. salina*, with significant growth inhibition at higher salinities. Conversely, Abu-Rezq et al. (2010) observed increased growth in *D. salina* with salinity elevation from 25 ppt to 45 ppt. Takagi and Yoshida (2006) found that *D. tertiolecta* experienced a sharp decline in biomass when salinity increased from 1 M to 2 M, but a less pronounced reduction occurred between 0.5 M and 1 M. Can et al. (2016) demonstrated that the optimal growth and biomass of *D. salina* were achieved at approximately 2 M NaCl, with a substantial decrease beyond this concentration. The high salinity tolerance of *Dunaliella* is a well-established characteristic (Borowitzka et al., 1977; Peeler et al.,

1989). However, further increases beyond an optimum can significantly impede biomass accumulation (Takagi and Yoshida, 2006).

In the present study, the increase in mean biomass production of *D. salina* when salinity was elevated from 35 g/L to 70 g/L aligns with the salt-tolerant nature of this microalga (Abu-Rezq et al., 2010; Peeler et al., 1989). This suggests that for the specific *D. salina* isolate used, 70 g/L may represent a more favorable salinity range for overall biomass production compared to standard seawater salinity. However, the highest individual biomass yield at 35 g/L under mixotrophic conditions indicates a potential interaction between salinity and carbon source availability in maximizing biomass.

Effect of nitrate and glucose on growth andbbiomass production

Nitrogen is a crucial macronutrient for the growth of all photosynthetic organisms, including microalgae. In this study, nitrate was employed as the nitrogen source at three concentrations: 100%, 50%, and 25% of the standard f/2 medium. Our findings indicated that varying nitrate concentrations did not exert a statistically significant effect on the final biomass yield of *D. salina*. This suggests that within the tested range, nitrogen availability may not have been the primary limiting factor for growth. Jiménez and Niell (1991) proposed that at certain concentrations, increased nitrogen availability might not directly translate to accelerated cell division due to limitations in the algal nitrogen uptake rate. Similarly, our results imply that the *D. salina* strain under these conditions may not have exhibited a proportional

increase in nitrogen uptake with increasing nitrate concentrations.

Gao et al. (2013) reported that nitrogen deficiency in the culture medium led to reduced biomass in *Chlorella muelleri* and *D. salina,* showing a less pronounced response to nitrogen limitation compared to *C. muelleri*. Given the lack of significant difference in biomass production across the tested nitrate concentrations in our study, it can be inferred that a concentration as low as 25% nitrate may adequately meet the nitrogen requirements of this Iranian *D. salina* strain over a 14-day cultivation period. This observation has significant implications for cost-effective nutrient management in large-scale microalgal cultivation.

In addition to inorganic nutrients, the role of carbon sources is critical for microalgal growth. While autotrophic growth relies on CO_2 as the primary carbon source, numerous studies, including Liu (2014), have demonstrated that incorporating of glucose as an organic carbon source can significantly enhance biomass and lipid production through mixotrophic or heterotrophic metabolism. Microalgae utilize light energy for growth under phototrophic conditions, and suboptimal lighting can limit growth rates. Under heterotrophic conditions (absence of light), a suitable organic carbon source like glucose becomes essential for achieving high biomass yields (Isleten-Hosoglu et al., 2012; Perez-Garcia et al., 2011). Glucose has been frequently identified as a preferred organic carbon source for various microalgae (Isleten-Hosoglu et al., 2012; Perez-Garcia et al., 2011).

Mixotrophic cultivation, which enables microalgae to simultaneously utilize light and organic carbon sources, is often more efficient in terms of biomass production compared to purely phototrophic or heterotrophic modes (Heredia-Arroyo et al., 2011). The ATP generated during photosynthetic processes can also enhance glucose metabolism and be reused in CO_2 fixation, leading to synergistic effects (Heredia-Arroyo et al., 2011; Li et al., 2014; Xu et al., 2004). Wan et al. (2011) observed the highest biomass and growth rate in *D. salina* under mixotrophic conditions with 15 g/L glucose supplementation. Similarly, Chandra et al. (2014) reported increased biomass production in a mixed microalgal culture with glucose addition. Our study also demonstrated that *D. salina* at different salinities exhibited varying responses to glucose supplementation (Fig. 4). At 35 g/L salinity, increasing glucose concentrations led to a significant increase in biomass, with the highest biomass yield (almost a three-fold increase) observed at 3 g/L glucose. However, this positive effect of glucose was less pronounced or absent at higher salinities (70 g/L and 105 g/L). This differential response could be attributed to the physiological adaptations of *D. salina* to increasing salinity, potentially affecting its ability to efficiently utilize exogenous glucose under high salt stress.

Lipid production

Microalgal lipid content exhibits significant variability, ranging from 1% to 85% of their dry weight, and is known to be influenced by environmental conditions (Chisti, 2007). Our findings demonstrate that in vitro manipulation of salinity and nutrient availability significantly impacted both the total lipid

content and the lipid production efficiency of *D. salina* (Fig. 3). The total lipid content in *D. salina* biomass across all treatments in this study ranged from 16.7% to 26.1%, which aligns with a previously reported value of 21.26% for this strain (Attaran Fariman, 2014). These values are within the broader range reported for other microalgae, such as 30% for some species (Fried et al., 1982) and 8% for others (Vanitha et al., 2007).

Studies by Azachi et al. (2002) and Takagi and Yoshida (2006) on *D. salina* indicated that increasing salinity from 0.5 M to 3.5 M led to an increase in total lipid content. In the present study, while elevated salinity generally increased the lipid percentage in *D. salina*, lipid biodegradation efficiency appeared to decline at salinities exceeding 70 g/L. Notably, changes in nutrient concentrations (glucose and nitrogen) did not significantly affect the overall percentage of lipid in *D. salina* biomass. The highest lipid percentage (26.17%) was observed at 70 g/L salinity with 3 g/L glucose, while the lowest (16%) occurred at 35 g/L with 0.05 g/L nitrate. This observation contrasts with Gu et al. (2012), who reported that while increased salinity enhanced the lipid percentage in *Nannochloropsis oculata*, the optimal oil production efficiency was achieved at lower salinity due to higher biomass yields. Consistent with Gu et al.'s (2012) findings, our study also showed that despite higher lipid percentages at higher salinities, the best lipid production efficiency was obtained at 35 g/L with 3 g/L glucose due to the significantly higher biomass accumulation under these conditions.

Nitrogen deficiency is known to inhibit protein synthesis in microalgae (Quigg and Beardall, 2003), while photosynthetic activity may persist. Consequently, the energy generated from photosynthesis can be redirected towards the synthesis of carbohydrates or lipids, depending on the algal species (Gao et al., 2013). In our study, reducing the nitrate level in the culture medium did not significantly increase the total lipid percentage (Table 4). This is consistent
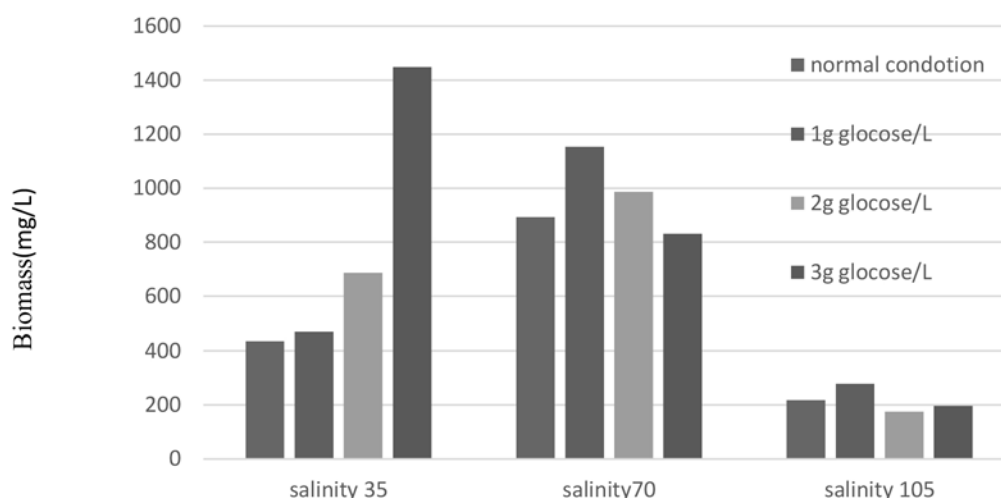

Fig. 5. The effect of different concentrations of glucose on the biomass of *D.salina*

with some research indicating no significant change in lipid percentage in certain *Dunaliella* species, such as *D. primolecta* (Uriarte et al., 1993) and *D. tertiolecta* (Lombardi and Wangersky, 1995), under nitrogen-limited conditions. Gordillo et al. (1998) found that *Dunaliella viridis* only increased lipid content during nitrogen deficiency when supplemented with 1% CO_2, suggesting the importance of the carbon to nitrogen ratio in lipid accumulation under nitrogen stress.

While some studies suggest that mixotrophic conditions can enhance both biomass and lipid content (Xu et al., 2004), others report increased lipid percentage under phototrophic conditions (Cheirsilp and Torpee, 2012), or no significant difference in intracellular lipid content across different trophic modes (Heredia-Arroyo et al., 2010). In our study, different glucose concentrations did not significantly affect the lipid percentage in *D. salina*, but the overall lipid production was enhanced due to increased biomass at higher glucose concentrations (especially at 35 g/L salinity). This aligns with reports of increased lipid production in *D. salina* under mixotrophic conditions (Wan et al., 2011). Tables 1-4 provide further comparative data on lipid production in different microalgae, including *D. salina*, under mixotrophic conditions.

Fatty acid composition and bBiofuel potential

The fatty acid composition of microalgae is influenced by various factors, including species, temperature, growth phase, light intensity, and nutrient availability. In this study, palmitic acid (C16:0) was the most abundant fatty acid in *D. salina* across all three tested salinities (Tables 2-4). Increasing salinity led to an increase in the proportion of palmitic acid, as well as the unsaturated fatty acids linoleic acid (C18:2) and linolenic acid (C18:3). This observation is partially consistent with Takagi and Yoshida (2006), who noted that most fatty acids in *Dunaliella* are composed of unsaturated C18 and saturated C16 fatty acids. However, Vanitha et al. (2007) reported C22 and C18:2 as the most abundant fatty acids in *D. salina* variants, highlighting potential strain-specific variations.

For biodiesel production, a higher content of saturated fatty acids (SFAs) and monounsaturated fatty acids (MUFAs), and a lower content of polyunsaturated fatty acids (PUFAs), is generally preferred for better fuel quality, particularly oxidative stability (Li et al., 2013). Deyab (2021) found increased SFAs in *D. salina* under nitrogen deficiency, while Chen et al. (2011) reported similar SFA and USFA profiles in *D. tertiolecta* with and without nitrate. Our study showed that changes in nitrate levels did influence the proportion of saturated and unsaturated fatty acids, with reduced nitrate leading to a decrease in the percentage of SFAs. However, very low nitrate concentrations (50% and 25%) resulted in similar SFA levels.

Overall, the *D. salina* strain isolated from Iran's southeast coast, with its total lipid content and significant proportions of SFAs (43.03% to 59.62%) and PUFAs (32.5% to 40.76%), demonstrates considerable potential for biofuel production. Notably, the observed changes in the proportions of saturated and unsaturated fatty acids in response

to varying salinity concentrations suggest that the lipid profile of this microalga can be tailored to suit different climatic conditions, with higher SFA content potentially advantageous in hot climates and higher USFA content in cold regions due to their lower freezing points.

Conclusion

This study demonstrated that salinity significantly affects the growth and lipid accumulation of an Iranian *D. salina* isolate, with optimal average biomass at 70 g/L but maximum yield under glucose supplementation at 35 g/L. While nitrate levels were not limiting, glucose enhanced biomass at lower salinity, highlighting the benefit of mixotrophic cultivation. Higher salinity generally increased lipid content, but maximum lipid production was linked to higher biomass at 35 g/L with glucose. Palmitic acid was the dominant fatty acid, and salinity influenced the proportions of saturated and unsaturated fatty acids, suggesting potential for biofuel production with a modifiable lipid profile. This research highlights the importance of optimizing salinity levels and exploring mixotrophic approaches to maximize biomass and lipid production in this *D. salina* isolate for biotechnological applications, particularly in biofuel production. Future work should focus on scaling up and assessing economic feasibility.

Acknowledgements

References

Abu-Rezq, T.S., Al-Hooti, S. and Jacob, D.A., 2010. Optimum culture conditions required for the locally isolated *Dunaliella salina*. *Journal of Algal Biomass Utilization*, 1(2), pp.12-19.

Attaran-Fariman, G., 2014. *Identification of native microalgae of the Oman Sea and their evaluation as live food in aquaculture*. Final report of Iranian Fisheries Institute, 166pp.

Azachi, M., Sadka, A., Fisher, M., Goldshlag, P., Gokhman, I. and Zamir, A., 2002. Salt induction of fatty acid elongase and membrane lipid modifications in the extreme halotolerant alga *Dunaliella salina*. *Plant Physiology*, 129(3), pp.1320-1329. DOI: https://doi.org/10.1104/pp.001909.

Bhola, V., Swalaha, F., Ranjith Kumar, R., Singh, M. and Bux, F., 2014. Overview of the potential of microalgae for CO_2 sequestration. *International Journal of Environmental Science and Technology*, 11, pp.2103-2118.

Bligh, E.G. and Dyer, W.J., 1959. A rapid method of total lipid extraction and purification. *Canadian Journal of Biochemistry and Physiology*, 37(8), pp.911-917. DOI: https://doi.org/10.1139/o59-099.

Borowitzka LJ, Kessly DS, Brown AD. 1977. The salt relation of *Dunaliella*. Further observation on glycerol production and its regulation. *Arch. Microbiol.,* 13: 131–38. DOI: https://doi.org/10.1007/BF00428592.

Borowitzka, M.A. and Siva, C.J., 2007. The taxonomy of the genus *Dunaliella* (Chlorophyta, Dunaliellales) with emphasis on the marine and halophilic species. *Journal of Applied Phycology*, 19(5), pp.567-590. DOI: https://doi.org/10.1007/BF00428592.

Bougaran, G., Rouxel, C., Dubois, N., Kaas, R., Grouas, S. and Cadoret, J.P., 2012. Enhancement of neutral lipid productivity in the microalga *Isochrysis affinis Galbana* (T-Iso) by a mutation-selection procedure. *Biotechnology and Bioengineering*, 109(11), pp.2737-2745. DOI: https://doi.org/10.1002/bit.24560.

Can, S.S., Cirik, S., Koru, E., Turan, G., Tekoğul, H. and Subakan, T., 2016. Effects of salinity, light and nitrogen concentration on growth and lipid accumulation of the green algae *Dunaliella salina*. *Fresenius Environmental Bulletin*, 25(5), pp.1437-1447.

Chandra, R., Rohit, M.V., Swamy, Y.V. and Mohan, S.V., 2014. Regulatory function of organic carbon supplementation on biodiesel production during growth and nutrient stress phases of mixotrophic microalgae cultivation. *Bioresource Technology*, 165, pp.279-287. DOI: https://doi.org/10.1016/j.biortech.2014.02.102.

Cheirsilp, B. and Torpee, S., 2012. Enhanced growth and lipid production of microalgae under mixotrophic culture condition: effect of light intensity, glucose concentration and fed-batch cultivation. *Bioresource Technology*, 110, pp.510-516. DOI: https://doi.org/10.1016/j.biortech.2012.01.125.

Chen, H., Jiang, J.G. and Wu, G.H., 2009. Effects of salinity changes on the growth of *Dunaliella salina* and its isozyme activities of glycerol-3-phosphate dehydrogenase. *Journal of Agricultural and Food Chemistry*, 57(14), pp.6178-6182 DOI: https://doi.org/10.1021/jf900447r.

Chen, M., Tang, H., Ma, H., Holland, T.C., Ng, K.S. and Salley, S.O., 2011. Effect of nutrients on growth and lipid accumulation in the green algae *Dunaliella tertiolecta*. *Bioresource Technology*, 102(7), pp.1649-1655. DOI: https://doi.org/10.1016/j.biortech.2010.09.062

Chisti, Y., 2007. Biodiesel from microalgae. *Biotechnology Advances*, 25(3), pp.294-306. DOI: https://doi.org/10.1016/j.biotechadv.2007.02.001.

Chu, W.L., 2012. Biotechnological applications of microalgae. *International e-Journal of Science, Medicine and Education*, 6(1), pp. S24-S37.

Deora, P.S., Verma, Y., Muhal, R.A., Goswami, C. and Singh, T., 2022. Biofuels: An alternative to conventional fuel and energy source. *Materials Today: Proceedings*, 48, pp.1178-1184. DOI: https://doi.org/10.1016/j.matpr.2021.08.227.

Deyab, M.A., El-Sadany, A., Ghazal, M.A. and El-Adl, M., 2021. Nitrogen deficiency maximizes the production and accumulation of β-carotene via induction of different macromolecule derivatives in *Dunaliella salina* (Dunal) Teodoresco. *Egyptian Journal of Botany*, 61(2), pp.453-466. doi: 10.21608/ejbo.2021.40359.1542.

Fried, A., Tietz, A., Ben-Amotz, A. and Eichenberger, W., 1982. Lipid composition of the halotolerant alga, *Dunaliella*

salina. *Biochimica et Biophysica Acta (BBA)-Lipids and Lipid Metabolism*, 713(2), pp.419-426. DOI: https://doi.org/10.1016/0005-2760(82)90261-2.

Gao, Y., Yang, M. and Wang, C., 2013. Nutrient deprivation enhances lipid content in marine microalgae. *Bioresource Technology*, 147, pp.484-491. DOI: https://doi.org/10.1016/j.biortech.2013.08.066

Gordillo, F.J., Goutx, M., Figueroa, F.L. and Niell, F.X., 1998. Effects of light intensity, CO_2 and nitrogen supply on lipid class composition of *Dunaliella viridis*. *Journal of Applied Phycology*, 10(2), pp.135-144. DOI: https://doi.org/10.1023/A:1008067022973.

Gu, N., Lin, Q., Li, G., Tan, Y., Huang, L. and Lin, J., 2012. Effect of salinity on growth, biochemical composition, and lipid productivity of *Nannochloropsis oculata* CS 179. *Engineering in Life Sciences*, 12(6), pp.631-637. DOI: https://doi.org/10.1002/elsc.201100204

Guillard, R.R. and Ryther, J.H., 1962. Studies of marine planktonic diatoms: I. *Cyclotella nana* Hustedt, and *Detonula confervacea* (Cleve) Gran. *Canadian Journal of Microbiology*, 8(2), pp.229-239. DOI: https://doi.org/10.1139/m62-029

Heredia-Arroyo, T., Wei, W. and Hu, B., 2010. Oil accumulation via heterotrophic/mixotrophic *Chlorella protothecoides*. *Applied Biochemistry and Biotechnology*, 162(7), pp.1978-1995. DOI: https://doi.org/10.1007/s12010-010-8974-4

Heredia-Arroyo, T., Wei, W., Ruan, R. and Hu, B., 2011. Mixotrophic cultivation of *Chlorella vulgaris* and its potential application for the oil accumulation from non-sugar materials. *Biomass and Bioenergy*, 35(6), pp.2245-2253. DOI: https://doi.org/10.1016/j.biombioe.2011.02.036

Hopkins, T.C., Graham, E.J.S. and Schuler, A.J., 2019. Biomass and lipid productivity of *Dunaliella tertiolecta* in a produced water-based medium over a range of salinities. *Journal of Applied Phycology*, 31(5), pp.3349-3358. DOI: https://doi.org/10.1007/s10811-019-01836-3 .

Iglina, T., Iglin, P. and Pashchenko, D., 2022. Industrial CO_2 capture by algae: a review and recent advances. *Sustainability*, 14(7), p.3801. DOI: https://doi.org/10.3390/su14073801.

IPCC. (2022). *Climate Change 2022: Mitigation of Climate Change. Contribution of Working Group III to the Sixth Assessment Report of the Intergovernmental Panel on Climate Change* [P.R. Shukla, J. Skea, R. Slade, et al. (eds.)]. Cambridge University Press. DOI: https://doi.org/10.1017/9781009157926 .

International Energy Agency (IEA). 2024. *CO_2 Emissions in 2023*, IEA, Paris. DOI: https://www.iea.org/reports/co2-emissions-in-2023.

International Energy Agency (IEA). 2025. *Global Energy Review 2025*, IEA, Paris. DOI: https://www.iea.org/reports/global-energy-review-2025.

Isleten-Hosoglu, M., Gultepe, I. and Elibol, M., 2012. Optimization of carbon and nitrogen sources for biomass and lipid production by *Chlorella saccharophila* under heterotrophic conditions and development of Nile red fluorescence-based method for quantification of its neutral lipid content. *Biochemical Engineering*

Journal, 61, pp.11-19. DOI: https://doi.org/10.1016/j.bej.2011.12.001

Jiménez, C. and Niell, F.X., 1991. Growth of *Dunaliella viridis* Teodoresco: effect of salinity, temperature and nitrogen concentration. *Journal of Applied Phycology*, 3(4), pp.319-327. DOI: https://doi.org/10.1007/BF02392885.

Li, T., Wan, L., Li, A. and Zhang, C., 2013. Responses in growth, lipid accumulation, and fatty acid composition of four oleaginous microalgae to different nitrogen sources and concentrations. *Chinese Journal of Oceanology and Limnology*, 31(6), pp.1306-1314. DOI: https://doi.org/10.1007/s00343-013-2316-7.

Li, T., Zheng, Y., Yu, L. and Chen, S., 2014. Mixotrophic cultivation of a *Chlorella sorokiniana* strain for enhanced biomass and lipid production. *Biomass and Bioenergy*, 66, pp.204-213. DOI: https://doi.org/10.1016/j.biombioe.2014.04.010.

Liu, J., 2014. Optimization of biomass and lipid production by adjusting the interspecific competition mode of *Dunaliella salina* and *Nannochloropsis gaditana* in mixed culture. *Journal of Applied Phycology*, 26(1), pp.163-171. DOI: https://doi.org/10.1007/s10811-013-0099-z.

Lombardi, A. and Wangersky, P.J., 1995. Particulate lipid class composition of three marine phytoplankters *Chaetoceros gracilis*, *Isochrysis galbana* (Tahiti), and *Dunaliella tertiolecta* grown in batch culture. *Hydrobiologia*, 306(1), pp.1-6. DOI: https://doi.org/10.1007/BF00007853.

Mairet, F., Bernard, O., Masci, P., Lacour, T. and Sciandra, A., 2011. Modelling neutral lipid production by the microalga *Isochrysis aff. galbana* under nitrogen limitation. *Bioresource Technology*, 102(1), pp.142-149. DOI: https://doi.org/10.1016/j.biortech.2010.06.138.

Mata, T.M., Almeidab, R. and Caetanoa, N.S., 2013. Effect of the culture nutrients on the biomass and lipid productivities of microalgae *Dunaliella tertiolecta*. *Chem Eng*, 32, p.973.

Moheimani, N.R., Borowitzka, M.A., Isdepsky, A. and Fon Sing, S., 2013. Standard methods for measuring growth of algae and their composition. In: Borowitzka, M.A. and Moheimani, N.R. (eds.) *Algae for Biofuels and Energy*. Dordrecht: Springer, pp.265-284. DOI: https://doi.org/10.1007/978-94-007-5479-9_16.

Morales, M., Aflalo, C. and Bernard, O., 2021. Microalgal lipids: A review of lipids potential and quantification for 95 phytoplankton species. *Biomass and Bioenergy*, 150, p.106108. DOI: https://doi.org/10.1016/j.biombioe.2021.106108.

Nigam, S., Rai, M.P. and Sharma, R., 2011. Effect of nitrogen on growth and lipid content of *Chlorella pyrenoidosa*. *American Journal of Biochemistry and Biotechnology*, 7(3), pp.124-129. http://thescipub.com/abstract/10.3844/ajbbsp.2011.124.129.

Pacheco, M.M., Hoeltz, M., de Souza, D., Benitez, L.B., Schneider, R.C. and Müller, M.V., 2017. Current approaches in producing oil and biodiesel from microalgal biomass. In: *Waste Biomass Management–A Holistic Approach*. Springer, pp.289-310. DOI: https://doi.org/10.1007/978-3-319-49595-8_13.

Peeler, T.C., Stephenson, M.B., Einspahr,

K.J. and Thompson, G.A., 1989. Lipid characterization of an enriched plasma membrane fraction of *Dunaliella salina* grown in media of varying salinity. *Plant Physiology*, 89(3), pp.970-976. DOI: https://doi.org/10.1104/pp.89.3.970.

Perez-Garcia, O., Bashan, Y. and Esther Puente, M., 2011. Organic carbon supplementation of sterilized municipal wastewater is essential for heterotrophic growth and removing ammonium by the microalga *Chlorella Vulgaris* 1. *Journal of Phycology*, 47(1), pp.190-199. DOI: https://doi.org/10.1111/j.1529-8817.2010.00934.x.

Quigg, A. and Beardall, J., 2003. Protein turnover in relation to maintenance metabolism at low photon flux in two marine microalgae. *Plant, Cell and Environment*, 26(5), pp.693-703. DOI: https://doi.org/10.1046/j.1365-3040.2003.01004.x.

Rios, L., Da Silva, C., Tasic, M., Wolf-Maciel, M. and Maciel Filho, R., 2016. Cultivation of three microalgae strains under mixotrophic conditions for biodiesel production. *Chemical Engineering Transactions*, 50, pp.409-414. http://dx.doi.org/10.3303/CET1650069.

Scragg, A., Morrison, J. and Shales, S., 2003. The use of a fuel containing *Chlorella vulgaris* in a diesel engine. *Enzyme and Microbial Technology*, 33(7), pp.884-889. DOI: https://doi.org/10.1016/j.enzmictec.2003.01.001.

Shokravi, Z., Shokravi, H., Chyuan, O.H., Lau, W.J., Koloor, S.S.R., Petrů, M. and Ismail, A.F., 2020. Improving 'lipid productivity'in microalgae by bilateral enhancement of biomass and lipid contents: A review. *Sustainability*, 12(21), p.9083. DOI: https://doi.org/10.3390/su12219083.

Takagi, M. and Yoshida, T., 2006. Effect of salt concentration on intracellular accumulation of lipids and triacylglyceride in marine microalgae *Dunaliella* cells. *Journal of Bioscience and Bioengineering*, 101(3), pp.223-226. DOI: https://doi.org/10.1263/jbb.101.223.

Talebi, A.F., Mohtashami, S.K., Tabatabaei, M., Tohidfar, M., Bagheri, A. and Ghasemi, Y., 2013. Fatty acids profiling: a selective criterion for screening microalgae strains for biodiesel production. *Algal Research*, 2(3), pp.258-267. DOI: https://doi.org/10.1016/j.algal.2013.04.003.

Thompson Jr, G.A., 1996. Lipids and membrane function in green algae. *Biochimica et Biophysica Acta (BBA)-Lipids and Lipid Metabolism*, 1302(1), pp.17-45. DOI: https://doi.org/10.1016/0005-2760(96)00045-8.

Truc, M.V., Phuc, N.H., Trung, V.P., Hieu, H.V. and Son, T.L., 2017. Accumulation of lipid in *Dunaliella salina* under nutrient starvation condition. *American Journal of Food and Nutrition*, 5(2), pp.58-61. DOI:10.12691/ajfn-5-2-2.

Uriarte, I., Farias, A., Hawkins, A.J.S. and Bayne, B.L., 1993. Cell characteristics and biochemical composition of *Dunaliella primolecta* butcher conditioned at different concentrations of dissolved nitrogen. *Journal of Applied Phycology*, 5(4), pp.447-453. DOI: https://doi.org/10.1007/BF02182737.

Vanitha, A., Narayan, M., Murthy, K. and Ravishankar, G.A., 2007. Comparative

study of lipid composition of two halo-tolerant algae, *Dunaliella salina* and *Dunaliella salina*. *International Journal of Food Sciences and Nutrition*, 58(5), pp.373-382. DOI: https://doi.org/10.1080/09637480701252252.

Vo, T.Q. and Tran, D.T., 2014. Effects of salinity and light on the growth of *Dunaliella* isolates. *Journal of Applied and Environmental Microbiology*, 2(6), pp.208-211.

Vo, T.Q., Tran, S.M., Nguyen, P.T. and Mai, T.T., 2017. Growth, carotenoid production, antioxidant capacity, and lipid accumulation of *Haematococcus* sp. under different light intensities. *American Journal of Plant Biology*, 2(4), pp.142-147.

Wan, M., Liu, P., Xia, J., Rosenberg, J.N., Oyler, G.A. and Betenbaugh, M.J., 2011. The effect of mixotrophy on microalgal growth, lipid content, and expression levels of three pathway genes in *Chlorella sorokiniana*. *Applied Microbiology and Biotechnology*, 91(3), pp.835-844. DOI: https://doi.org/10.1007/s00253-011-3399-8.

Xu, F., Hu, H.H., Cong, W., Cai, Z.L. and Ouyang, F., 2004. Growth characteristics and eicosapentaenoic acid production by *Nannochloropsis* sp. in mixotrophic conditions. *Biotechnology Letters*, 26(1), pp.51-53. DOI: https://doi.org/10.1023/B:BILE.0000009460.81267.cc.

Phylogenetic, Structural, and Immunogenic Analysis of Algal L-Asparaginases: Potential Alternatives for ALL Treatment

Mahdis Mofidi[1], Mohammad Yaghoubi-Avini*[1]

Abstract

L-asparaginase is an essential drug used in the treatment of acute lymphoblastic leukemia (ALL), a highly prevalent cancer in children. However, its immunogenicity and allergenicity often lead to adverse reactions in patients. As a result, alternative strategies, such as identifying novel enzyme sources and employing protein engineering, have been explored. This study aimed to elucidate the molecular structure and predict the immunogenic profile of L-asparaginases from *Spirulina subsalsa*, *Nannochloropsis gaditana* CCMP526, and *Gracilaria domingensis* to propose potential substitutes for bacterial asparaginases, such as EcAII and ErAII. The corresponding enzyme sequences were retrieved from GenBank. Phylogenetic analysis revealed three distinct clusters corresponding to class 1,2, and 3 L-asparaginases. Algal enzymes from *N. gaditana* CCMP526 (GenBank ID: EWM28374.1) and *G. domingensis* (GenBank ID: KAI0567449.1) clustered within class 2 L-asparaginases, whereas *S. subsalsa* (NCBI Reference Sequence ID: WP_265263300.1) exhibited a closer evolutionary relationship with class 3 asparaginases. These findings suggest that algal asparaginases possess unique functional characteristics compared to their bacterial counterparts. Immunogenicity assessment indicated that the T-cell and B-cell epitope densities of *S. subsalsa*, *N. gaditana* CCMP526, and *G. domingensis* were comparable to those of EcAII but significantly lower than ErAII. Additionally, these algal asparaginases demonstrated lower epitope density for the *HLA-DRB1*07:01 allele, which is associated with hypersensitivity reactions, suggesting a reduced likelihood of triggering immune responses. Among the algal sources, *N. gaditana* exhibited the lowest epitope density, followed by *G. domingensis* and *S. subsalsa*. However, in the B-cell epitope analysis, *S. subsalsa* demonstrated the least potential to elicit allergenic reactions, as it contained only one allergenic epitope. Structural modeling using AlphaFold 3 predicted highly reliable three-dimensional models for the algal asparaginases.

1-Department of Microbiology and Microbial Biotechnology, Faculty of Life Sciences and Biotechnology, Shahid Beheshti University, Tehran, Iran
*Corresponding author email address: m_yaghoubi@sbu.ac.ir

Introduction

L-asparaginase (ASNase) is an enzyme with industrial and therapeutic applications. It is primarily recognized for its ability to reduce acrylamide formation in the food industry and its crucial role in treating acute lymphoblastic leukemia (ALL). This enzyme is an essential component of combination chemotherapy for ALL, playing a key role in inhibiting the proliferation of asparagine-dependent cancer cells. Given the high prevalence of ALL, accounting for approximately 30% of childhood malignancies, extensive research is being conducted to identify and optimize ASNase sources from various microorganisms (Andrade et al. 2024; Belén et al. 2019). The antitumor properties of ASNase arise from the hydrolysis of L-asparagine into aspartic acid and ammonia. While healthy cells can synthesize asparagine, neoplastic cells rely on external sources for growth and survival. ASNase depletes circulating asparagine, leading to the inhibition of leukemic cells, nutrient depletion, DNA damage, cell cycle arrest, and ultimately apoptosis. This mechanism makes ASNase a key agent in chemotherapy for ALL (Pedroso et al. 2023). Structurally, L-asparaginases are classified into three groups (Loch and Jaskolski 2021): Class 1 includes tetrameric enzymes, initially identified in bacteria but also found in yeasts and mammals (Karamitros and Konrad 2014). This class comprises cytoplasmic (Type I) enzymes that exhibit low substrate affinity (mM) and periplasmic (Type II) enzymes that demonstrate a higher affinity (μM) for L-asparagine (Srikhanta et al. 2013). Class 2 contains Type III enzymes,

divided into potassium-dependent and potassium-independent proteins. These enzymes are initially inactive and acquire catalytic activity through self-maturation (Linhorst and Lübke 2022a; Loch et al. 2022). Class 3 includes Type IV (thermostable) and Type V (thermolabile) enzymes, originally identified in *Rhizobium etli*. These enzymes exist as homodimers with low substrate affinity for L-asparagine (Borek and Jaskólski 2001; Loch et al. 2023).

Currently, only Type II (Class 1) ASNases from *Escherichia coli* (EcAII) and *Erwinia chrysanthemi* (ErAII) are approved for ALL treatment (Tosta Pérez et al. 2023a). However, in addition to glutaminase activity, which contributes to severe side effects, these enzymes exhibit high immunogenicity and allergenicity, triggering adverse immune responses in patients (Belén et al. 2020). Hypersensitivity reactions associated with ASNase include anaphylaxis, bronchospasm, urticaria, itching, limb swelling, and erythema. 30–75% of patients experience hypersensitivity reactions, and up to 70% develop anti-ASNase antibodies, altering the drug's pharmacokinetics, shortening its half-life, and reducing therapeutic efficacy (Bowman et al. 2011). In some cases, this condition occurs asymptomatically while significantly diminishing drug effectiveness, known as silent inactivation (Fernandez et al. 2014; Schalk et al. 2014).

Due to these challenges, the research actively explores alternative ASNase sources with reduced immunogenicity to mitigate side effects while maintaining therapeutic efficacy. However, ASNases from Classes 2 and 3 have largely been overlooked due

to their initially perceived low substrate affinity, even though their antileukemic and immunogenic properties remaining underexplored.

This study aims to evaluate algal alternatives to bacterial ASNase using computational tools. Specifically, it focuses on the structural and immunogenic profile of ASNase derived from *Spirulina subsalsa*, *Nannochloropsis gaditana* CCMP526, and *Gracilaria domingensis*, which are economically significant algae due to their widespread applications in the food and pharmaceutical industries. These algae are recognized for their high growth rate, valuable biochemical compounds, and broad industrial utility, making them promising sources for safer and more effective therapeutic ASNase.

Material and methods

Phylogenetic Tree Reconstruction

The sequences of Class 1 (InterPro ID: IPR027474), Class 2 (InterPro ID: IPR000246), and Class 3 (InterPro ID: IPR010349) L-asparaginases (Andrade et al. 2024), along with the sequences of the three L-asparaginases studied in this research, were obtained from the InterPro database (Blum et al. 2021). Sequence alignment was performed using the MUSCLE algorithm in MEGA 7 software (Kumar, Stecher, and Tamura 2016). Then, a phylogenetic tree was constructed using the Maximum Likelihood (ML) method with the WAG+G model and 500 bootstrap replicates.

The NetMHCII 4.0 server (Kagami et al. 2020) was used to predict T-cell epitopes using default parameters. Peptides with lengths ranging from 9 to 15 amino acids were analyzed for selected alleles. The peptides were classified into three categories based on their predicted rank scores: strong binding (SB ≤ 1%), weak binding (WB ≤ 5%), and non-binding (> 5%). The epitope density was calculated using the formula $f_i = n_i/N$, where n_i represents the number of predicted immunogenic epitopes (SB and WB), and N is the total number of epitopes for each allele. The alleles analyzed included HLA-DRB101:01, HLA-DRB103:01, HLA-DRB104:01, HLA-DRB107:01, HLA-DRB108:01, HLA-DRB111:01, HLA-DRB113:01 and HLA-DRB115:01.

Statistical analysis was performed utilizing Python, which included libraries such as pandas (McKinney 2010), scipy (Virtanen et al. 2020), seaborn (Waskom 2021), and matplotlib (Hunter 2007). Non-parametric methods were employed to address the potential non-normal distribution of the data. Pairwise comparisons were conducted using the Mann-Whitney U test, while the Kruskal-Wallis test was used for comparisons among multiple groups. Results, including test statistics and p-values, were considered statistically significant when $p < 0.05$. Data were presented as medians with interquartile ranges and visualized through boxplots and strip plots to illustrate the distribution of epitope densities across the different groups.

Prediction of B-cell Epitopes, Allergenicity, Antigenicity, and 3D Structure of L-Asparaginase

The topology of the outer membrane influences linear B-cell epitopes on the cell surface. To predict the linear B-cell epitopes of asparaginases from *S. subsalsa*, *N. gaditana* CCMP526, and *G. domingensis*, the AB-

CPred server (Saha and Raghava 2006a) was used. A threshold of 0.8 was applied, and the sequence length was set to 16- mers.

The allergenicity of each epitope was assessed using the AlgPred server (Saha and Raghava 2006b), while the antigenicity of these proteins was predicted using the VaxiJen server (Doytchinova and Flower 2007), with default parameters retained and tumors selected as the target organisms.

For the three-dimensional structure prediction of the enzyme, the amino acid sequences of L-asparaginase from *S. subsalsa*, *N. gaditana* CCMP526, and *G. domingensis* were input into AlphaFold 3. AlphaFold 3 is a deep learning model developed by DeepMind that predicts protein structures based on their amino acid sequences. This model provides highly accurate predictions of protein folding and spatial arrangements.

The quality of the predictions was assessed using the predicted local distance difference test (pLDDT) and predicted aligned error (PAE) metrics (Abramson et al., 2024). Finally, epitope map visualization was performed using PyMOL software (Kagami et al., 2020).

Results

Phylogenetic tree of algal L-asparaginases

The phylogenetic tree was constructed using the alignment of the L-asparaginase gene sequences from the algae *N. gaditana* CCMP526, *S. subsalsa*, and *G. domingensis*, along with 25 L-asparaginase sequences from classes 1, 2, and 3, specifically types I and II L-asparaginase. The tree (Figure 1) revealed three distinct clusters: class 3 L-asparaginases, class 2 L-asparaginases, and class 1 L-as-

paraginases, supported by strong bootstrap values. The cluster of class 3 L-asparaginases was distinct from class 2 enzymes, supported by a strong bootstrap value. The L-asparaginase from *S. subsalsa* was positioned within the class 3 cluster, indicating that the *S. subsalsa* enzyme shares the highest structural similarity with class 3 L-asparaginases.

The L-asparaginases from *N. gaditana* CCMP526 and *G. domingensis* were grouped within the class 2 Ntn-hydrolase family of L-asparaginases, which are mainly found in eukaryotic organisms.

Class 1 L-asparaginases were grouped into closely related branches and were distinct from the central cluster of class 2 and 3 L-asparaginases. The therapeutic asparaginases from *E. coli* and *E. chrysanthemi* were within this cluster.

Prediction of immunogenicity

Epitope density is used to evaluate the immunogenicity of proteins. It emphasizes that more epitope density is directly related to higher immunogenic potential. This concept was applied to assess the immunogenicity of asparaginases from the selected algal sources compared with clinical asparaginases from EcAII and ErAII. The results showed no significant difference in immunogenicity between the algal asparaginases and the EcAII asparaginase. However, a significant difference was observed with ErAII, which demonstrated higher immunogenicity compared to algal asparaginases and EcAII.

The algal asparaginases exhibited lower immunogenicity than clinical asparaginases, with *N. gaditana* CCMP526 showing lower immunogenicity than the others (Figure 2).

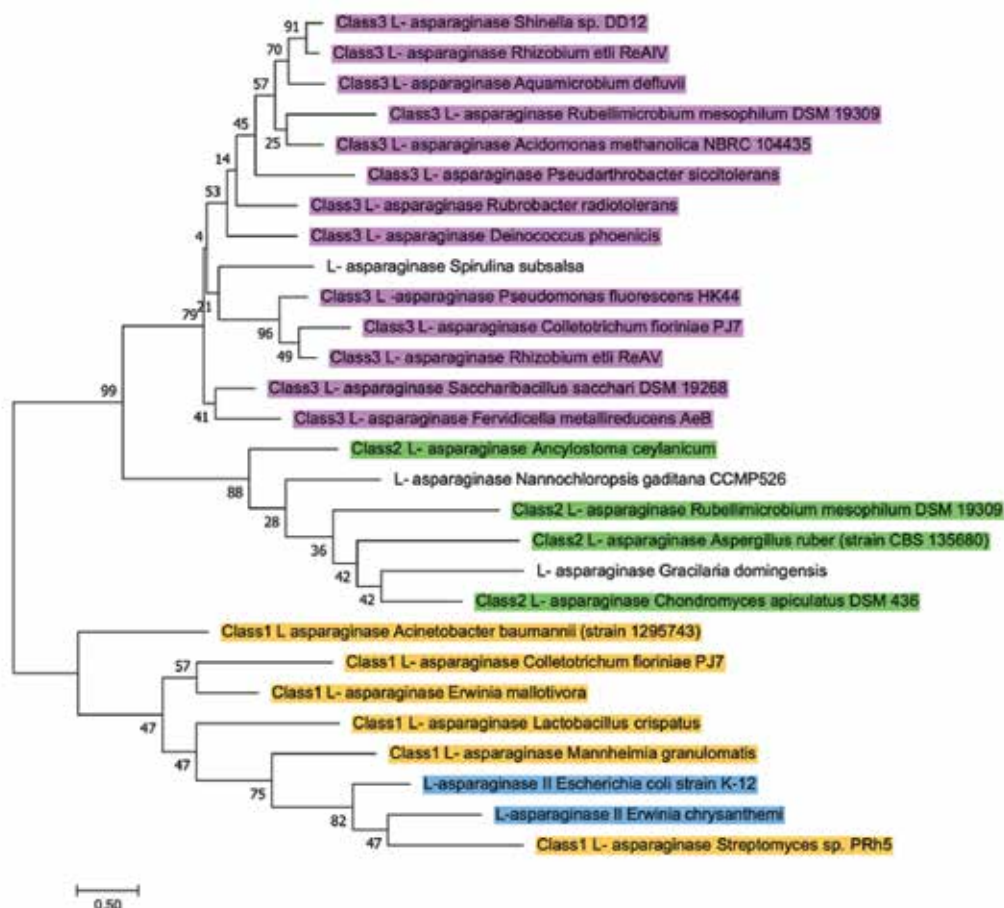The T-cell epitope density for each of the

Fig. 1. The phylogenetic tree of the L-asparaginase enzyme was constructed using the maximum likelihood method and the WAG+G model. The blue color indicates microorganisms currently used in the commercial production of drugs; the classes 1, 2, and 3 are represented in yellow, green, and purple, respectively
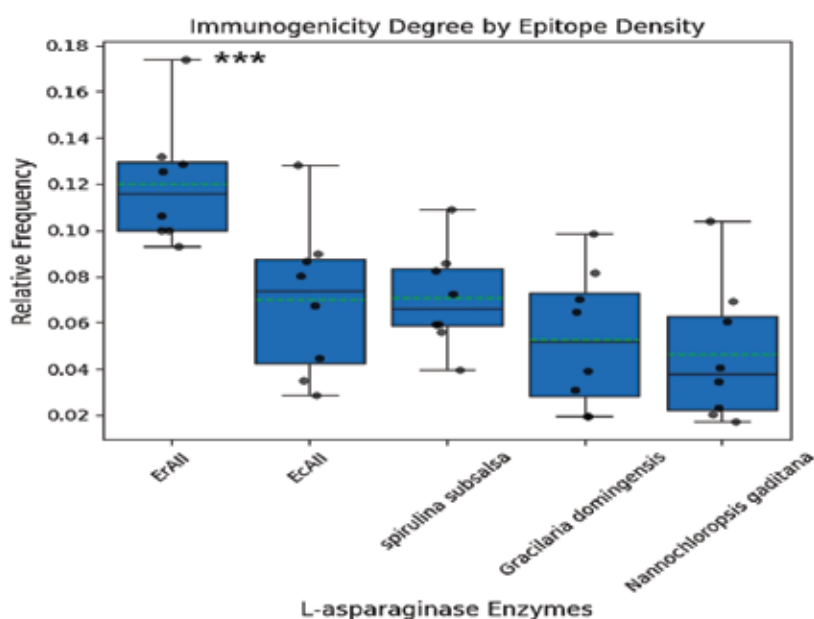

Fig. 2. Comparison of the epitope density and immunogenicity between asparaginases from *S. subsalsa*, *N. gaditana* CCMP526, *G. domingensis*, and clinical asparaginases EcAII and ErAII. The asterisk indicates the significant difference

eight (*HLA-DRB1*01:01, *HLA-DRB1*03:01, *HLA-DRB1*04:01, *HLA-DRB1*07:01, *HLA-DRB1*08:01, *HLA-DRB1*11:01, *HLA-DRB1*13:01 and *HLA-DRB1*15:01) alleles is shown in Figure 3, and the results indicate variability in distribution for each species depending on the allele. In most cases, the epitope density of *S. subsalsa*, *N. gaditana* CCMP526, and *G. domingensis* was lower than that of ErAII (Figure 3).

The HLA-DRB107:01 alleles are associated with hypersensitivity reactions and a higher risk of allergic reactions during treatment with bacterial asparaginase. The results showed that algal asparaginases exhibited lower epitope density for the HLA-DRB107:01 allele comparing EcAII and ErAII asparaginases.

Structure prediction

The AlphaFold 3 predicted the three-dimensional structure of *S. subsalsa* L-asparaginase, resulting in five structural models. The generated graphs and indicators demonstrated that the predicted structures are highly reliable. Among these structural models, the rank 1 structure was selected for its highest reliability, with a pLDDT index of approximately 100 and a PTM index of 0.96. The structures of *G. domingensis* and *N. gaditana* CCMP526 were also predicted with PTM indices of 0.84 and 0.85, respectively, indicating good structural reliability (Figure 4).

Prediction and analysis of linear B-Cell epitopes in algal asparaginases

The linear B-cell epitopes of asparaginases from *S. subsalsa*, *N. gaditana* CCMP526, and *G. domingensis* were predicted to evaluate their potential for antibody production in serum. The results revealed that *S. subsalsa* had 11 epitopes, of which one was allergenic, 10 were non-allergenic, 7 were immunogenic, and 4 were non-immunogenic. In *N. gaditana* CCMP526, 20 epitopes were identified, including 13 allergenic, 7 non-allergenic, 10 immunogenic, and 10 non-immunogenic epitopes. Similarly, *G. domingensis* exhibited 17 epitopes, with 10 allergenic, 7 non-allergen-
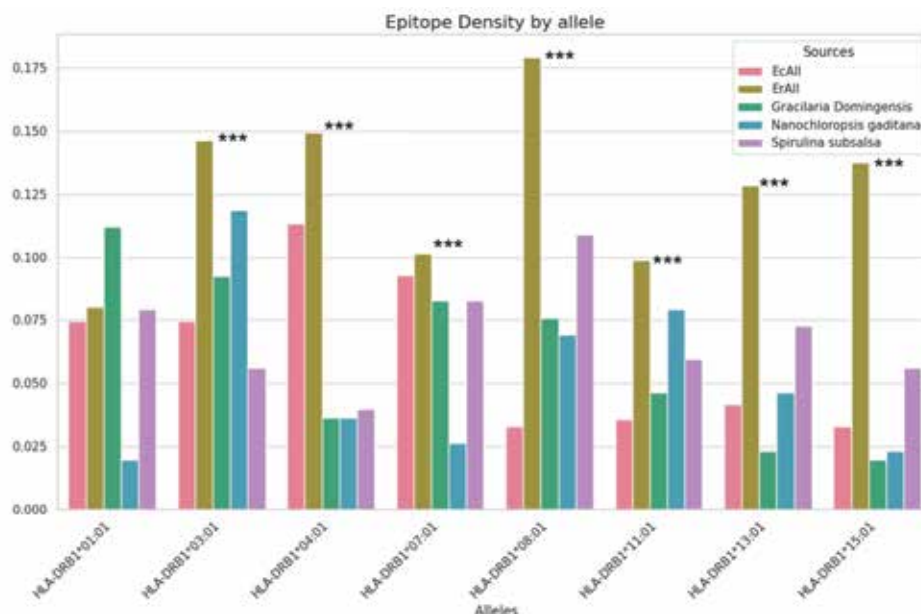

Fig. 3. The calculated epitope density for the alleles *HLA-DRB1*01:01, *HLA-DRB1*03:01, *HLA-DRB1*04:01, *HLA-DRB1*07:01, *HLA-DRB1*08:01, *HLA-DRB1*11:01, *HLA-DRB1*13:01, and *HLA-DRB1*15:01 reflects the proportion of immunogenic epitopes relative to the total peptides

ic, 11 immunogenic, and 6 non-immunogenic epitopes.

The mapping of allergenic epitopes, as shown in Figure 5, indicates that most regions of *S. subsalsa* are covered by non-allergenic epitopes, making it less likely to induce hypersensitivity reactions compared to asparaginases from *N. gaditana* CCMP526 and *G. domingensis*.

In contrast, *N. gaditana* CCMP526 exhibited the highest allergenic epitopes among the analyzed species, suggesting a greater potential for unwanted immune responses. Similarly, *G. domingensis* contains many allergenic and immunogenic epitopes, which may influence its immunogenic potential and likelihood of triggering immune responses.
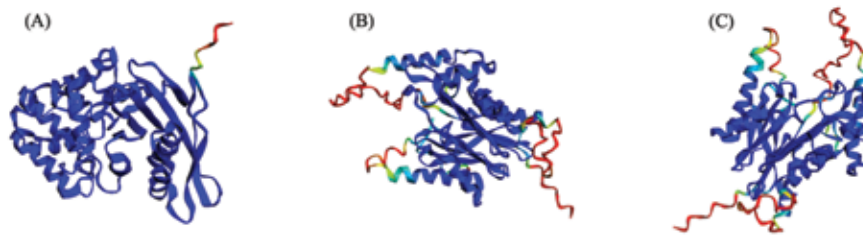

Fig. 4. Prediction of the 3D structures of asparaginases with AlphaFold 3, with colors shading from blue (high confidence) to yellow (low confidence) for each structure. Predicted enzyme structures of (A) *S. subsalsa*, (B) *G. domingensis*, and (C) *N. gaditana* CCMP526
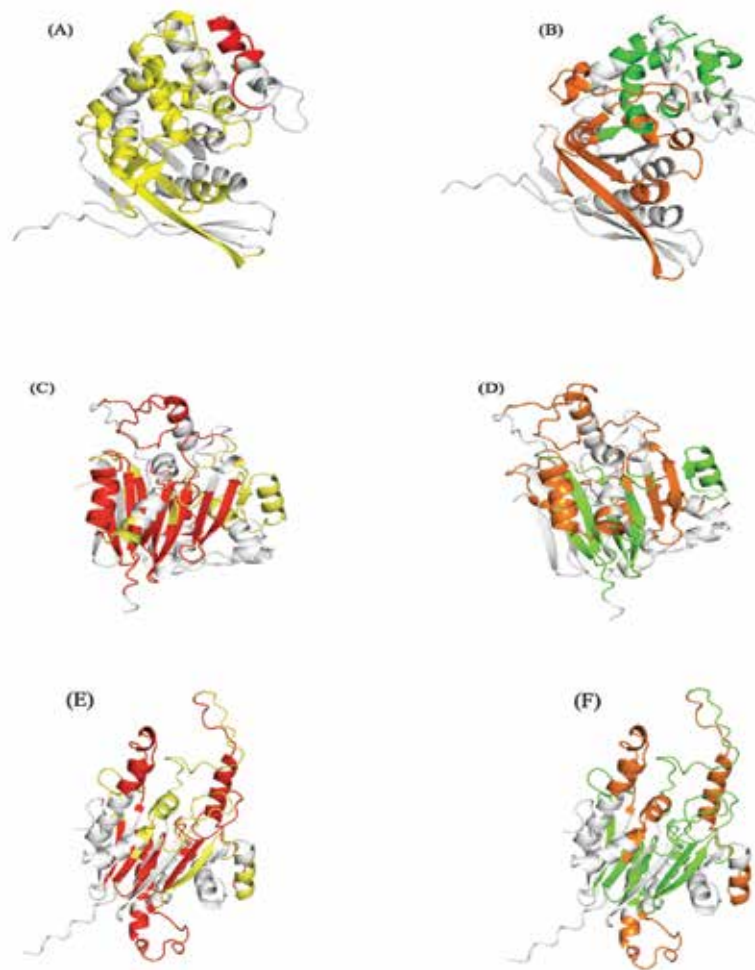

Fig. 5. Structural distribution of B-cell epitopes in the asparaginases monomers of (A, B) *S. subsalsa*; (C, D) *G. domingensis*, and (E, F) *N. gaditana* CCMP526. Panels (A, C, E) show the

Discussion

In this study, a phylogenetic tree of L-asparaginase was constructed using sequences from three algae species: *N. gaditana CCMP526*, *S. subsalsa*, and *G. domingensis*, along with 25 L-asparaginase sequences from classes 1, 2, and 3. The L-asparaginase from *S. subsalsa* was found to cluster with the L-asparaginases belonging to class 3. This class of enzymes encompassesboth permanent (thermophilic, type IV) and inducible (thermosensitive, type V) enzymes, which were initially discovered in *Rhizobium etli* (Ściuk et al. 2024). The phylogenetic tree revealed that class 3 enzymes differ significantly in amino acid sequence and structural features from the other classes. These differences are primarily attributed to unique features in their active sites and homodimeric structure. Until now, no phylogenetic studies have been conducted on the *S. subsalsa* L-asparaginase.

L-asparaginases from *N. gaditana* CCMP526 and *G. domingensis* clustered within the L-asparaginase class 2. Class 2 L-asparaginases consist of type III enzymes, which can be further divided into potassium-dependent (K-dependent) and potassium-independent (K-independent) enzymes (Sodek, Lea, and Miflin 1980). Type III L-asparaginases belong to the Ntn-hydrolase family (Linhorst and Lübke 2022b) and are produced as inactive precursors, which gain catalytic activity through self-activation.

Currently, only type II enzymes (class 1) from *E. coli* (EcAII) and *E. chrysanthemi* (ErAII) are approved for the treatment of acute lymphoblastic leukemia (ALL) (Tosta Pérez et al. 2023b). On the other hand, the potential therapeutic use of other L-asparaginases (from class 2 or class 3) has often been overlooked due to their low substrate affinity. However, recent studies have reported that class 3 L-asparaginase exhibits favorable properties and efficacy in treating ALL and AML (Ściuk et al. 2024).

This study compared the immunogenicity of L-asparaginases from *S. subsalsa*, *N. gaditana* CCMP526, and *Gracilaria domingensis* with clinical enzymes EcAII and ErAII utilizing epitope density. Epitope density measures immunogenic potential, with higher epitope densities indicating greater immune system stimulation (Belén et al. 2020). The results showed that the L-asparaginases from *S. subsalsa*, *N. gaditana* CCMP526, and *G. domingensis* exhibited immunogenicity similar to EcAII. However, significant immunogenicity was observed in ErAII, which showed a higher immunogenic potential than the other enzymes. In comparison to other algal enzymes, *N. gaditana* CCMP526 L-asparaginase showed the lowest immunogenicity. This finding suggests that some algae-derived enzymes may have better immunogenic profiles for clinical use, with *N. gaditana* demonstrating the lowest epitope density and, therefore, the least potential for unwanted immune responses.

Further analysis of T-cell epitope density revealed differences based on *HLA-DRB* alleles. Notably, the *HLA-DRB1*07:01 allele, associated with hypersensitivity reactions and an increased risk of allergic reactions during L-asparaginase treatment for leukemia (Fernandez et al. 2014), showed lower epitope density in *S. subsalsa*, *N. gaditana* CCMP526, and *G. domingensis* compared to

the clinical enzymes EcAII and ErAII. This suggests that algae-derived L-asparaginases may present a lower risk of hypersensitivity reactions. Furthermore, the type III enzyme from *N. gaditana* CCMP526 exhibits a lower allergenicity compared to other algal sources.

In addition to T-cell epitope analysis, linear B-cell epitopes were predicted to evaluate the potential for antibody production in serum. The results indicated that *S. subsalsa* had fewer allergenic epitopes than *N. gaditana* CCMP526 and *G. domingensis*, making it a safer option for clinical use. On the other hand, *N. gaditana* CCMP526 had the highest number of allergenic epitopes among the species studied, which could lead to unwanted immune responses. Moreover, *G. domingensis* displayed more allergenic epitopes and immunogenicity, which may affect its immunogenic profile and increase immune responses.

Combining the results from both T-cell and B-cell epitope analyses, it can be concluded that *S. subsalsa* represents the most appropriate candidate for clinical use. This species not only demonstrated low epitope density in both T-cell and B-cell analyses but also exhibited a reduced risk of allergic reactions, making it a safer alternative for clinical applications. In contrast, while *N. gaditana* CCMP526 exhibited the lowest T-cell epitope density, it had the highest number of allergenic epitopes in the B-cell analysis, which could potentially lead to unwanted humoral responses. *G. domingensis*, although showing some advantages over *N. gaditana*, still presented more allergenic epitopes than *S. subsalsa* and could trigger more immune reactions.

Therefore, *S. subsalsa* stands out as the most promising option for clinical use, as it offers a lower epitope density and a potentially safer immunogenic profile, with a reduced risk of triggering immune responses.

References

Abramson, Josh, Jonas Adler, Jack Dunger, Richard Evans, Tim Green, Alexander Pritzel, Olaf Ronneberger, Lindsay Willmore, Andrew J. Ballard, and Joshua Bambrick. 2024. "Accurate Structure Prediction of Biomolecular Interactions with AlphaFold 3." *Nature,* 630 (8016): 493–500.

Andrade, Kellen Cruvinel Rodrigues, Mauricio Homem-de-Mello, Julia Almeida Motta, Marina Guimarães Borges, Joel Antônio Cordeiro de Abreu, Paula Monteiro de Souza, Adalberto Pessoa, Georgios J. Pappas Jr., and e Pérola de Oliveira Magalhães. 2024. 'A Structural In Silico Analysis of the Immunogenicity of L-Asparaginase from *Penicillium Cerradense*'. *International Journal of Molecular Sciences,* 25 (9): 4788.

Belén, Lisandra Herrera, Jorge F. Beltrán Lissabet, Carlota de Oliveira Rangel-Yagui, Gisele Monteiro, Adalberto Pessoa, y Jorge, and G. Farías. 2020. 'Immunogenicity Assessment of Fungal L-Asparaginases: An in Silico Approach'. *SN Applied Sciences,* 2 (2): 222. DOI: https://doi.org/10.1007/s42452-020-2021-z.

Belén, Lisandra Herrera, Jorge Beltrán Lissabet, Carlota de Oliveira Rangel-Yagui, Brian Effer, Gisele Monteiro, Adalberto Pessoa, and Jorge G. Farías Avendaño.

2019. 'A Structural in Silico Analysis of the Immunogenicity of L-Asparaginase from Escherichia Coli and Erwinia Carotovora'. *Biologicals,* 59:47–55.

Blum, Matthias, Hsin-Yu Chang, Sara Chuguransky, Tiago Grego, Swaathi Kandasaamy, Alex Mitchell, Gift Nuka, et al. 2021. 'The InterPro Protein Families and Domains Database: 20 Years On'. *Nucleic Acids Research,* 49 (D1): D344–54. DOI: https://doi.org/10.1093/nar/gkaa977.

Borek, Dominika, and Mariusz Jaskólski. 2001. 'Sequence Analysis of Enzymes with Asparaginase Activity.' *Acta Biochimica Polonica,* 48 (4): 893–902.

Bowman, W. Paul, Eric L. Larsen, Meenakshi Devidas, Stephen B. Linda, Laurie Blach, Andrew J. Carroll, William L. Carroll, et al. 2011. 'Augmented Therapy Improves Outcome for Pediatric High Risk Acute Lymphocytic Leukemia: Results of Children's Oncology Group Trial P9906'. *Pediatric Blood & Cancer,* 57 (4): 569–77. DOI: https://doi.org/10.1002/pbc.22944.

Doytchinova, Irini A, and Darren R Flower. 2007. 'VaxiJen: A Server for Prediction of Protective Antigens, Tumour Antigens and Subunit Vaccines'. *BMC Bioinformatics,* 8 (1): 4. DOI: https://doi.org/10.1186/1471-2105-8-4.

Fernandez, Christian A., Colton Smith, Wenjian Yang, Mihir Daté, Donald Bashford, Eric Larsen, W. Paul Bowman, Chengcheng Liu, Laura B. Ramsey, and Tamara Chang. 2014. 'HLA-DRB1* 07: 01 Is Associated with a Higher Risk of Asparaginase Allergies'. *Blood, The Journal of the American Society of Hematology,* 124 (8): 1266–76.

Hunter, John D. 2007. 'Matplotlib: A 2D Graphics Environment'. *Computing in Science & Engineering,* 9 (03): 90–95.

Kagami, Luciano Porto, Gustavo Machado das Neves, Luís Fernando Saraiva Macedo Timmers, Rafael Andrade Caceres, and Vera Lucia Eifler-Lima. 2020. 'Geo-Measures: A PyMOL Plugin for Protein Structure Ensembles Analysis'. *Computational Biology and Chemistry* 87:107322.

Karamitros, Christos S., and Manfred Konrad. 2014. 'Human 60-kDa Lysophospholipase Contains an N-Terminal L-Asparaginase Domain That Is Allosterically Regulated by L-Asparagine'. *Journal of Biological Chemistry,* 289 (19): 12962–75.

Kumar, Sudhir, Glen Stecher, and Koichiro Tamura. 2016. 'MEGA7: Molecular Evolutionary Genetics Analysis Version 7.0 for Bigger Datasets'. *Molecular Biology and Evolution,* 33 (7): 1870–74. Doi: https://doi.org/10.1093/molbev/msw054.

Linhorst, Arne, and Torben Lübke. 2022a. 'The Human Ntn-Hydrolase Superfamily: Structure, Functions and Perspectives'. *Cells,* 11 (10): 1592.

Loch, Joanna I., and Mariusz Jaskolski. 2021. 'Structural and Biophysical Aspects of L-Asparaginases: A Growing Family with Amazing Diversity'. *IUCrJ,* 8 (4): 514–31.

Loch, Joanna I., Agnieszka Klonecka, Kinga Kądziołka, Piotr Bonarek, Jakub Barciszewski, Barbara Imiolczyk, Krzysztof Brzezinski, Mirosław Gilski, and Mariusz Jaskolski. 2022. 'Structural and Biophysical Studies of New L-Asparaginase

Variants: Lessons from Random Mutagenesis of the Prototypic Escherichia Coli Ntn-Amidohydrolase'. *Acta Crystallographica Section D: Structural Biology,* 78 (7): 911–26.

Loch, Joanna I., Paulina Worsztynowicz, Joanna Sliwiak, Marta Grzechowiak, Barbara Imiolczyk, Kinga Pokrywka, Mateusz Chwastyk, Miroslaw Gilski, and Mariusz Jaskolski. 2023. 'Rhizobium Etli Has Two L-Asparaginases with Low Sequence Identity but Similar Structure and Catalytic Center'. *Acta Crystallographica Section D: Structural Biology,* 79 (8). Doi: https://journals.iucr.org/d/issues/2023/08/00/dw5237/dw5237.pdf.

McKinney, Wes. 2010. 'Data Structures for Statistical Computing in Python.' In *SciPy*, 445:51–56. http://conference.scipy.org.s3.amazonaws.com/proceedings/scipy2010/pdfs/mckinney.pdf.

Pedroso, Alejandro, Lisandra Herrera Belén, Jorge F. Beltrán, Rodrigo L. Castillo, Adalberto Pessoa, Enrique Pedroso, and Jorge G. Farías. 2023. 'In Silico Design of a Chimeric Humanized L-Asparaginase'. *International Journal of Molecular Sciences,* 24 (8): 7550.

Saha, Sudipto, and G. P. S. Raghava. 2006a. 'Prediction of Continuous B-cell Epitopes in an Antigen Using Recurrent Neural Network'. *Proteins: Structure, Function, and Bioinformatics,* 65 (1): 40–48. DOI: https://doi.org/10.1002/prot.21078.

Saha, Sudipto, and Gajendra Pal Singh Raghava. 2006b. 'AlgPred: Prediction of Allergenic Proteins and Mapping of IgE Epitopes'. *Nucleic Acids Research,* 34 (suppl_2): W202–9.

Schalk, Amanda M., Hien-Anh Nguyen, Coraline Rigouin, and Arnon Lavie. 2014. 'Identification and Structural Analysis of an L-Asparaginase Enzyme from Guinea Pig with Putative Tumor Cell Killing Properties'. *Journal of Biological Chemistry,* 289 (48): 33175–86.

Ściuk, Anna, Kinga Wątor, Izabela Staroń, Paulina Worsztynowicz, Kinga Pokrywka, Joanna Sliwiak, Marta Kilichowska, Kamila Pietruszewska, Zofia Mazurek, and Anna Skalniak. 2024. 'Substrate Affinity Is Not Crucial for Therapeutic L-Asparaginases: Antileukemic Activity of Novel Bacterial Enzymes'. *Molecules,* 29 (10): 2272.

Sodek, Ladaslav, Peter J. Lea, and Benjamin J. Miflin. 1980. 'Distribution and Properties of a Potassium-Dependent Asparaginase Isolated from Developing Seeds of Pisum Sativum and Other Plants'. *Plant Physiology* 65 (1): 22–26.

Srikhanta, Yogitha N., John M. Atack, Ifor R. Beacham, and Michael P. Jennings. 2013. 'Distinct Physiological Roles for the Two L-Asparaginase Isozymes of Escherichia Coli'. *Biochemical and Biophysical Research Communications,* 436 (3): 362–65.

Tosta Pérez, María, Lisandra Herrera Belén, Pablo Letelier, Yolanda Calle, Adalberto Pessoa, and Jorge G. Farías. 2023a. 'L-Asparaginase as the Gold Standard in the Treatment of Acute Lymphoblastic Leukemia: A Comprehensive Review'. *Medical Oncology,* 40 (5): 150. Doi: https://doi.org/10.1007/s12032-023-02014-9.

Virtanen, Pauli, Ralf Gommers, Travis E.

Oliphant, Matt Haberland, Tyler Reddy, David Cournapeau, Evgeni Burovski, Pearu Peterson, Warren Weckesser, and Jonathan Bright. 2020. 'SciPy 1.0: Fundamental Algorithms for Scientific Computing in Python'. *Nature Methods,* 17 (3): 261–72.

Waskom, Michael L. 2021. 'Seaborn: Statistical Data Visualization'. *Journal of Open Source Software,* 6 (60): 3021.

Seed Protein Analysis as a Tool for Taxonomy of *Alcea* (Malvaceae) in Iran

Maneezheh Pakravan*

Abstract

The genus *Alcea* L. consists of over 50 species, which are primarily distributed in the Irano-Turanian region but have also spread into the Caucasus and the Eastern Mediterranean. Due to the high phenotypic plasticity observed in this genus, species identification requires a combination of traits that are often not all present in a single herbarium specimen. In this study, the electrophoresis of seed proteins is investigated in 24 species and 4 varieties of the genus *Alcea.* Plant samples were collected from 18 different provinces. This study aimed to apply the seed protein pattern in *Alcea* species to determine the boundary between *Alcea* species by using Sodium Dodecyl Sulfate Polyacrylamide Gel Electrophoresis (SDS-PAGE). The observed protein bands provided a basis for comparing the species. A total of 7 common bands were found among all species, which can be considered characteristic markers of the genus *Alcea.* Similarity coefficients and Jaccard indices were used to create a similarity matrix, and a cluster analysis was performed using the Ward method with SPSS software. The results showed that *A. aucheri* was closely related to *A. arbelensis, A. koelzii, A. rechingerii, A. kurdica,* and *A. schirazana* based on seed protein storage. A close relationship was observed between *A. arbelensis* and *A. rechingerii*, with a 90% protein similarity. Additionally, 92% protein similarity was found between *A. gorganica* and *A. popovi*. In the cluster analysis, the species were grouped into 7 clusters, which were nearly identical to the morphological grouping of the species. The seed electrophoresis results were compared with previous molecular phylogenetic studies. We can conclude that seed protein analysis is more useful in determining the relationship of closely related species and subspecies within the genus *Alcea*.

Keywords: *Alcea*, Electrophoresis, Iran, SDS-PAGE, Storage proteins

Introduction

The Malvaceae family was initially recognized as a separate family by de Jussieu in the 18th century (Judd & Manchester,1997). In the early 20th century, the Malvaceae family was divided into subfamilies such as Malvoideae (Hutchinson, 1967; Judd & Manchster, 1997; Alverson et al*.,* 1999; Takhtajan, 1980). In the late 20th and early 21st centuries, advancements in genetic

technologies, the family relationships within Malvaceae were reassessed using DNA analysis. These changes led to the merger of the Tiliaceae and Sterculiaceae families into Malvaceae (Kubitzki & Bayer, 2003; Stevens, 2001, 2014; APG III, 2009 & APG IV, 2016; Le Péchon & Gigord, 2014; Walker & Eggli, 2023; Hanes et al., 2024).

Currently, the Malvaceae family includes four main subfamilies: Malvoideae, Bombacoideae, Sterculioideae, and Matisioideae. This classification is based on genetic evidence and morphological characteristics (Colli-Silva et al. 2025).

The genus *Alcea* L., a prominent genus within the Malvaceae family, encompasses more than 50 species. These species are primarily distributed in the Irano-Turanian region, although they have also spread into the Caucasus and the Eastern Mediterranean (Zohary, 1963). Among the 33 species that grow in Iran, he majority are located in the western regions (Pakravan 2008). Most species of *Alcea* are tall hemicryptophytes with palmate to simple or lobed leaves, covered with stellate or branched hairs (Pakravan, 2008). The flowers have five sepals and 5 to 9 epicalyxes, and they are large and colorful. Zohary suggested nine informal species groups for *Alcea* based on leaf shape, epicalyx, and mericarp characters (Zohary, 1963a, b). *Althea* L. (the sister group of *Alcea* [Tate et al., 2005; Escobar et al., 2009]) is similar to *Alcea*, but distinguished from *Alcea* by having flowers smaller than 30 mm, a cylindrical stamen tube, and one chambered carpel (Escobar et al., 2012). *Alcea* is one of the most challenging genera in Central Asia (Iljin, 1949; Zohary, 1963b;

Riedl, 1976; Townsend, 1980). Any classification in this genus encounters similarities in the characteristics of various organs. Due to the high phenotypic plasticity observed in this genus, species identification requires a combination of traits, such as leaf shape, the ratio of the calyx to epicalyx, and the shape of mature mericarps, which are often not all present in a single herbarium specimen.

There have been few morphological studies on this genus, including the classification of the subgenus by Bossier (1867), Zohary (1963), Riedl (1976), and Pakravan (2001, 2003, 2005, 2006a, 2006b, 2008). Studies on pollen (Arabameri et al., 2023), fruit, and seed (Özbek & Uzunhisarcıklı, 2023) have been attempted to assist in the classification of *Alcea* species. Research on seed proteins, which serves as a valuable approach for determining species relationships, has thus far been limited to the family level within the Malvaceae family (Ibrahim et al., 2023). They analyzed seed proteins in 49 species of 34 genera, and the results contributed to establishing the family classification. This research confirmed the effectiveness of utilizing seed proteins as a reliable approach for the classification of taxa within the Malvaceae subfamilies.

Several phylogenetic studies have been conducted on the Malvaceae family and the *Althea* genus (Escobar et al. 2009); however, the only comprehensive molecular phylogenetic analysis was conducted by Escobar et al. (2012), focusing on the *Alcea* genus. Using three molecular markers (nrDNA, the plastid spacers *psbA-trnH* and *trnL-trnF*), they confirmed the monophyly of the *Alcea* and distinguished it from the *Althea*.

Given that seed proteins are considered valuable molecular markers at the protein level for plant classification and have not been studied within the genus *Alcea*, this study aims to utilize the seed protein patterns in *Alcea* species to ascertain the accurate taxonomic positioning of the species and subsequently aid in their classification. Lastly, the study will investigate the alterations that have occurred within the intraspecific divisions observed in specific species.

Material and methods

Seed collection and protein extraction

Seeds of 24 species and four varieties were collected from 18 provinces (Table 1). A minimum of two to three individuals from the accessions of each species were utilized for the analysis. Since the number of individuals with ripe seeds in each population was small and the seeds were also light in weight, fewer individuals were examined despite multiple collections.

0.5 gram of each seed were ground using liquid nitrogen in a cold environment, and the protein extract was prepared using seed powder in a Tris-Glycine buffer (pH = 7.2) at a ratio of 1:6 (including 30 grams of Tris, 144g of Glycine, 10g of SDS, 70cc of water, 15µg of Temed, and 30 g of Acrylamide, 0.8 g of Bis-acrylamide). The extract was centrifuged for 45 minutes at 1500g.

Electrophoresis

SDS-PAGE electrophoresis was performed on polyacrylamide gels following the method of Laemmli (1976). After injecting the protein extract, the gels were transferred to an electrophoresis tank and subjected to a 5mA current at room temperature. Due to the large number of samples, electrophoresis was conducted on three separate gels, each containing 18 columns. To determine the molecular weight of unknown proteins, a standard solution (including Bovine serum albumin, egg serum albumin, Pepsin, trypsinogen, β-lactat albumin, Lysozyme) was used (Table 2). Protein concentration was measured using the Bradford method (Bradford, 1976).

Gel staining

Following electrophoresis, the gels were washed several times with distilled water and then stained with Coomassie Blue solution (containing 0.25 grams of Coomassie Blue, 125 mL of methanol, 25 mL of glacial acetic acid, and 100 mL of water) overnight (Smith, 1984). After staining, excess dye was removed by destaining the gels in a solution of acetic acid and methanol for 15hours.

Statistical analysis

The number and location of protein bands, and their Rm values, were determined. Cluster analysis based on the Jaccard and similarity coefficient using the Ward method (Podani, 2000) was performed using SPSS software. Based on these coefficients, the similarity percentage was calculated, and a matrix was created.

Results and Discussion

Overall, 37 protein bands were observed in different species of *Alcea* through protein electrophoresis. By comparing the protein bands and measuring the RM, it can be observed that Bands 1, 15, 22, and 30 are present in all species, so these bands may serve

Table 1. Voucher details of *Alcea* species

Species	Location	Collector & Number	Voucher
A. angulata Freyn & Sint	Tehran: 87 Km from Tehran to Firuzkuh, 35.6053276, 52.4592907	Pakravan & Darrehshuri 26433	TUH
	Tehran: 3 Km to Robat-Karim on the road from Saveh to Tehran, 35.5345503, 51.1035845	Pakravan & Darrehshuri 26391	TUH
A. arbelensis Boiss. & Hausskn.	Fars: 45 Km to Yasuj from Esfahan, Tange-Tizab, 30.3690210, 51.7875348	Pakravan & Darrehshuri 26406	TUH
	Kermanshah: 4 Km from Sahneh to Kangavar, 34.4466768, 47.7419318	Pakravan & Hayelmoghadam 26449	TUH
A. aucheri (Boiss.) Alef.	Fars: Noorabad to Kazerun road, research institute, 29.5696222, 51.7416341	Sardabi & Latifian 42157	TARI
A. glabrata Alef.	Tehran: Ghazvin road, 31 Km from Takestan to Buin Zahra, 35.8731861, 49.5497782	Pakravan & Hayelmoghadam 26384	TUH
A. glabrata Alef. var. *microcarpa*	Tehran: 30 Km from Karaj to Challus, 36.2006439, 51.3617076	Pakravan & Darrehshuri 26372	TUH
	Tehran: Kan, near the river, 35.8005378, 51.2589569	Pakravan & Darrehshuri 26397	TUH
A. gorganica (Rech. f.., Aell. & Esfand.) Zoh.	Golestan: Golestan National Park, 450 m, 37.4443110, 56.1424860	Akhani 11819	W
	Khorassan: Between Bojnurd and Maraveh tappeh, 38.0817152, 56.4403929	Assadi & Mozaffarian 35605	TARI
A. popovii Iljin	Golestan: 5 Km from Galikesh to Golestan National Park, 250 m, 37.3267723, 55.4897674	Mozaffarian & Maasoumi 79112	TARI
A. mazandaranica	Mazandaran: Kelardasht, Roodbarak, 1650 m, 36.4821203, 51.1279873	Mozaffarian 45495	TARI
A. kurdica (Schlecht.) Alef.	KurdestanSanandaj, Abidar Park, 35.3099883, 46.9701690	Pakravan & Hayelmoghadam 26401	TUH
A. kurdica (Schlecht.) Alef. var. *laxiflora* (Riedle) Pakravan	Kermanshah: Between Khamseh and Bisotun, 34.4374004, 47.4986567	Pakravan & Hayelmoghadam 26443	TUH
A. rechingeri (Zohary) Riedl	Kermanshah: Tagh-e Bostan, 34.3857435, 47.1344034	Pakravan & Hayelmoghadam 26439	TUH
A. shirazana Alef.,	Fars: Between Ardakan & Komeh, 30.3318827, 51.9687954	Pakravan & Darreh shuri 26408	TUH
A. koelzii I. Riedl	Markazi: Between Arak and Salafchegan, 34.2975075, 50.2345917	Ghahreman 10098	TUH
	Kohgiluyeh: Yasuj, 30.6661864, 51.6230154	Ghahreman 10095	
A. tiliacea (Bornm. Zohary	Khorassan: Neyshabur, upper Mirab, 1600-1900 m, 36.0934766, 58.7878643	Assadi & Mozaffarian 36099	TARI
	Khorassan: 14 Km from Kashmar to Neyshabur, 1400-1500 m, 32.4214271, 58.5088468	Assadi & Maasoumi 35622	TARI

A. sulphurea (Boiss. & Hohen.) Alef.,	Tehran: Tehran: Fasham, 35.9368816, 51.5048014	Pakravan & Darreh shuri 26433	TUH
	Tehran: Damavand, 3 Km from Darbandsar to Fasham, 35.9891013, 51.4861346	Pakravan & Darreh shuri 26378	TUH
A. striata (DC.) Alef.,	Bushehr: Kuh-e Haft-Chah, 1600 -2000 m, 27.6834441, 52.4473810	Mozaffarian 74085	TARI
A. tabrisiana (Boiss. & Buhse) Iljin	Tehran: 37 Km from Tehran to Ghazvin, 36.1188777, 50.3946687	Pakravan & Hayelmoghadam 26455	TUH
A. wilhelminae Riedl	Azerbaijan: Ghuschi pass, between Salmas and Urumiyeh, 38.0130092, 44.9547488	Pakravan & Hayelmoghadam 26418	TUH
A. wilhelminae Riedl var. *lineariloba* *(*Riedl)Pakravan	Azerbaijan: Ghuschi pass, 38.0131846, 44.9402488	Pakravan & Hayelmoghadam 26389	TUH
A. sachsachanica Iljin,	Azerbaijan: Ghushchi pass, 38.0131846, 44.9402488	Pakravan & Hayelmoghadam 26390	TUH
A. mozaffarianii Ghahreman, Pakravan & Assadi	Ardebil: Road of Ardebil to Khalkhal, 2000-2500 m, 37.8482705, 48.3729127	Mozaffarian & Maasoumi 78245	TARI
A. iranshahri Pakravan, Ghahreman & Assadi	Fars: Kuh-e Dena, Bijan pass, 2500 m, 30.8629268, 51.4947690	Assadi & Mozaffarian 31162	TARI
A. flavovirens (Boiss. & Buhse) Iljin	Hamedan: Avaj pass 35.5365856, 49.1372051	Pakravan & Hayelmoghadam 26388	TUH
A. flavovirens (Boiss. & Buhse) Iljin var. *albiflora* Zohary	Azerbaijan: 81 Km from Tabriz to Mianeh, 37.3053915, 47.1045185	Pakravan & Hayelmoghadam 26387	TUH
A, ghahremanii Pakravan, Maasoumi & Assadi	Azerbaijan: Mianeh, 1700 m, 37.4760113, 47.6628803	Attar & Dadjoo 18044	TUH
A. transcaucasica (Iljin) Iljin	Kurdestan: 101 Km from Marivan to Paveh, 35.2731969, 46.1621723	Runemark & Assadi 27434	TARI
A. calverti (Boiss.) Boiss. var. *albiflora* Zohary	Kohgiluyeh &Boyerahmad: Between Yasuj & Dehdasht, Kuh-e Saverz, 2300-3200 m, 30.7059248, 51.1285056	Assadi & Abuhamzeh 46386	TARI
A. tarica Pakravan	Tehran: Road Firuzkuh to Damavand, Tar Lake, 35.7300093, 522224757	Pakravan & Darreh shuri 26380	TUH

Table 2. Molecular weight and logarithm of molecular weight of proteins used in SDS-PAGE

Proteins	Molecular Weight (kDa)	Logarithm of molecular weight
Albumin bovine	66000	4.820
Albumin egg	45000	4.652
Pepsin	34700	4.540
Trypsinogen (Bovine Pancreas)	24000	4.380
B-Lactalbumin	18400	4.265
Lysozyme	14300	4.155

as the genus markers. Band 32 was observed in the *A. kurdica* group (such as: *A. arbelensis* Boiss. & Hausskn*., A koelzii, A. rechingerii, A. kurdica* (Schlecht.) Alef*., A. schirazana* Alef.), as well as in *A. striata* (DC.) Alef. and *A. iranshahrii* Pakravan, Ghahreman & Assadi (Fig. 2). Based on the common bands, the closeness of the taxa can be inferred. In this study, *A. wilhelminae* Riedl and *A. wilhelminae* var. *lineariloba* (Riedl) Pakravan share 33 bands (Fig.1), indicating a very close relationship between these two taxa. Therefore, based on this closeness, the reduction of *A. lineariloba* at the varietal level of *A. wilhelminae* (Pakravan 2008) is confirmed. Additionally, *A. gorganica* (Rech. f., Aell. & Esfand.) Zoh., and *A. popovii* Iljin share 35 bands, indicating a high degree of similarity between these two species (Fig. 1). Furthermore, *A. glabrata* Alef. and *A. glabrata* var. *microcarpa* (Zohary) Pakravan & Ghahreman share 33 bands (Fig. 1).

Using the similarity matrix table derived from the protein data (Table 3), the proximity of the above species can be expressed in a better way. As shown in Figure 1, within the *A. kurdica* species group, *A. arbelensis* and *A. koelzii* have a similarity of 0.68%, but the similarity between *A. arbelensis* Boiss. & Hausskn. and *A. rechingerii* (Zohary) Riedl is higher (0.90%). In this group, the similarity between *A. kurdica* var. *laxiflora* (Riedle) Pakravan and *A. kurdica* is 0.68%. Additionally, the similarity between *A. kurdica* and *A. arbelensis* is 0.75%. This degree of similarity among the species confirms their placement in the same species group. The similarity percentage between *A. gorganica* and *A. popovi* is 0.92%, which confirms a decline of *A. popovi* as a variety of *A. gorganica*.

In the *A. flavovirens* group, a high similarity of 0.71% is observed between *A. glabrata* and var. *microcarrpa*. Based on this percentage of similarity, the classification of var. *microcarpa* as a variety of *A. glabrata is* supported.

In the dendrogram obtained from cluster analysis (Fig. 3), the placement of *A. aucheri* (Boiss.) Alef, along with *A. kurdica* var. *laxiflora*, *A. rechingerii*, *A. koelzii I. Riedl* and *A. arbelensis* do not consistently align with the species grouping based on morphological traits. Considering the phylogenetic tree in the previous study (Escobar et al., 2012), our results somewhat agree with the phylogenetic tree of *Alcea* species based on molecular data. In the phylogenetic studies
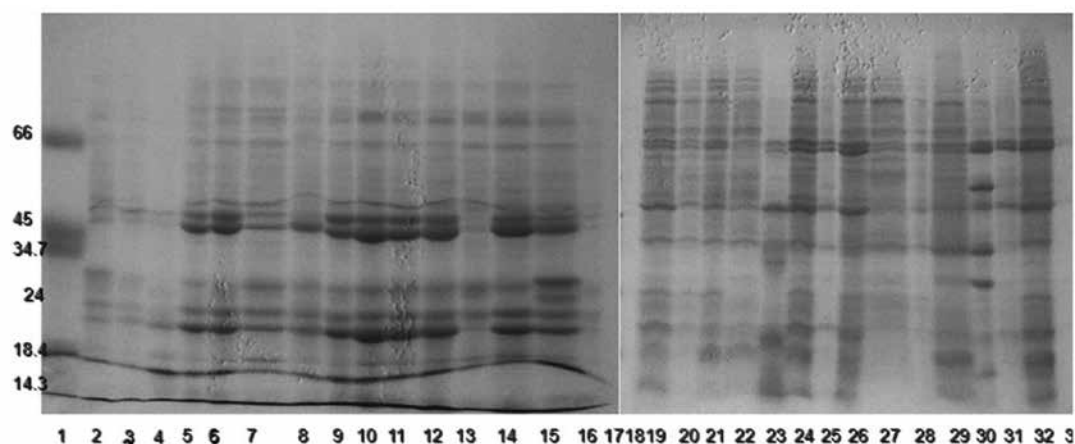
Fig. 1. SDS-PAGE polyacryl amid gel electrophoresis of seed proteins extracted of *Alcea* species studied: sequences of taxa from left to right: 1: Marker, 2, 3, 5: *A. angulata*; 4: *A. transcaucasica*; 6: *A.popovii*; 7: *A. gorganica*; 8,9: *A. wilhelminae* var. *lineariloba*; 10: *A. ghahremanii*; 11: *A. flavovirens*; 12: *A. flavovirens* var. *albiflora*; 13: *A. sachsachanica*; 14, 15: *A. wilhelminae*; 16: *A. tabrisiana*; 17: *A. tarica*; 18, 28, 31,32: *A. glabrata*; 19: *A. rhyticarpa* var. *tiliacea*; 21: *A. calverti*; 21, 22: *A. striata*; 23, 26: *A. glabrata* var. *microcarpa*; 24, 25, 33: *A. angulata*; 27: *A. tarica*; 29, 30: *A. sulphurea*
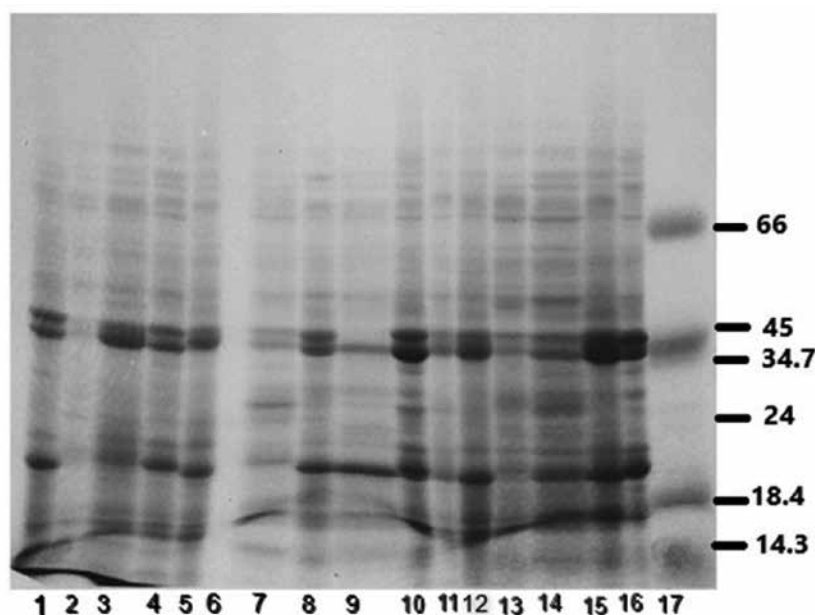
Fig. 2. SDS-PAGE polyacryl amid gel electrophoresis of seed proteins extracted of *Alcea* species studied: sequences of taxa from left to right: 1: *A. tarica*; 2: *A. aucheri*; 3: *A. sulphurea*; 4: *A. iranshahrii*; 5: *A. mazandaranica*; 6: *A. mozaffarianii*; 7: *A. koelzii* (Kohgiluyeh accession); 8: *A. koelzii* (Arak accession); 9, 10: *A. arbelensis*; 11: *A. rechingeri*; 12: *A. kurdica* var. *laxiflora*; 13: *A. schirazana*; 14, 15, 16: *A. kurdica*; 17: Marker

Table 3. Jaccard similarity coefficients for protein profiles of 24 species and four varieties of the genus *Alcea* from 50 samples representing the relatedness of similarity between the whole couples of *Alcea* species

Cod	an	Su-d	Su	lo	gl.d	ani	st	ca	t	gl	ta	w	sa	f	fl.a	gh	w-d	go	po	an	tr	ku	sc	la	re	ko	ko-e	mo	ma	ir	au
an	1.000
Su-d	0.632	1.000
Su	0.432	0.438	1.000
lo	0.424	0.371	0.824	1.000
gl.d	0.429	0.348	0.406	0.352	1.000
ani	0.500	0.429	0.543	0.600	0.500	1.000
st	0.542	0.520	0.677	0.687	0.321	0.353	1.000
ca	0.609	0.520	0.625	0.636	0.480	0.586	0.571	1.000
t	0.489	0.412	0.624	0.882	0.424	0.600	0.636	0.687	1.000
gl	0.344	0.419	0.611	0.714	0.344	0.576	0.471	0.515	0.667	1.000
ta	0.375	0.406	0.639	0.743	0.375	0.559	0.545	0.564	0.743	0.839	1.000
w	0.400	0.357	0.639	0.686	0.400	0.500	0.531	0.531	0.735	0.867	0.719	1.000
sa	0.364	0.394	0.667	0.722	0.364	0.543	0.529	0.529	0.722	0.812	0.903	0.439	1.000
f	0.333	0.333	0.639	0.649	0.333	0.514	0.500	0.503	0.694	0.781	0.871	0.306	0.967	1.000
fl.a	0.406	0.354	0.714	0.771	0.406	0.543	0.576	0.578	0.824	0.706	0.789	0.781	0.615	0.788	1.000
gh	0.333	0.364	0.639	0.694	0.333	0.514	0.500	0.684	0.781	0.871	0.306	0.967	0.933	0.844	1.000
w-d	0.344	0.375	0.611	0.667	0.344	0.529	0.429	0.471	0.967	0.759	0.727	0.967	0.812	0.781	0.812	0.839	1.000
go	0.323	0.355	0.556	0.657	0.281	0.515	0.412	0.455	0.611	0.800	0.774	0.655	0.606	0.774	0.750	0.833	0.929	1.000
po	0.367	0.400	0.556	0.657	0.323	0.515	0.455	0.500	0.657	0.742	0.833	0.710	0.606	0.774	0.806	0.833	0.862	0.926	1.000
an	0.267	0.393	0.472	0.571	0.357	0.484	0.406	0.452	0.571	0.645	0.733	0.613	0.790	0.677	0.710	0.733	0.750	0.815	0.885	1.000
tr	0.441	0.429	0.730	0.730	0.441	0.611	0.647	0.647	0.686	0.722	0.778	0.750	0.778	0.750	0.676	0.622	0.667	0.583	1.000
ku	0.424	0.412	0.676	0.730	0.382	0.600	0.588	0.588	0.733	0.667	0.694	0.639	0.771	0.743	0.722	0.743	0.676	0.611	0.611	0.571	0.833	1.000
Sc	0.500	0.433	0.639	0.448	0.645	0.531	0.485	0.639	0.618	0.647	0.983	0.556	0.583	0.556	0.526	0.514	0.559	0.471	0.743	0.735	1.000
la	0.370	0.357	0.444	0.500	0.423	0.533	0.419	0.375	0.500	0.471	0.500	0.441	0.486	0.500	0.486	0.457	0.429	0.412	0.455	0.412	0.600	0.687	0.815	1.000
re	0.406	0.394	0.667	0.722	0.452	0.687	0.529	0.486	0.676	0.687	0.689	0.541	0.622	0.595	0.622	0.595	0.611	0.600	0.600	0.559	0.730	0.722	0.761	0.625	1.000
ar	0.438	0.382	0.649	0.750	0.438	0.719	0.472	0.472	0.703	0.686	0.667	0.651	0.649	0.622	0.649	0.622	0.630	0.629	0.543	0.757	0.750	0.871	0.710	0.906	1.000
ko	0.444	0.379	0.500	0.600	0.500	0.778	0.394	0.484	0.556	0.529	0.514	0.500	0.543	0.514	0.543	0.514	0.486	0.471	0.471	0.489	0.611	0.679	0.730	0.704	0.887	0.774	1.000
ko-e	0.222	0.211	0.253	0.219	0.222	0.192	0.261	0.208	0.218	0.207	0.161	0.172	0.156	0.161	0.156	0.126	0.094	0.100	0.111	0.206	0.219	0.250	0.261	0.253	0.226	0.292	1.000
mo	0.414	0.355	0.556	0.611	0.519	0.667	0.495	0.548	0.657	0.500	0.571	0.606	0.556	0.528	0.600	0.528	0.459	0.425	0.444	0.441	0.714	0.758	0.767	0.714	0.647	0.727	0.786	0.269	1.000
ma	0.375	0.406	0.595	0.649	0.517	0.656	0.457	0.545	0.684	0.583	0.657	0.074	0.639	0.611	0.541	0.486	0.526	0.529	0.500	0.794	0.750	0.700	0.606	0.765	0.767	0.241	0.897	1.000
ir	0.375	0.214	0.412	0.515	0.500	0.448	0.379	0.379	0.515	0.438	0.516	0.503	0.500	0.489	0.500	0.469	0.438	0.419	0.467	0.414	0.529	0.515	0.607	0.600	0.500	0.581	0.615	0.250	0.571	1.000
au	0.408	0.390	0.660	0.725	0.459	0.680	0.531	0.489	0.675	0.590	0.675	0.667	0.645	0.543	0.620	0.590	0.618	0.670	0.580	0.590	0.740	0.720	0.780	0.622	0.250	0.518	0.667	0.544	0.622	0.450	0.890	1.000

Abbreviations: an: *A. angulata;* Su-d: *A. sulphurea* (Damavand accession); Su: *A. sulphurea* (Firuzkuh accession); lo: *A. glabrata Alef. var. microcarpa;* gl. d: *A. tarica;* ani: *A. gorganica* (Khorasan accession); St: *A. striata;* Ca: *A. calverti* var. *albiflora;* t: *A. tiliacea* ; gl: *A. glabrata;* ta: *A. tabrisiana;* W: *A. wilhelminae;* Sa: *A. sachsachanica;* Fl.: *A. flavovirens;* Fl.a: *A. flavovirens* var. *albiflora;* gh: *A, ghahremanii;* W-li: *A. wilhelminae* var. *lineariloba;* go: *A. gorganica;* po: *A. popovii;* an: *A. gorganica* (Khorasan accession); tr: *A. transcaucasica;* ku: *A. kurdica;* Sc: *A. shirazana;* la: *A. kurdica* var. *laxiflora;* re: *A. rechingeri;* ko: *A. koelzii;* ko-e: *A. koelzii* (Kohgiluyeh accession); mo: *A. mozaffarianii;* ir: *A. iranshahrii;* au: *A. aucheri*
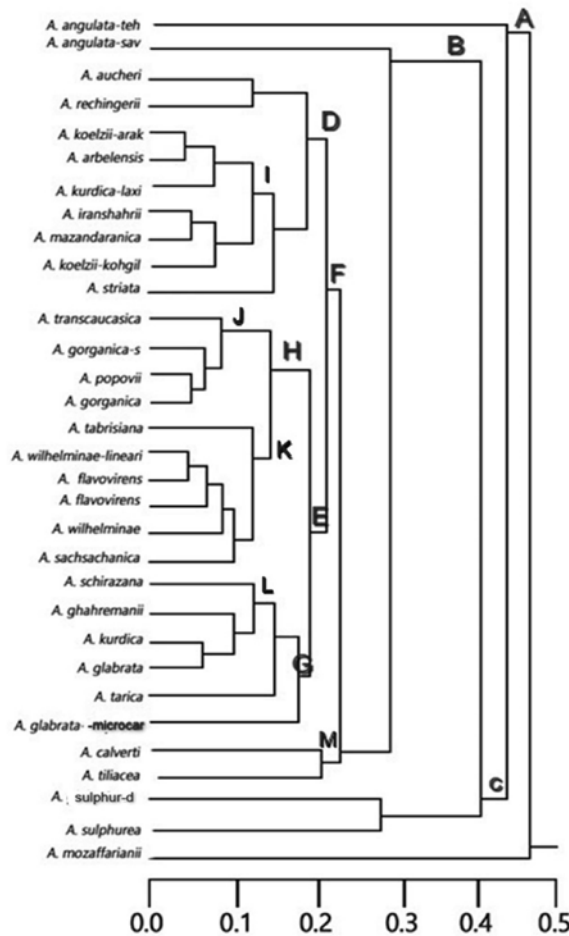

Fig. 3. Cluster analyses of SDS-PAGE patterns observed in Alcea accessions (Jaccard association coefficient index)

we conducted using some nuclear and chloroplast genes of *Alcea* species in the Irano-Turanian region, the phylogenetic trees did not closely match the species groupings based on morphological traits. The position of the species in the phylogenetic tree showed greater similarity to the dendrogram obtained from the present study (Escobar et al., 2012).

Furthermore, the placement of *A. rechingeri*, *A. koelzii*, and *A. arbelensis* in the same cluster confirms the morphological results (Pakravan, 2008). These species are all part of the same species group, characterized by mericarps that possess broad wings and lack folds, with their distribution located in western Iran. Additionally, *A. kurdica* var. *laxiflora* is also placed in this cluster, confirming the closeness of *A. laxiflora* to *A. kurdica,* leading to its classification at the varietal level of *A. kurdica* (Pakravan, 2001) On the other hand, a population of *A. koelzii* with red flowers, collected from the Kohgiluyeh and Boyer-Ahmad province, is located in this cluster. This taxon is separated from *A. koelzii* (with white flowers) at the 0.1 level in the dendrogram (Fig. 3), which suggests the variation of this taxon. Thus, it can be proposed as a variety of A. koelzii. However, a definitive statement about the position of this taxon requires further research in other biosystematics fields.

In the second cluster (branch H), the placement of *A. gorganica* and *A. popovi* alongside the subcluster of species group *A. flavovirens* align with the phylogenetic tree obtained from molecular phylogeny. Furthermore, *A. gorganica* is located next to *A popovi*, which differ only in flower color and wrinkling mericarp. Their placement in adjacent branches confirms their close relationships. Moreover, a sample identified as *A. sycophylla* in the Flora Iranica (Riedel, 1976), which is investigated morphologically (by the author), is placed in a branch next to *A. gorganica* and *A. popovi*. Since this sample shows no difference from *A. gorganica*, the presence of *A. sycophylla* Iljin & Nikitin in Iran, based on the samples reported by Riedel, is not confirmed.

In the subcluster K, the placement of *A. wilhelminae*, *A. flavovirens*, and *A. sachsacanica* Iljin together in the same branches fully confirms the morphological results as well as the phylogenetic tree obtained from molecular phylogeny. All of these species all classified within the *A. flavovirens* species group and exhibit several morphological similarities. These characteristics include a sparse, star-shaped hairy covering, palmate leaves with relatively deep lobes, and mericarps that possess well-developed wings and radially arranged wrinkles.

The positioning of *A. schirazana* within a common cluster alonside *A. kurdica,* is consistent with the morphological results. However, the placement of *A. schirazana* in a cluster with *A. glabrata*, *A. ghahremanii*, and *A. tarica* does not correspond with the morphological data. This discrepancy arises because all these species exhibit sparse hairs and mericarps that are either nearly wingless or possess degenerated wings. On the other hand, the placement of *A. tarica*, which has been introduced in recent years for the Flora of Iran (Pakravan, 2008), in a distinct cluster next to this one, further supports the distinction of this species.

Furthermore, the placement of *A. calverti* (Boiss.) Boiss. and *A. tiliacea* (Bornm.) Zohary, in a separate cluster (Fig. 3 subcluster M), does not align with the morphological results.

The placement of *A. sulphurea* far from *A. rhyticarpa* and *A. angulata*, which share many morphological similarities (having dense woolly hairs, shallowly cut leaves, and wingless mericarps), is not confirmed. *A. sulphurea* was placed in the *A. aucheri* species group by Zohary (1963a). *A. flavovirens* var. *alba*, with its white flowers, hairy ovaries, and veined sepals, is distinct from *A. flavovirens*. Therefore, the placement of *A. flavovirens* var. *alba* in a cluster distant from *A. flavovirens* indicates that this taxon could be elevated to the species level (Fig. 3), as its genetic distance is greater than that of a variety. However, this would require further investigations into gene sequencing.

A. mozaffarianii Ghahreman, Pakravan & Assadi was introduced in recent years for the Flora of Iran (Ghahreman et al. 2000). The placement of this species in a branch separated from other species confirms the distinction of this species as an independent and distinct unit.

From the results of the seed protein analysis in *Alcea* species, it can be concluded that the use of seed proteins is very useful for separating closely related taxa (such as varieties *A. kurdica*, *A. flavovirens*, and *A. glabrata*). Still, it has limited use in resolving interspecific relationships, which can be attributed to the phenotypic plasticity of morphological traits in the genus *Alcea*. As Escobar et al. (2012) concluded from their phylogenetic study, high species diversity in *Alcea* is due to rapid and recent radiation and low molecular divergence observed within the genus *Alcea*. Our work provides the first seed protein study in *Alcea* species.

Acknowledgements

References

Alverson, W. S., Whitlock, B.A., Nyffeler, R., Bayer, C., and Baum, D.A. 1999. Phylogenetic analysis of the core Malvales based on ndhF sequences. *American Journal of Botany,* 86, pp. 1474-1486.

APG III (Angiosperm Phylogeny Group). 2009. An update of Angiosperm Phylogeny Group classification for the orders and families of flowering plants: APG III. *Botanical Journal of The Linnean Society,* 161 (2), pp. 1005-121. DOI: 10.1111/j.1095-8339.2009.00996.x

APG IV (Angiosperm Phylogeny Group). 2016. An update of Angiosperm Phylogeny Group classification for the orders and families of flowering plants: APG IV. *Botanical Journal of The Linnean Society,* APG IV (Angiosperm Phylogeny Group). 181 (2), pp. .1-20.

Arabameri, M., Mehrabian, A., and Khodayari, H. 2023. Pollen Morphology of Malvaceae in Iran: A Case Study to Complete Pollen Atlas of Iran. *Plant, Algae, and Environment*,7(1), pp. 1093- 1110. DOI: 10.48308/jpr.2023.104476

Boissier, PE. 1867. Flora orientalis, vol. 1.

Basel.

Bradford, H.G.M.M. 1976. A rapid and sensitive method for the quantitation of microgram quantities of protein utilizing the principle of protein-dye binding. *Analytical biochemistry,* 72(1-2), pp. 248-254.

Colli-Silva, M., Pérez-Escobar, O.L., Ferreira, C. D.M., Costa, M.T.R., Gerace, S., Coutinho, T. S., Yoshikawa, V.N., Antonio-Domingues, H., Gutiérrez, R. H., Bovini, M.G., Duarte, M.C., Cheek, M., Chase, M.W., Fay, M.F., Christenhusz, M.J.M., Dorr, L. J., Schoeplein, C., Corcoran, M., Roy, S., Cable, S., McLay, T., Maurin, O., Forest, F., Baker1, W.J., & Antonelli, A. 2025. Taxonomy in the light of incongruence: An updated classification of Malvales and Malvaceae based on phylogenomic data. Taxon, 0, 0, 1-25. DOI:.org/10.1002/tax.13300.

Escobar García, P., Schönswetter, P., Fuertes Aguilar, J., Nieto Feliner, G. and Schneeweiss, G.M. 2009. Five molecular markers reveal extensive morphological homoplasy and reticulate evolution in the *Malva* alliance (Malvaceae). *Molecular Phylogenetics and Evolution,* 50, pp. 226-239. DOI: 10.1016/j.ympev.2008.10.015.

Escobar Garcia, P., Pakravan, M., Schönswetter, P., Fuertes Aguilar, J., and Schneeweiss, G.M. 2012. Phylogenetic relationships in the species-rich Irano-Turanian genus *Alcea* (Malvaceae). *Taxon*, 61(2), pp. 324-332. DOI: 10.1002/tax.612004.

Hutchinson, J. 1967. *The Genera of Flowering Plants (Angiospermae)*, vol. II. Clarendon Press, Oxford.

Hanes, M.M., Blanchard, O.J., Jr., Valencia-D., J., McLay, T., Abbott, J.R., McDaniel, S.F., Barrett, R.L., Mathews, S., & Neubig, K.M. 2024. Phylogenetic relationships within tribe Hibisceae (Malvaceae) reveal complex patterns of polyphyly in Hibiscus and Pavonia. Systematic Botany. 49, p.p. 77–116. DOI: org/10.1600/036364424X17114831879189.

Ibrahim, Z.M. and Hassan, S.H., Karakish, E.A., and Ismail, M. 2023. Significance of Seed Storage Protein and Seed Morphological Characters in the Classification of Some Species of Malvaceae *s.l. Egyptian Journal of Botany*, 63(2): 431-455. DOI: 10.21608/ejbo.2022.165769.2154.

Iljin, M.M. 1949. Malvaceae. In: Komarov, V.L., Shishkin, B.K., Bobrov, E.G. (Eds.), *Flora SSSR*, vol. 15. Botanical Institute of the Academy of Sciences of the USSR, Leningrad, pp. 21–137.

Judd, W.S. & Manchester, S.R. 1997. Circumscription of Malvaceae. (Malvales) as determined by a preliminary cladistic analysis of morphological, anatomical, palynological, and chemical characters. Brittonia, 49, p Judd, W.S. & Manchester, S.R. 1997. Circumscription of Malvaceae (Malvales) as determined by a preliminary cladistic analysis of morphological, anatomical, palynological, and chemical characters. *Brittonia*, 49, p.p. 340-405. DOI: org/10.2307/2807839.

Kubitzki, K. & Bayer, C. 2003. Malvales In: Kubitzki (ed.) *The Families and Genera of Vascular Plants, Malvales, Capparales and Non-Betalain Caryophyllales,* vol. 5, p.p. 225-311. Springer, Berlin, Heidelberg, New York.

Laemmli, U.K. 1970. Cleavage of structural

proteins during the assembly of the head of bacteriophage T4. *Nature*, 227, pp. 680–685.

LePéchon, T. & Gigord, L.D.B. 2014. On the relevance of molecular tools for taxonomic revision in Malvales, Malvaceae s.l., and Dombeyoideae. P.p. 337–363 in: Besse, P. (ed.), Molecular plant taxonomy: Methods and protocols. *Methods in Molecular Biology,* 1115. Totowa: Humana Press. DOI: org/10.1007/978-1-62703-767-9_17

Ghahreman, A., Pakravan, M. and Assadi, M. 2000. A new species of *Alcea* (Malvaceae) from Iran. *Nordic Journal of Botany*, 20(6), pp. 701-704.

Pakravan, M. 2001. Biosystematic study of the genus *Alcea* L. (Malvaceae) in Iran. Dissertation, University of Tehran, Tehran.

Pakravan, M. 2003. *Alcea Ilamica*, a new species from Iran. *Rostaniha*, 4(34), pp. 93-97.

Pakravan, M. 2005. New findings of the genus *Malva* L. (Malvaceae) in Iran. *The Iranian Journal of Botany*, 11(2), pp. 247-249.

Pakravan, M. 2006. A new combination in *Alcea* (Malvaceae) from Iran. The *Iranian Journal of Botany*, 12 (1), pp. 97-98.

Pakravan, M. 2006. Novelties in the genus *Alcea* in Iran. *The Iranian Journal of Botany*, 12 (2), pp.183-186.

Pakravan, M. 2008. A new species and a new combination in Iranian *Alcea* (Malvaceae)

Annales Botanici Fennici, 45(2), pp. 133-136. DOI:10.5735/085.045.0207.

Podani, J. 2000. Introduction to the Exploration of Multivariate Data [English translation]. Leide, Netherlands: Backhuys.

Riedl, I. 1976. *Alcea*. 41–80 in: Rechinger KH. (ed) *Flora Iranica*, 120. Graz, Akademische Druck- und Verlagsanstalt.

Smith, B.J. 1984. SDS-Polyacrylamide gel electrophoresis of proteins. *Method in Molecular Biology*, 1, pp. 41-55.

Stevens, P.F. 2001 (onwards 2014)**.** Angiosperm Phylogeny Website. Version 13, Retrieved *15 July* 2014. http://www. mobot. org/ MOBOT/research/APweb/ Includes

Takhtajan, A.L. 1980. Outline of the classification of flowering plants (Magnoliophyta). *Botanical Review*. (Lancaster) 46: 225–359. DOI: org/10.1007/bf0286155

Tate, J.A., Fuertes Aguilar, J., Wagstaff, S.J., La Duke, J.C., Bodo Slotta, T.A. and Simpson, B.B. 2005. Phylogenetic relationships within the tribe Malveae (Malvaceae, subfamily Malvoideae) as inferred from ITS sequence data. *American Journal of Botany*, 92, pp. 584-602.

Townsend, C.C. 1980. *Alcea*. In: Townsend CC, Guest E. (Eds.), *Flora of Iraq*, vol. 4(1). Ministry of Agriculture, Baghdad, pp. 248–258.

Özbek, F. and Uzunhisarcıkli, M.F. 2023. Taxonomic significance of seed macro-micromorphology of Turkish *Alcea* L. (Malvaceae) through light microscopy and scanning electron microscopy. *Microscopy and Technique*. 86 (12), pp. 1551-1567. DOI:org/10.1002/jemt.24385

Walker, C.C. & Eggli, U. 2023. Adansonia Malvaceae. Pp. 807–820 in: Eggli, U. & Nyffeler, R. (eds.), Dicotyledons: Rosids, 2nd ed. Illustrated handbook of succulent

plants. Cham: Springer. DOI:org/10.1007/978-3-030-93492-7_75

Zohary, M. 1963a. Taxonomical studies in *Alcea* of South-Western Asia. Part I. *Bulletin of the Research Council of Israel*, 11D4, pp. 210–229.

Zohary, M., 1963b. Taxonomical studies in *Alcea* of South-Western Asia. Part II. *Israel Journal of Botany*, 121, pp. 1-26.